MODULATION OF THROMBOSPONDIN-1 IN THE LUNG MICROENVIRONMENT: IMPLICATIONS FOR TARGETING METASTASIS

A Dissertation

Presented to the Faculty of the Weill Cornell Graduate School

of Medical Sciences

in Partial Fulfillment of the Requirements for the Degree of

Doctor of Philosophy

by

Tina El Rayes

May 2015

MODULATION OF THROMBOSPONDIN-1 IN THE LUNG MICROENVIRONMENT: IMPLICATIONS FOR TARGETING METASTASIS

Tina El Rayes

Cornell University 2015

Metastasis of cancer to distant organs is the major cause of its lethality. With recent studies highlighting the role of the premetastatic niche in supporting metastatic progression, we focused our efforts on understanding the interplay between reprogrammed microenvironments in distal organs and tumor cells, to determine novel mechanisms that contribute to metastasis progression and identify potential targets for metastasis suppression. Our investigations unraveled a critical role of the anti-tumorigenic factor thrombospondin-1 (Tsp-1) in the reprogrammed lung microenvironment.

Premetastatic niches generated in the lungs by metastasis-incompetent primary tumors showed elevated Tsp-1 expression. Interestingly, $Gr1^+$ myeloid cells in the lungs were the major producers of Tsp-1, and they responded to the tumor-derived factor prosaposin (psap), abundantly secreted by metastasis-incompetent tumors compared to their metastatic counterparts. Further analysis led to the identification of the pentapeptide sequence, DWLPK, within psap that retains Tsp-1-inducing activity. Using DWLPK, recapitulated Tsp-1 induction in $Gr1^+$ cells in the lungs and suppressed

metastasis of Lewis lung carcinoma cells. These results suggest that DWLPK can potentially serve as a therapeutic agent for metastasis suppression.

Studying metastasis in the setting of pre-existing lung inflammation, we observed loss of Tsp-1 in the lung microenvironment. Intranasal administration of bacterial lipopolysaccharide (LPS) induced lung inflammation, characterized by recruitment of $Ly6G^+$ neutrophils, and it enhanced metastatic burden. Inflammation was accompanied by an increase in neutrophil elastase (NE) and cathepsin G (CG) protease activity, and loss of Tsp-1 protein in lungs. Our studies confirmed that NE and CG degrade Tsp-1 in lungs in response to LPS-induced inflammation, thus promoting metastasis. Interestingly, blocking the neutrophil proteases pharmacologically using the dual protease inhibitor Sivelestat suppressed metastasis, indicating that the proteases are clinically viable anti-metastatic therapeutic targets.

Our studies demonstrate the novel finding that metastasis-incompetent tumors render the distal site metastasis-suppressive, by systemically inducing Tsp-1 expression in recruited myeloid cells. On the other hand, we have described a novel mechanism, where inflammation leads to Tsp-1 degradation via neutrophil proteases, generating a metastasis-promoting microenvironment. Our findings highlight the context-dependent plasticity of $Ly6G^+$ cells at distal sites, functioning as the main source of anti-tumorigenic Tsp-1 and the proteases that degrade it.

BIOGRAPHICAL SKETCH

Tina was born in the suburbs of Beirut, the capital of Lebanon. After high school, she was admitted into the prestigious American University of Beirut, where she completed her Bachelor of Sciences degree in biology, graduating with High Distinction, and minoring in psychology. Determined to pursue a research career, Tina volunteered in the research lab of Dr. Hala Muhtasib during her senior undergraduate year, where she was trained in basic molecular biology techniques. After graduating, she enrolled in the Master of Sciences program at the American University of Beirut, where she completed two years of research work in the lab of Dr. Rabih Talhouk, culminating in a Master's thesis in the field of breast cancer. Wanting to take her education and research career to a higher level, Tina looked to the United States for opportunities. She was offered a graduate student position at Weill Cornell Graduate School of Medical Sciences, where she joined the lab of Dr. Vivek Mittal and has since then been exploring the role of the premetastatic microenvironment on tumor metastasis.

To téta Antoinette and jeddo Philippe

Though you are greatly missed, your love is ever so present.

ACKNOWLEDGEMENTS

I want to start by thanking Dr. Vivek Mittal for recognizing the potential in me as a young graduate student and giving me the opportunity to participate in the exciting research conducted in his lab. Under your mentorship, I have matured as a scientist, and I am ready to join the scientific community, more confident in my critical thinking and technical abilities.

I would also like to thank my collaborator, Dr. Randolph Watnick, and members of his lab. Scientific discussions with you were always insightful. Thank you for giving me the chance to work on projects with you.

Dr. Gudas and Dr. Benezra, my committee members, thank you for your continued guidance over the past years.

Next, all the members of the Mittal lab, past and present. Thank you for all the support, scientific and otherwise, that you provided. Ding, you were always ready to discuss science and help out with experiments, despite everything else you had on your plate. I can see how much you enjoy what you do, and I hope you always feel this way. Raul, you taught me everything I needed to be a productive member of the lab. I enjoyed working on projects with you. We were like a well-oiled machine! Natasha, you were very welcoming when I first joined the lab and made me feel like I belonged. I am very happy for you and Raul, and I hope we can all meet again soon, like the old times, maybe in a setting involving a guitar! Mary, heavy metal fan and my dear friend, I am so happy I met you. You were always very knowledgeable in the lab. Thank you for showing me all the little tricks for troubleshooting problems (e.g. 3 dye pellets of alexa 568 for 2 hours). And outside the lab, I am thankful to have

you as a friend. Thank you for all the support you've shown me over the years. I wish you the best of luck on becoming the world's most awesome doctor! Seongho, you were a source of constant positive energy in the lab. I appreciate all the feedback and advice you were ready to give me to drive me in the right direction, science-wise and career-wise. I wish you all the best in Korea, because you deserve nothing less. Hyejin, my senior and my friend, as a graduate student, you led by example. I admire your hard work and the effort you put into everything you do. Thank you for all the talks we had and all the advice you shared. I felt like you were my older sister in the lab, and I appreciate the help you always gave so readily. Good luck with your scientific pursuit. Who knows, we might be neighbors again one day! Kari, my junior and my buddy. I hope I gave you some good advice that you can thank me for in your thesis next year! Thank you for being so patient while I complained about something new every day. And thank you for your support when times got tough; it made a huge difference. I want you to know that you are super smart (but I'm sure you know that), and one day you will take the world by storm. Just give yourself more credit. Anna, I had the best time digging into my activist self, thanks to you. You showed me that the life of a scientist doesn't have to be dull. Good luck with your new adventure, the most important one anyone can embark on. You're gonna be a great mom. Murtaza, I will never forget your legendary rapping skills! Thank you for being on top of everything all the time, and keeping this ship going. Chris, you beautiful orange-haired man, having you around was always fun (also helpful in case of medical emergencies). Good luck becoming a rich doctor (who remembers his friends). Esi, thank you for being so friendly and warm. I always enjoyed our talks. I wish you luck in dental school. You will do great, I'm sure of it. Sharrell, you

always accomplished a million tasks in your calm and quiet way. Thank you for helping out on projects even when you were swamped with work. Good luck with everything you do. Lauren and Jen, although you guys both joined the lab more recently, I already feel like I've known you for a long time. Lauren, I can see that you are going to accomplish great things in the lab. Jen, I'm happy that you are officially a member of the lab now. Thanks for helping out with experiments and providing moral support when I needed it. Good luck with your grad school applications!

I want to also thank my family for supporting my decision to go to grad school. Mom, I know it was hard for you to see me leave for another country. Thank you for being strong and for believing in me. Dad, thank you for your support and your constant encouragement. I hope I can always make both of you proud.

TABLE OF CONTENTS

LIST OF FIGURES

CHAPTER ONE

INTRODUCTION

Metastasis is the major cause of cancer-related deaths. This has fueled studies to understand mechanisms of metastasis for the purpose of devising novel therapeutic approaches. Earlier studies examining mechanisms of metastasis focused solely on cancer cell-intrinsic properties that drive steps in the metastatic cascade, such as tumor cell invasion, migration, and extravasation, as well as homing to specific distant organs (Nguyen and Massagué, 2007; Yang et al., 2004a). However, recent studies have shed light on the critical role of immune/inflammatory cells that make up the microenvironment of the metastatic organ in supporting the steps of the metastatic cascade, including metastatic seeding and outgrowth (Joyce and Pollard, 2009). By understanding how changes in the premetastatic microenvironment impact tumor cell metastatic ability, our aim is to target the more genetically stable cell components of the microenvironment to hinder metastatic progression.

My doctoral thesis has focused on uncovering the reprogrammed microenvironments in distant metastatic organs generated by metastasis-incompetent and metastasis-competent tumors. Moreover, I have evaluated the effect of heightened inflammatory conditions in the distant organs on metastasis progression. The hope is that understanding the mechanisms operating in the metastatic organs can pave the way to new therapeutic approaches that target the metastasis-promoting microenvironment, irrespective of tumor-intrinsic properties or disparities among tumors.

1-1. The premetastatic niche

In 1889, Stephen Paget proposed the “seed and soil” hypothesis, where he posited that cancer cells, “the seed”, had an affinity for and colonized organs that were conducive to their growth, or had the proper “soil”, and that metastasis was not a random event (Fidler, 2003). Strikingly in agreement with the “seed and soil” hypothesis, emerging evidence from recent studies shows that a conducive microenvironment is required for disseminated tumor cells to engraft distant sites. Furthermore, metastatic tumors themselves systemically establish bone marrow (BM)-derived “premetastatic niches” in distant organs that serve as permissive hubs for supporting future metastasis (Psaila and Lyden, 2009). These premetastatic niches are characterized by the induction of organ-specific chemoattractants, growth factors and extracellular matrix (ECM)-related proteins, as well as the recruitment of bone marrow-derived cells, like vascular endothelial growth factor receptor (VEGFR)1^+ hematopoietic progenitor cells and $CD11b^+$ myeloid cells (Gao et al., 2012; Hiratsuka et al., 2006; Kaplan et al., 2005; Kim et al., 2009; Qian et al., 2011) (**Figure 1.1**).

The “premetastatic niche” model implies that it is not only a tumor cell’s intrinsic properties that dictate its metastatic fate but that the generation of a conducive environment at the distant site is necessary to allow the outgrowth of disseminated tumor cells into secondary metastases (Kaplan et al., 2005).

The first description of the premetastatic niche involved the clustering of hematopoietic progenitor cells in the lungs, preceding and necessary for tumor

Figure 1.1

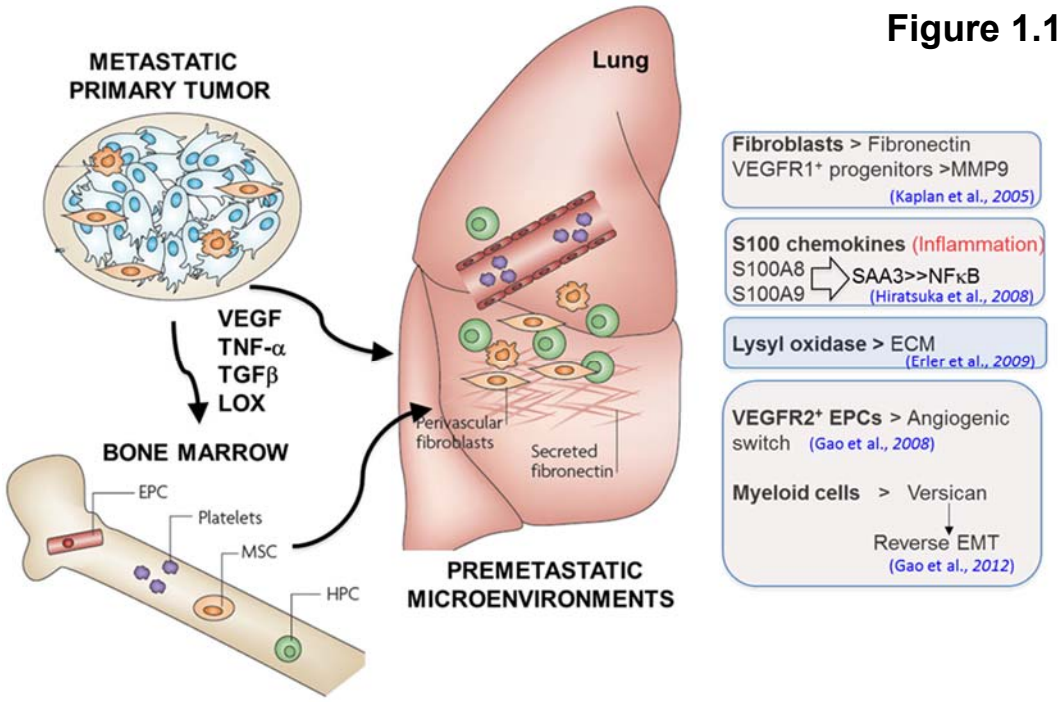

Figure 1.1. The premetastatic niche. Metastatic primary tumors, by systemically secreting VEGF, TNFα, and TGFβ, induce the recruitment of bone marrow-derived cells (BMDCs), such as endothelial progenitor cells (EPCs), platelets, mesenchymal stem cells (MSCs), and hematopoietic progenitor cells (HPCs) to the lung. These BMDCs form the premetastatic niche, together with induced chemoattractants, proteases, and ECM components. For instance, metastatic primary tumors systemically induce the expression of fibronectin in lung fibroblasts, leading to the recruitment of VEGFR1$^+$ HPCs via their fibronectin receptor, VLA-4. VEGFR1$^+$ cells in turn secrete MMP9 in response to tumor-derived VEGF, modifying the lung ECM. VEGF, TNFα, and TGFβ secreted by primary tumors induce the expression of S100A8 and S100A9 in the lung microenvironment, recruiting myeloid cells. S100A8 and S100A9 activate the expression of SAA3, leading to TLR4 signaling and NF-κB activation, promoting an inflammatory state. Hypoxic primary tumors release lysyl oxidase (LOX), which crosslinks collagen in the lungs, increasing the retention of myeloid cells and tumor cells. Myeloid cells recruited to the lungs secrete the factor versican, which induces MET in disseminated tumor cells, allowing metastatic outgrowth. And VEGFR2$^+$ EPCs are recruited to induce the angiogenic switch, allowing micrometastases to develop to macrometastases in the lungs. *(Modified from Psaila and Lyden, 2009)*.

metastasis. In this model, tumor cells systemically upregulated the expression of fibronectin in lung resident fibroblasts, leading to the recruitment of bone marrow-derived VEGFR1$^+$ hematopoietic progenitor cells via their fibronectin receptor, VLA-4 (Kaplan et al., 2005). A more recent study found that CXCR4-mediated recruitment of Gr1$^+$ myeloid cells into the lungs enhanced lung metastasis, independent of vascular endothelial growth factor (VEGF)/VEGFR1-mediated recruitment of tumor–associated macrophages (TAMs) (Hiratsuka et al., 2011).

Primary tumors, by secreting VEGFA, transforming growth factor β (TGFβ), and tumor necrosis factor α (TNFα), can systemically induce the expression of chemoattractants, like S100A8 and S100A9, in the premetastatic lungs, leading to recruitment of CD11b$^+$ myeloid cells, which in turn express migration-stimulating factors, such as TNFα and TGFβ, enhancing tumor cell metastasis (Hiratsuka et al., 2006). In addition, S100A8 and S100A9 induce the expression of serum amyloid A3 (SAA3) in premetastatic lungs, resulting in the activation of NF-κB signaling via toll-like receptor 4 (TLR4) on myeloid cells, creating an inflammatory state and further accelerating lung metastasis (Hiratsuka et al., 2008). Furthermore, primary tumor-derived CCL2 can stimulate CCR2 on lung endothelial cells, inducing the secretion of S100A8 and SAA3, which signal via TLR4 to increase vascular permeability, creating hyperpermeable foci in the lungs that attract leukocytes and tumor cells (Hiratsuka et al., 2013).

VEGF secreted by primary tumors induces the expression of matrix metalloprotease 9 (MMP9) in the premetastatic lung in cells that express VEGFR1, including CD11b$^+$ myeloid cells and endothelial cells (Hiratsuka et

al., 2002). MMP9 in the premetastatic niche can facilitate tumor cell extravasation, as well as release growth factors from the ECM, like VEGF to promote angiogenesis (Bergers et al., 2000), and chemokines like soluble KIT ligand, which further recruits bone marrow-derived cells expressing the KIT receptor (Heissig et al., 2002).

Bladder cancer-derived proteoglycan versican enhances tumor cell metastasis to the lungs via a mechanism that upregulates CCL2 chemokine levels in the lungs and increases macrophage infiltration (Said et al., 2012). Consistent with that study, the recruitment of CCR2-expressing monocytes and macrophages to the lungs in response to metastatic tumor cell-derived and host tissue-derived CCL2 enhances breast tumor metastasis to the lungs, in part due to the expression of VEGF by recruited monocytes, promoting tumor cell extravasation (Qian et al., 2011). Furthermore, versican expressed by LLC tumor cells activates TLR2:TLR6 complexes on myeloid cells, inducing TNFα secretion by myeloid cells and enhancing tumor cell metastatic growth (Kim et al., 2009). On the other hand, versican expressed by $CD11b^{+}$ $Gr1^{+}$ $Ly6C^{high}$ myeloid progenitor cells in the premetastatic lung contributes to the mesenchymal-to-epithelial transition (MET) of disseminated metastatic tumor cells, consequently increasing cell proliferation and accelerating lung metastasis of breast tumors (Gao et al., 2012).

It has also been shown that hypoxic primary tumors secrete lysyl oxidase (LOX), which acts systemically to crosslink collagen in lungs. This allows the retention of $CD11b^{+}$ myeloid cells in the lungs, which in turn secrete MMP2, releasing collagen fragments that are chemoattractive to myeloid cells and tumor cells, hence promoting metastatic progression (Erler et al., 2009).

Together these studies have established the ability of metastasis-competent primary tumors to generate a premetastatic niche. This thesis will first characterize the premetastatic niches generated by metastasis-incompetent tumors to determine mechanisms of metastasis suppression. Next, it will address the role of extrinsic inflammation in promoting metastasis, based on the hypothesis that the inflammatory microenvironment created would resemble the tumor-derived inflammatory component of the premetastatic niche.

1-2. Thrombospondin-1 (Tsp-1)

In the year 1990, thrombospondin-1 (Tsp-1) was identified as the first endogenous inhibitor of angiogenesis, inhibiting endothelial cell migration and neovascularization in the rat cornea (Good et al., 1990). The identification of endogenous angiogenesis inhibitors paved the way to the understanding that regulation of angiogenesis depends on a balance between promoter and inhibitor activities. In the context of tumors, angiogenesis is required for tumor progression, so Tsp-1 is an important regulator of tumor progression.
Tsp-1 expression is regulated by a tumor suppressor (Good et al., 1990), later identified as p53 (Dameron et al., 1994; Kang et al., 2009).

Structure of Tsp-1

Tsp-1 is one of five thrombospondins in mammals (Tsp-1 - Tsp-5). Tsp-1 protein consists of three polypeptide chains of equivalent molecular weight. The trimer has a molecular weight of around 450 kDa, while each monomeric chain has a molecular weight of 150 kDa (**Figure 1.2**). The three chains are crosslinked proximal to the N-terminal domain via inter-chain disulfide bonds.

Figure 1.2

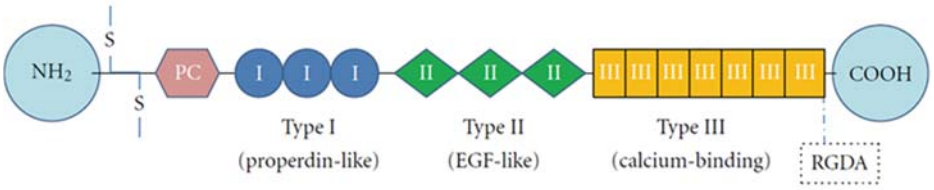

Figure 1.2. The structure of Tsp-1. Tsp-1 exists as homotrimer. Each monomer (pictured above) consists of a globular NH2-terminal domain, known as the heparin-binding domain, interchain disulfides, which allow Tsp-1 monomers to trimerize, a procollagen homology domain (PC), Type I, II, and III repeats, and a globular carboxyl terminal. The RGD sequence within the last Type III repeat is the binding site for integrins. *(Modified from Lopez-Dee et al., 2011)*.

Structurally, a Tsp-1 monomer consists of an NH2-terminal globular domain, known as the heparin-binding domain, inter-chain disulfides, a procollagen domain, three type I repeats (TSR), three EGF-like repeats, seven Ca^{2+}-binding repeats, the last of which contains an RGD sequence that allows it to interact with αvβ3 integrin, and a COOH terminal domain (Bornstein, 1992; Lopez-Dee et al., 2011).

Tsp-1 in wound healing

Under conditions of wound healing, the synthesis of Tsp-1 occurs in megakaryocytes. Platelet Tsp-1 is stored in α-granules and released upon the binding of thrombin to platelets. A thrombin-thrombospondin complex forms on the surface of platelets, and this occurs through a thiol-disulfide bond between a free thiol group on Tsp-1 and a disulfide on thrombin (Lawler, 1986). Tsp-1 binds platelets through its carboxyl-terminal and mediates platelet aggregation (Rabhi-Sabile et al., 1996). Tsp-1 is found in clots, bound to fibrinogen via its TSR domain (Lawler, 1986; Lee et al., 2006b; Panetti et al., 1999).Tsp-1 also binds von Willebrand factor and coagulation factors IXa and Xa (Lawler, 1986).

Tsp-1 binding partners

Tsp-1 is synthesized and secreted by diverse cell types, including endothelial cells, fibroblast, epithelial cells (Lawler, 1986), as well as monocytes and macrophages (Jaffe et al., 1985). However, activated macrophages reduce their secretion of Tsp-1 (Jaffe et al., 1985).

Tsp-1 binds numerous ECM proteins, including heparin, fibronectin, fibrinogen, type V collagen, and plasminogen (Lawler, 1986).

The different functions of Tsp-1 depend on its presence in the ECM environment. However, Tsp-1 undergoes different fates, including cellular uptake, proteolysis, or ECM retention. For instance, interaction of the N-terminal domain of Tsp-1 with heparan sulfate proteoglycans or low-density lipoprotein receptor-related protein (LRP) leads to its endocytic internalization and intracellular proteolysis (Gupta et al., 1999), while in the ECM, Tsp-1 can undergo processing by different enzymes (Bonnefoy and Legrand, 2000; Hogg et al., 1994; Lee et al., 2006b; Rabhi-Sabile et al., 1996). Finally, Tsp-1 retention in the ECM is mediated by the C-terminal domain of Tsp-1 trimers, and depends on the C-terminal RGD motif as well as a site in the L-lectin domain, but is independent of CD47, β1-integrins, αvβ3 integrin, and fibronectin (Adams et al., 2008).

Tsp-1 cleavage fragments and their functions

In the ECM, Tsp-1 is exposed to proteases that mediate its cleavage. Exposure of Tsp to α-thrombin in the presence of Ca^{2+} leads to selective cleavage of a 25 kDa amino-terminal heparin-binding fragment and an anti-angiogenic 140 kDa carboxyl-terminal fragment (Lawler, 1986; Taraboletti et al., 1997). Cleavage of the Tsp-1 amino-terminal heparin-binding domain is also mediated by thermolysin, plasmin, trypsin, chymotrypsin, and cathepsin G (Lawler, 1986; Rabhi-Sabile et al., 1996).

The anti-angiogenic function of Tsp-1 has been attributed to three peptide sequences in the 140 kDa carboxyl-terminal fragment, one being in the procollagen domain and the other two in the type I repeats (TSR domain) (Tolsma et al., 1993; Vogel et al., 1993). More recently, it was shown that ADAMTS1, a secreted metalloprotease, cleaves Tsp-1 within the procollagen

domain, in the proximity of the inter-chain disulfide bonds, releasing a trimeric N-terminal domain, composed of individual 36 kDa fragments, and soluble 110 kDa C-terminal monomers, which suppress VEGF- and FGF2-activated endothelial cell proliferation (Lee et al., 2006b).

Interestingly, the 25 kDa amino-terminal heparin-binding fragment of Tsp-1, released through thrombin cleavage, induces angiogenesis in the rabbit cornea by promoting endothelial cell invasiveness. The 25 kDa fragment induces the synthesis and activation of MMP2, and downregulates the expression of the MMP2 inhibitor TIMP2 in endothelial cells (Taraboletti et al., 2000). This account demonstrates that Tsp-1 can be a source of smaller fragments that mediate angiogenesis, hence opposing the antiangiogenic function of full-length Tsp-1, or the 140 kDa fragment of Tsp-1.

Non-receptor-mediated Tsp-1 anti-angiogenic functions

bFGF binds to full-length Tsp-1 and the C-terminal 140 kDa antiangiogenic fragment generated by thrombin cleavage. Tsp-1 thus inhibits binding of bFGF to endothelial cells, and concurrently inhibits endothelial cell proliferation in response to bFGF (Taraboletti et al., 1997).

Tsp-1 binds inactive MMP2 and MMP9 zymogens, inhibiting their activation (Bein and Simons, 2000), consequently inhibiting MMP9-mediated release of VEGF from the ECM (Rodriguez-Manzaneque et al., 2001). Tsp-1 also directly binds VEGF and leads to its clearance from the ECM via intake of the Tsp1-bound VEGF by LRP1 (Gupta et al., 1999; Lawler and Lawler, 2012).

Receptor-mediated Tsp-1 anti-angiogenic functions

Tsp-1 can induce apoptosis of endothelial cells. Binding of Tsp-1 to the CD36 receptor on endothelial cells induces their apoptosis via the activation of mitochondrial-dependent and independent apoptotic cascades, downstream of the Src family kinase Fyn (Jiménez et al., 2000; Lawler and Lawler, 2012; Ren et al., 2009).

Tsp-1 can inhibit endothelial cell proliferation in response to VEGF. Binding of Tsp-1 to endothelial CD36 promotes the association of CD36 with β1 integrins, inhibiting phosphorylation of VEGFR2 in response to VEGF, hence blocking the downstream Akt survival and proliferation signals (Lawler and Lawler, 2012; Primo et al., 2005). Furthermore, in capillary endothelial cells, the binding of Tsp-1 to very-low-density lipoprotein receptor (VLDLR) inhibits cell cycle progression via Akt and MAPK pathways (Oganesian et al., 2008), whereas in larger vessels, Tsp-1 inhibits cell cycle progression by binding to CD36, activating p53 and p21 (Lawler and Lawler, 2012; Yamauchi et al., 2007).

Although binding of Tsp-1 to CD36 or CD47 blocks nitric oxide (NO) production in endothelial cells, only CD47 is required, and this leads to inhibition of endothelial cell migration, proliferation, and survival, as well as vascular permeability (Isenberg et al., 2007).

Receptor-mediated Tsp-1 anti-tumor functions

Tsp-1 can also act directly on tumors, blocking their proliferation or inducing their apoptosis. Tsp-1 type I repeats inhibit melanoma proliferation via a CD36-independent mechanism, which seems to require a protein tyrosine phosphatase, since the effect is blocked by the tyrosine phosphatase inhibitor

vanadate (Guo et al., 1998). Furthermore, Tsp-1 inhibits cell proliferation of B16-F10 melanoma cells in a TGFβ-dependent manner (Miao et al., 2001), which requires the TSR2 domain of Tsp-1 containing the RFK sequence that activates latent TGFβ (Miao et al., 2001; Schultz-Cherry et al., 1994, 1995). *In vivo*, Tsp-1 was able to increase melanoma tumor apoptosis, through TGFβ activation (Miao et al., 2001).

1-3. Thesis Aims

The ability of metastasis-competent primary tumors to generate metastasis-promoting premetastatic niches in distal organs is well described. However, similar information on metastasis-incompetent tumors is lacking. We considered three potential scenarios that could explain the inability of metastatic-incompetent tumors to metastasize. 1- Metastasis-incompetent tumors generate a premetastatic niche, but tumor-intrinsic properties prevent metastasis. 2- Metastasis-incompetent tumors do not generate a premetastatic niche. 3- Metastasis-incompetent tumors generate a niche in the distant organ that is molecularly different than the one generated by metastasis-competent tumors. Chapter two of this thesis will address this question and evaluate the distal microenvironment established by metastasis-incompetent tumors, in the goal of finding tumor-derived factors that systemically alter the distal site and block metastatic outgrowth, and making use of them therapeutically.

Another key question that will be addressed in chapter three of this thesis is whether external inflammation has the potential to promote metastasis, as the inflammatory microenvironment resembles the tumor-derived inflammatory component of the premetastatic niche. The aim is to recapitulate the

mechanism(s) that enhance metastatic outgrowth, revealing therapeutically actionable targets for metastasis suppression.

CHAPTER TWO[1]

METASTASIS-INCOMPETENT TUMORS SYSTEMICALLY INDUCE TSP-1 IN LUNG GR1^{+} MYELOID CELLS.

2-1. INTRODUCTION

Emerging data demonstrate that metastatic primary tumors systemically alter the distal site of metastasis, creating a premetastatic niche that is required for metastatic tumor colonization and outgrowth. However, the impact of metastasis-incompetent tumors on the premetastatic niche has not been previously described. This chapter will interrogate the ability of metastasis-incompetent tumors to systemically influence distant metastatic organs, with a focus on the tumor-derived secreted factor prosaposin, which systemically alters the lung microenvironment by modulating Tsp-1 production, rendering it metastasis-suppressive.

Preceding our studies, prosaposin had been described as an anti-metastatic factor highly secreted by cancer cells with a low metastatic potential, and capable of inducing Tsp-1 expression in stromal cells (Kang et al., 2009). We demonstrated that tumor-derived psap induced Tsp-1 expression in myeloid cells recruited to the lungs, leading to metastasis suppression. In addition, the psap-derived pentapeptide DWLPK likewise induced Tsp-1 expression in lung myeloid cells and inhibited metastasis, indicating a potential for therapeutic intervention.

[1] Results presented in this chapter have been published in: Catena R, Bhattacharya N, El Rayes T, Wang S, Choi H, Gao D, Ryu S, Joshi N, Bielenberg D, Lee SB, Haukaas SA, Gravdal K, Halvorsen OJ, Akslen LA, Watnick RS, Mittal V. Bone marrow-derived Gr1+ cells can generate a metastasis-resistant microenvironment via induced secretion of thrombospondin-1. Cancer Discov. 2013 May;3(5):578-89.

2-1.1. Prosaposin structure and processing

Prosaposin is a 75 kDa polypeptide precursor of four saposin proteins, which are heat-stable activators of glycosphingolipid hydrolases that reside in the lysosome, and hence play a role in glycosphingolipid metabolism. Proteolytic processing of prosaposin in the lysosome releases the four saposins A-D, of lower molecular weight (9-11 kDa) (Hiesberger et al., 1998; Sandhoff and Kolter, 1997).

Prosaposin is synthesized as a 65 kDa polypeptide in the endoplasmic reticulum (ER), and then further converted into the 73 kDa form in the Golgi apparatus after glycosylation. Furthermore, both the 65 and the 73 kDa prosaposin forms contain phosphate groups on N-linked oligosaccharide chain (carbohydrate-linked phosphate) on saposin C and saposin D domains while only the 73 kDa prosaposin has sulfate residues on the saposin A and saposin C domain, suggesting that phosphorylation occurs in the ER and sulfation in the Golgi (Vielhaber et al., 1996).

A major fraction of synthesized prosaposin is secreted outside the cell, whereas part of it is directly intracellularly shuttled to the lysosome, for processing into saposins. This occurs through the binding of the mannose-6-phosphate (M-6-P) residues on prosaposin to the mannose-6-phosphate receptor (MPR) (Vielhaber et al., 1996). On the other hand, most of the endocytic re-uptake of secreted prosaposin occurs independently of MPR, via the mannose receptor on macrophages and LRP1 expressed ubiquitously on most cells (Hiesberger et al., 1998).

Once endocytosed, prosaposin is delivered to the lysosome, where it undergoes processing into the saposins by the aspartyl protease, cathepsin D (Hiraiwa et al., 1997). Interestingly, the binding of prosaposin to the

glycosphingolipid ganglioside GM1 protects it from processing by cathepsin D (Hiraiwa et al., 1997).

2-1.2. Known functions of Psap

In addition to being a lysosomal precursor, prosaposin has been described to have additional functions, especially since it exists as a secreted protein in human milk, cerebrospinal fluid, and seminal plasma (Hiraiwa et al., 1993), and its unprocessed form is highly abundant in the brain (O'Brien et al., 1988).

Prosaposin is important for the development of male reproductive organs (Morales and Badran, 2003), is secreted by Sertoli cells in the testes, and is involved in spermatogenesis (McKinnell and Sharpe, 1997) and fertilization (Hammerstedt et al., 2001).

In muscle tissue, prosaposin plays a role in the differentiation of myoblasts to myotubes (Rende et al., 2001).

Prosaposin has neurotrophic functions, and its active region is located in the saposin C domain. It stimulates neurite outgrowth of a mouse neuroblastoma cell line and choline acetyltranferase (ChAT) activity in a human neuroblastoma cell line (O'Brien et al., 1994). Prosaposin also exerts a neuroprotective and glioprotective role (Campana et al., 1999; Tsuboi et al., 1998) via the activation of ERK signaling downstream of the G-protein-coupled receptors GPR37 and GPR37L1 (Meyer et al., 2013).

2-1.3. Psap functions in cancer

In the context of tumorigenesis, prosaposin was found to be secreted by the human breast cancer cell lines MDA-MB-231, MDA-MB-435, and MCF7, and

its secretion was upregulated in response to 17β-estradiol (Campana et al., 1999). Higher expression levels of Psap protein and mRNA were observed in malignant androgen-independent (AI) prostate cancer cells than in androgen-sensitive (AS) cells or normal prostate epithelial cells, and this could be attributed in some cases to genomic amplification of the Psap gene (Koochekpour et al., 2005). Moreover, in prostate cancer, Psap levels in serum were found to be downregulated in patients with localized primary tumors, but upregulated in patients with castrate-resistant metastatic prostate cancer (Koochekpour et al., 2012). Psap can induce the expression of androgen receptor (AR), its phosphorylation, and nuclear localization in AR-positive LNCaP prostate cancer cells (Koochekpour et al., 2007a), while on the other hand being an androgen-regulated gene (ARG), where AR binds to a hormone-responsive element in the proximal region of the Psap promoter and activates Psap expression (Koochekpour et al., 2007b).
The same is true in AR-expressing prostate stromal cells, where Psap functions as an androgen-agonist and an androgen-regulated gene, with the interesting addition that conditioned medium from prostate stromal cells can induce Psap promoter activity in AI and AS prostate cancer cells, indicating paracrine signaling (Koochekpour et al., 2008).

Of specific interest for the purpose of our project is the observation that prosaposin secretion is elevated in non-metastatic breast and prostate cancer cell lines compared to their metastatic counterparts, and that Psap acts as an inhibitor of metastasis via its Tsp-1 induction activity on stromal fibroblasts (Kang et al., 2009). Furthermore, Psap mRNA expression was lower in human primary tumors that gave rise to metastases than in localized non-metastatic

primary tumors (Kang et al., 2009). These studies suggest that Psap is secreted by metastasis-incompetent tumors and has the potential to systemically alter the microenvironment at the distal site.

2-1.4. LRP1 receptor

As mentioned above, LRP1 has been reported as a receptor for psap, mediating its endocytosis. The LRP1 receptor was identified in the liver as a receptor that bound apolipoprotein E (apoE)-containing lipoprotein remnants and removed them from circulation (Beisiegel et al., 1989). Interestingly, apoE is secreted by cells that themselves express LRP1 or are in close proximity to cells that express it, as in the case of hepatocytes, which express LRP1 and secrete apoE, and this is thought to drive the synergistic function in the hepatic uptake of lipoproteins (Krieger and Herz, 1994). LRP1 was soon after found to be the receptor responsible for clearing from the circulation the proteinase inhibitor α2-macroglobulin bound to proteases (Kristensen et al., 1990; Strickland et al., 1990). LRP1 in the liver is also highly expressed on Kupffer cells, the liver resident macrophages, where it internalizes protease inhibitors complexed with proteases, chylomicron remnants, and activated coagulation factors, leading to their intracellular degradation (Lillis et al., 2008).
Since then, LRP1 has been reported to have high affinity for numerous ligands and to internalize them (Lillis et al., 2008). For instance, LRP1 has been shown to bind and clear the plasminogen activators, tissue-type plasminogen activator (tPA) and urokinase-type plasminogen activator (uPA), bound to their inhibitor, plasminogen activator inhibitor-1 (PAI-1) (Nykjaer et al., 1992; Orth et al., 1992). Plasminogen activators are serine proteases that convert plasminogen into active plasmin, a broad spectrum protease that plays a role

in matrix restructuring, wound healing, and invasion. Hence, LRP1 regulates pericellular proteases and can influence cell invasion. On one hand, LRP1 expression was associated with a less invasive phenotype of breast and prostate cancer cell lines, possibly due to the endocytosis of the proteases (Kancha et al., 1994). On the other hand, LRP1 cell surface expression was positively correlated with invasiveness of several breast cancer cell lines (Li et al., 1997, 1998), and LRP1 was expressed on the leading edge of invading cells (Chazaud et al., 2002).

Based on all these observations, LRP1 was originally thought to function simply as an endocytic receptor, but data now suggests that it also plays a role in intracellular signaling.

LRP1 is expressed on a number of cell types, including hepatocytes and Kupffer cells in the liver, monocytes in lung and lymphoid tissue, and neuronal cells and astrocytes in the brain (Moestrup et al., 1992), where it can bind amyloid precursor protein (APP) (May et al., 2002). LRP1 deletion in mice causes embryonic lethality, demonstrating its essential role during development, with one study suggesting it plays a role in embryo implantation (Herz et al., 1992).

LRP1 transcription and protein expression are downregulated in macrophages by lipopolysaccharide (LPS) and interferon-γ (IFN- γ) (LaMarre et al., 1993), and upregulated by colony-stimulating factor-1 (CSF1) (Hussaini et al., 1990). Furthermore, LRP1 is redistributed from intracellular compartments to the cell membrane in response to insulin (Descamps et al., 1993).

LRP1 is synthesized in the ER as a single polypeptide precursor and is cleaved by the processing protease furin in the Golgi into the 85 kDa single-pass transmembrane C-terminal subunit and an N-terminal 515 kDa large extracellular domain that remains non-covalently associated with the 85 kDa subunit (Krieger and Herz, 1994; Willnow et al., 1996a). The 515 kDa extracellular subunit contains the ligand-binding domains of LRP1, whereas the 85 kDa subunit consists of the transmembrane domain and the cytoplasmic domain of LRP1. In the ER, a resident chaperone protein called receptor associated protein (RAP) prevents newly translated LRP1 from binding to ligands and aggregating, hence allowing proper delivery of LRP1 to the cell membrane (Herz et al., 1991; Williams et al., 1992; Willnow et al., 1996b). The lower pH encountered by the RAP/LRP1 complex in the Golgi leads to the release of LRP1 from RAP (Bu et al., 1995; Lee et al., 2006a).

Being a member of the low density lipoprotein (LDL) receptor family, the extracellular domain of LRP1 contains cysteine-rich complement-type repeats (CR), arranged into four clusters, termed clusters I-IV. Most binding to LRP1 occurs at clusters II and IV (Neels et al., 1999). Furthermore, the extracellular domain of LRP1 is made up of two cysteine-rich EGF-like repeats, a β-propeller YWTD repeat, and a third EGF-like repeat. The β-propeller domain functions in the uncoupling of LDL receptor family members from ligands under the low pH conditions of the endosome (Mikhailenko et al., 1999). The cytoplasmic domain of LRP1 is 100 amino acids long and contains two NPxY motifs that are tyrosine phosphorylated by PDGFR-β, v-scr, and connective tissue growth factor (Barnes et al., 2003; Boucher et al., 2002;

Yang et al., 2004b). In addition, LRP1 cytoplasmic domain can bind several adaptor molecules (Gotthardt et al., 2000).

LRP1 and PDGFR-β are closely located in caveolae (Boucher et al., 2002). PDGF-BB binds PDGFR and can bind directly to the extracellular domain of LRP1 (Loukinova et al., 2002). This leads to the tyrosine phosphorylation of the second NPxY motif of the LRP1 cytoplasmic domain by scr-family kinases, via a mechanism dependent on PDGFR-β, creating a docking site for Shc adaptor protein on LRP1, allowing LRP1 to function in intracellular signaling events (Boucher et al., 2002; Loukinova et al., 2002). Furthermore, another possible signaling mechanism of LRP1 involves the cleavage and release of its intracellular domain from the cell membrane by a gamma secretase-like activity, where it has the potential to translocate to the nucleus and participate in transcriptional regulation (May et al., 2002). LRP1 intracellular domain (LRPICD) has been described to translocate to the nucleus and negatively regulate amyloid precursor protein (APP)- Fe65 scaffold protein transcriptional activity (Kinoshita et al., 2003).

LRP1 is involved in cell migration. The binding of Tsp-1 to a calreticulin-LRP1 co-complex, where Tsp-1 binds calreticulin, which in turn binds LRP1, leads to the phosphorylation of scr and focal adhesion kinase (FAK), activating ERK and PI3K, leading to downstream RhoA inactivation, focal adhesion disassembly, and stimulation of cell migration (Orr et al., 2002, 2003a, 2003b, 2004). Interestingly, direct binding of Tsp-1 to LRP1 leads to its internalization and degradation (Mikhailenko et al., 1997).

This chapter will explore the ability of metastasis-incompetent tumors to generate a premetastatic niche. We determined that metastasis-incompetent tumors generate a metastasis-suppressive lung microenvironment that is characterized by the induction of Tsp-1 in recruited $Gr1^+$ myeloid cells. We further evaluated the therapeutic benefits of exogenously inducing Tsp-1 in the lung microenvironment on metastatic outgrowth. To this end, we used a peptide derived from the tumor-secreted protein prosaposin, and showed that we can suppress metastatic outgrowth. Moreover, mechanistic studies were conducted that implicate LRP1 as the receptor that mediates signaling leading to Tsp-1 induction in response to prosaposin.

2-2. RESULTS

2-2.1. Poorly metastatic tumors recruit BM-derived cells to the lungs.

Studies have shown that metastatic tumors generate a premetastatic niche characterized by the recruitment of BM-derived cells to the future site of metastasis. However, this phenomenon has not been explored for metastasis-incompetent tumors, and it remains unknown whether these tumors fail to form premetastatic niches, or generate metastasis-refractory niches.

To determine the nature of the premetastatic niche generated by tumors with low metastatic potential, we used human prostate and breast cancer cell lines that include the weakly metastatic parental cells, PC3 or MDA-MB-231, and their highly metastatic variants, PC3M-LN4 (LN4) and MDA-MB-LM2 (LM2), respectively, both of which metastasize to lungs. Furthermore, to recapitulate the systemic effect of tumor-secreted factors acting on the lung microenvironment *in vivo*, we administered tumor cell conditioned media (CM) intraperitoneally (i.p.) into mice. To be able to visualize the recruitment of bone

marrow-derived cells (BMDCs) to the lung microenvironment, we performed BM transplantation (BMT) of GFP^+ BM into irradiated wild type (WT) syngeneic mice. The CM from metastatic LN4 cells significantly increased the recruitment of GFP^+ BMDCs to the lungs, forming a premetastatic niche, as expected. Strikingly, CM from the metastasis-incompetent PC3 cell line similarly generated a GFP^+ BM-derived premetastatic niche in the lungs (**Figure 2.1a, b**). Furthermore, the majority of recruited GFP^+ cells were $CD11b^+$ myeloid cells (**Figure 2.1a, c**).

2-2.2. Poorly metastatic tumors induce Tsp-1 expression in the BM-derived cells recruited to the lung microenvironment.

Having observed no difference in the cellular composition of the premetastatic lungs generated by metastasis-competent and incompetent tumors, we hypothesized that the BMDCs recruited to the lungs could harbor molecular differences that might explain the metastasis-resistant phenotype seen in metastasis-incompetent tumors. To explore this possibility further, we performed gene expression analysis of lungs from mice challenged with PC3 CM or LN4 CM (**Figure 2.2a**). We focused our selection criteria on genes that encoded secreted proteins, which were negative regulators of metastatic outgrowth and were upregulated in PC3 CM-treated mouse lungs. Among the candidate genes, we selected thrombospondin-1 (Tsp-1) for further analysis, since it is a known inhibitor of angiogenesis and tumor progression, and since several regulators of Tsp-1 function were also upregulated in these lungs, including the CD47 receptor and ADAMTS1 (**Figure 2.2a**). Analysis of PC3 CM-treated lungs validated that Tsp-1 was upregulated compared to LN4 CM-

Figure 2.1

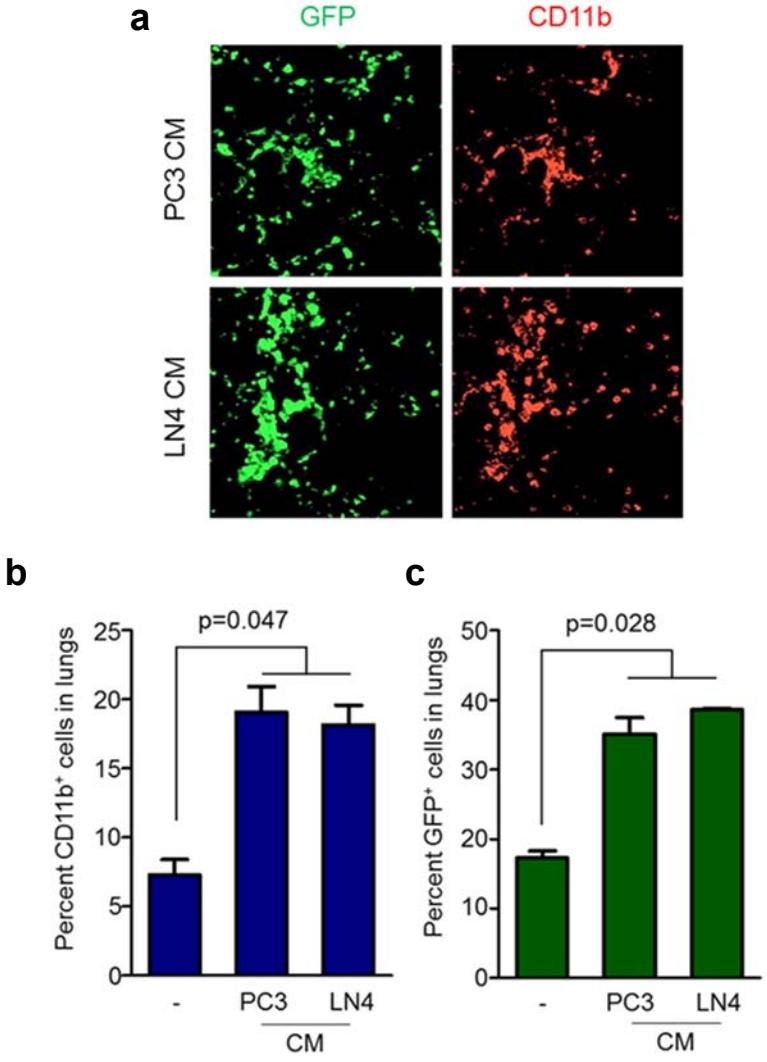

Figure 2.1. Metastasis-incompetent tumor cells generate a bone marrow-derived myeloid cell premetastatic niche in the lungs.
(a) Representative immunofluorescence images showing recruitment of GFP^+ BM-derived cells (green), and $CD11b^+$ myeloid cells (red) in the lungs of mice treated with PC3 CM compared to LN4 CM. DAPI was used to label the nuclei of cells.
(b) Flow cytometry-based quantitation of recruited BM-derived GFP^+ cells in lungs of mice treated with serum-free RPMI media (-), PC3 CM, or LN4 CM (n=3 per group). p= 0.047 (one-tailed Mann-Whitney U) between RPMI-treated and CM-treated mice.
(c) Flow cytometry-based quantitation of recruited $CD11b^+$ myeloid cells in lungs of mice treated with serum-free RPMI media (-), PC3 CM, or LN4 CM (n=3 per group). p= 0.028 (one-tailed Mann-Whitney U) between RPMI-treated and CM-treated mice.
*(Data in Figure 2.1 generated in collaboration with Dr. R. Catena. Panels **a, b, c** generated by R. Catena.)*

Figure 2.2. Metastasis-incompetent tumor cells upregulate Tsp-1 in the lung microenvironment.
(a) A portion of the heat map obtained from hierarchical clustering of gene expression profiling of lungs from mice treated with LN4 CM or PC3 CM. Gene expression data was filtered using gene ontology so that only secreted proteins were considered. Each row represents a gene that was differentially upregulated (≥ 1.5 fold) in PC3 CM-treated lungs and each column represents data from one animal. The relatively high expression is indicated in Red, while the relatively low expression is in Green. Tsp-1 is depicted by an arrow.
(b) Quantitative RT-PCR analysis of Tsp-1 expression in lungs of RPMI-, PC3 CM-, or LN4 CM-treated mice (n= 3 mice/ group).
(c) Quantitation of Tsp-1^+ cells/field in sections of lungs from LN4 CM- and PC3 CM-treated mice stained for Tsp-1, with DAPI as nuclear stain. $p<0.001$ (one-tailed t test).
(d) Representative immunofluorescence stain of Tsp-1 (white) in lungs of PC3 CM- and LN4 CM-treated mice.
For **c** and **d**, n=3 mice/ group; 2 sections per mouse, 10 fields per section.
*(Data in Figure 2.2 generated in collaboration with Dr. R. Catena. Panels **c** and **d** generated by R. Catena.)*

Figure 2.2

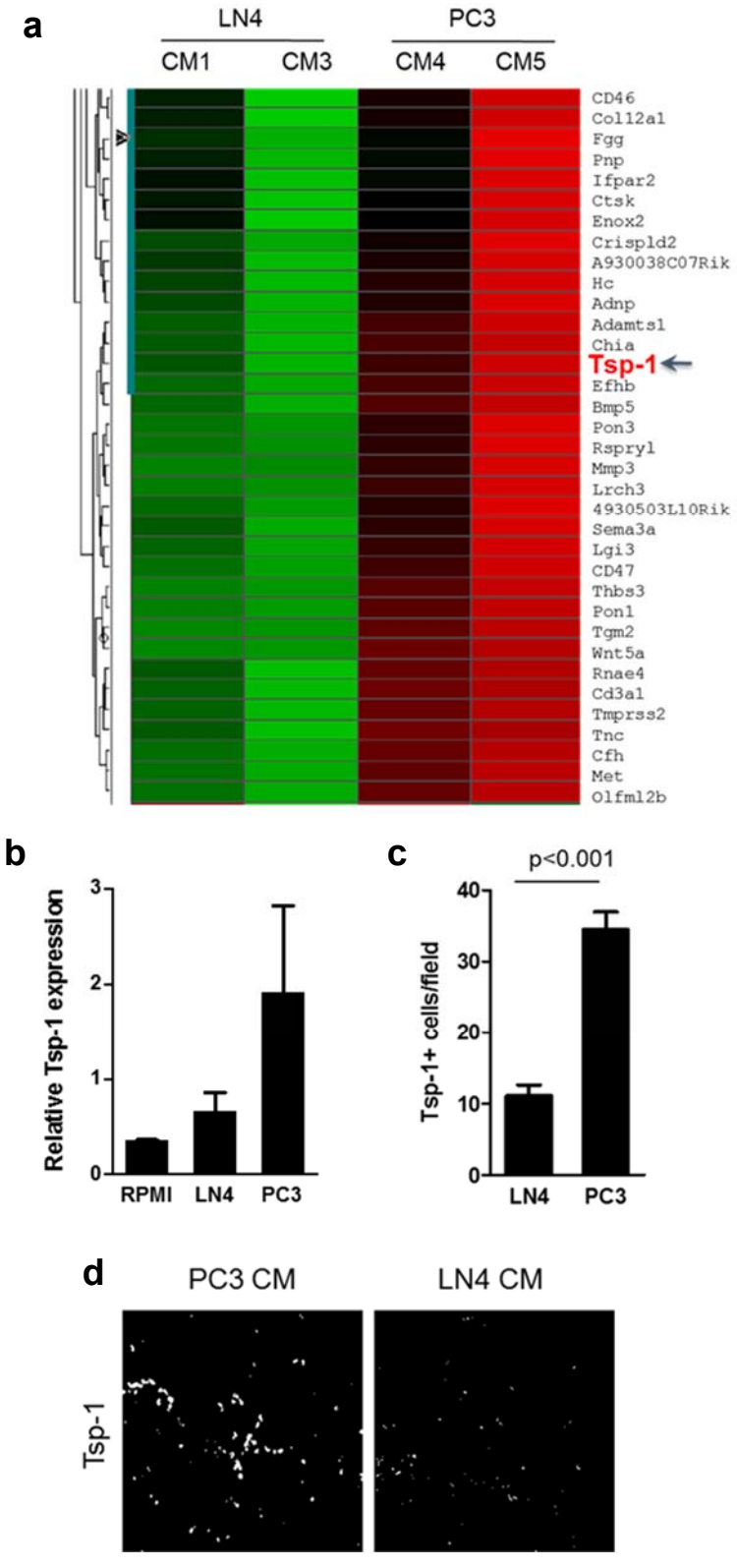
a
LN4
PC3
CM1
CM3
CM4
CM5
CD46
Col12a1
Fgg
Pnp
Ifpar2
Ctsk
Enox2
Crispld2
A930038C07Rik
Hc
Adnp
Adamtsl
Chia
Tsp-1
Efhb
Bmp5
Pon3
Rspryl
Mmp3
Lrch3
4930503L10Rik
Sema3a
Lgi3
CD47
Thbs3
Pon1
Tgm2
Wnt5a
Rnae4
Cd3a1
Tmprss2
Tnc
Cfh
Met
Olfml2b
b
Relative Tsp-1 expression
RPMI
LN4
PC3
c
p<0.001
Tsp-1+ cells/field
LN4
PC3
d
PC3 CM
LN4 CM
Tsp-1

treated lungs, both at the mRNA level by qRT-PCR, and at the protein level by immunostaining (**Figure 2.2b-d**).

2-2.3. BM-derived CD11b$^+$ Gr1$^+$ myeloid cells are the major contributors of Tsp-1.

Immunostaining for Tsp-1 revealed that Tsp-1 expression was mainly confined to the CD11b$^+$ myeloid cell population in the lungs of PC3 CM-treated mice (**Figure 2.3a**). This finding was reproduced using a different myeloid cell marker, Gr1, in a breast cancer model, where CM from the weakly metastatic MDA-MB-231 cells induced upregulation of Tsp-1 in Gr1$^+$ cells in lungs, compared to the highly metastatic MDA-LM2 cells (**Figure 2.3b**). To more accurately determine the cell population expressing Tsp-1 in the lungs, we sorted cells from mouse lungs treated with PC3 CM, and analyzed Tsp-1 expression in the sorted populations by qRT-PCR. Tsp-1 was mainly contributed by the Gr1$^+$ myeloid cell population, but not other hematopoietic populations or non-hematopoietic cells (**Figure 2.4a**). To further exclude the possibility that non-myeloid cell types express the Tsp-1 protein, we performed Western blot analysis on different cellular compartments from peripheral blood of wild type or Tsp-1$^{-/-}$ mice. Strikingly, the Gr1$^+$ cells expressed abundant levels of Tsp-1 protein compared to Gr1$^-$ cells (**Figure 2.4b**), and as expected, Tsp-1 protein was absent in all cells sorted from Tsp-1$^{-/-}$ mice. Given that the Gr1$^+$ cell population can be subdivided into Ly6G$^+$ granulocytic myeloid cells, and Ly6C^{high} myelomonocytic cells, we further analyzed Tsp-1 expression in these Gr1$^+$ subpopulations and found that both subsets expressed Tsp-1 (**Figure 2.4c**). These data suggest that BM-derived Gr1$^+$ cells are the major source of Tsp-1 in the premetastatic microenvironments generated by

Figure 2.3. Metastasis-incompetent tumor cells induce Tsp-1 in myeloid cells recruited to the lungs.
(a) Representative immunofluorescence staining of PC3 CM-treated mouse lungs depicting $CD11b^+$ myeloid cell recruitment, and Tsp-1 protein expression in the $CD11b^+$-staining cells. CD11b is in red; Tsp-1 is in magenta.
(b) Representative immunofluorescence staining depicting $Gr1^+$ myeloid cell recruitment, and Tsp-1 protein expression in the $Gr1^+$-staining cells in lungs of mice treated with CM from MDA-MB-231 or its highly metastatic derivative MDA-LM2. CM was administered daily for 6 days and then lungs were analyzed. Gr1 is in white; Tsp-1 is in red.
(c) Quantitation of Tsp-1 fluorescence intensity in lungs treated with MDA-MB-231 CM (MDA CM) and MDA-LM2 CM (LM2 CM), described above, and stained for Tsp-1. (n=3 mice per group).
*(Data in Figure 2.3 generated in collaboration with Dr. R. Catena. Panel **a** generated by R. Catena.)*

Figure 2.3

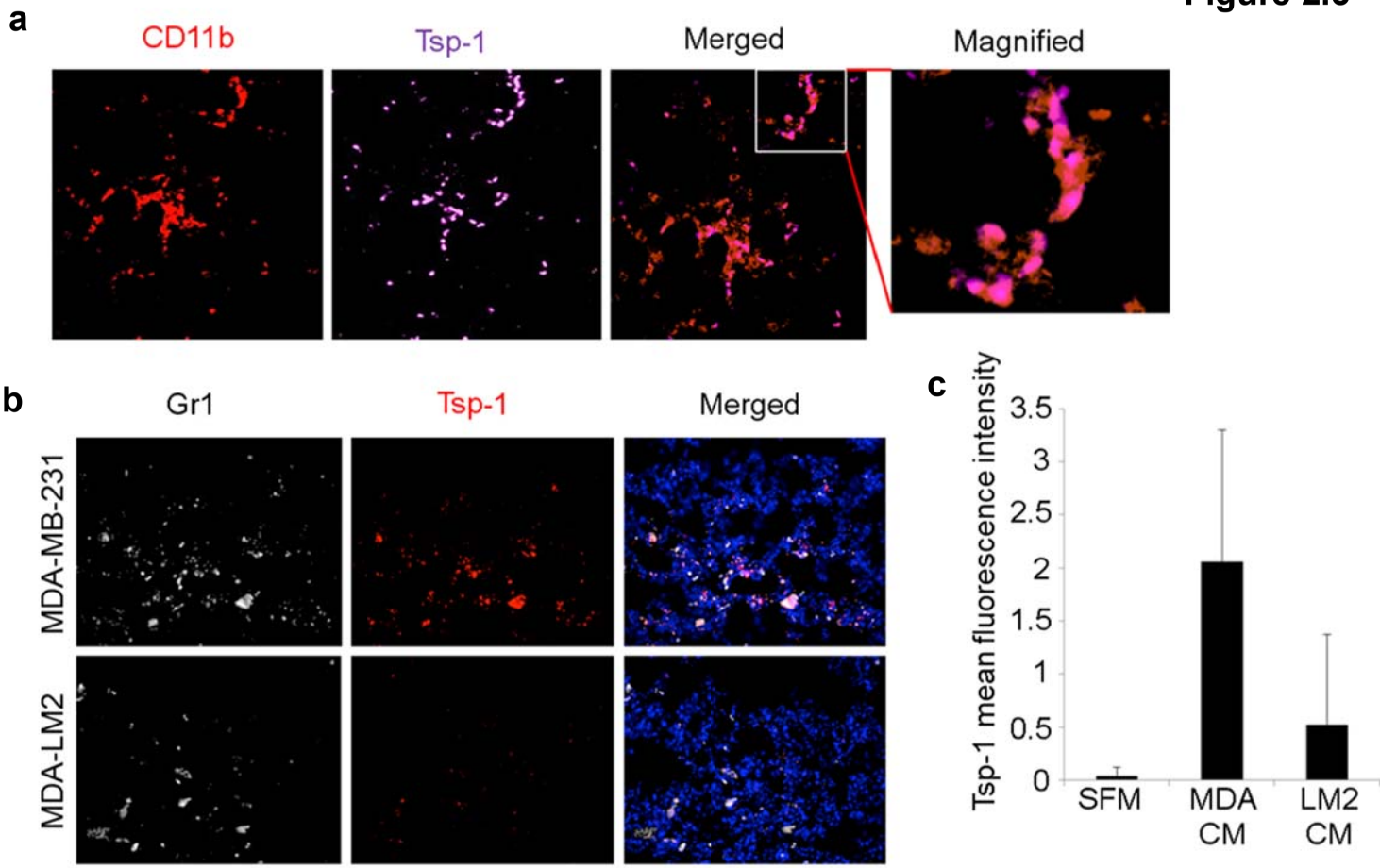
a
CD11b
Tsp-1
Merged
Magnified
b
Gr1
Tsp-1
Merged
MDA-MB-231
MDA-LM2
c
Tsp-1 mean fluorescence intensity
3.5
3
2.5
2
1.5
1
0.5
0
SFM
MDA CM
LM2 CM

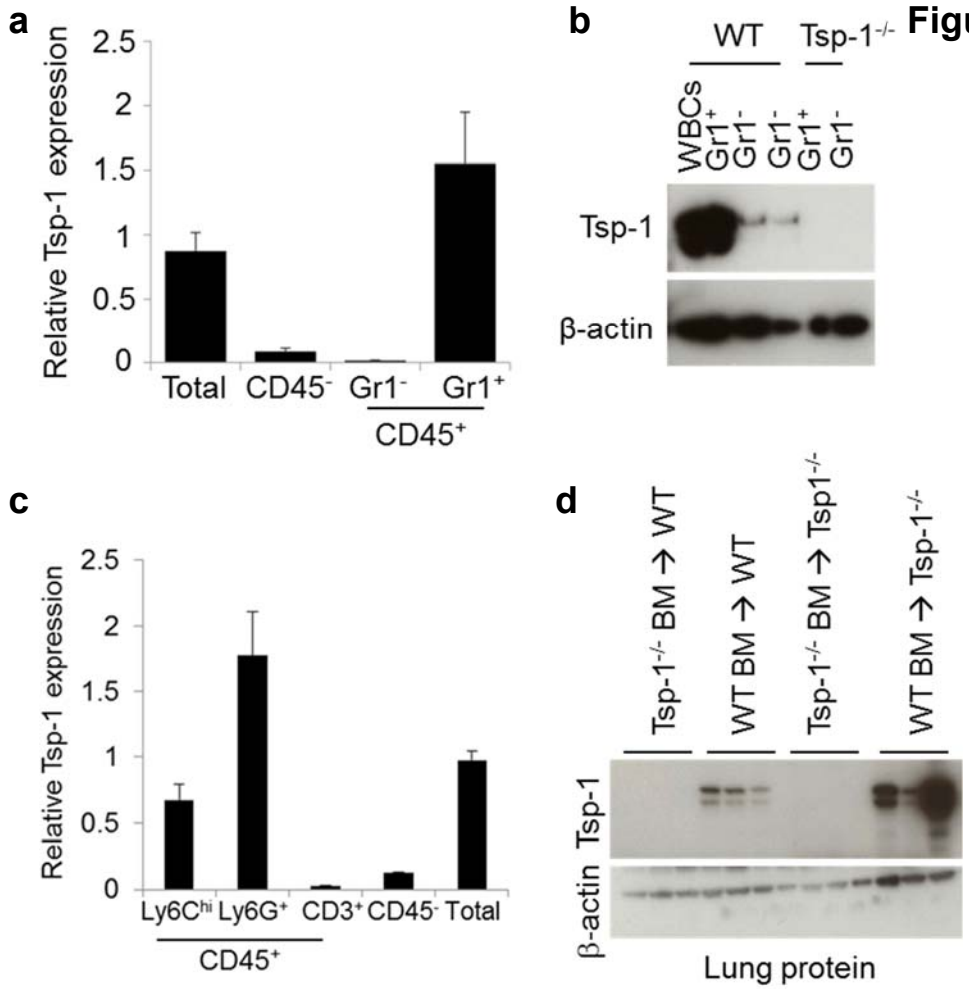

Figure 2.4

Figure 2.4. Tsp-1 is expressed by bone marrow-derived myeloid cells in the lungs.
(a) Quantitative RT-PCR analysis of Tsp-1 expression in different subsets of flow cytometry-sorted cells isolated from the lung. Of these, the $CD45^+$ $Gr1^+$ cells showed elevated Tsp-1 compared to $CD45^+$ $Gr1^-$ cells or other $CD45^-$ cells. $CD45^+$: hematopoietic cells; $CD45^-$: non-hematopoietic cells; $Gr1^+$: myeloid cells; $Gr1^-$: non-myeloid hematopoietic cells; total: all lung cells.
(b) Western blot analysis of Tsp-1 levels in cellular hematopoietic compartments in the peripheral blood from WT mice and $Tsp\text{-}1^{-/-}$ mice show $Gr1^+$ cells as a major source of Tsp-1. WBC: white blood cells.
(c) Quantitative RT-PCR analysis of Tsp-1 expression in different subsets of flow cytometry-sorted cells from the lung. Both subsets of $Gr1^+$ cells, $Ly6C^{high}$ (monocytes) cells and $Ly6G^+$ (neutrophils) cells express Tsp-1. $CD3^+$: T-cells.
(d) Western blot analysis of Tsp-1 levels in lungs of mice after BM transplantation. Transplantation of $Tsp\text{-}1^{-/-}$ BM to WT recipients ($Tsp\text{-}1^{-/-}$ BM →WT) rendered lungs devoid of Tsp-1. Conversely, transplantation of WT BM to $Tsp\text{-}1^{-/-}$ recipients (WT BM →$Tsp\text{-}1^{-/-}$) restored Tsp-1 expression in the lung. WT BM →WT: transplantation of WT BM into WT recipients. $Tsp\text{-}1^{-/-}$ BM →$Tsp\text{-}1^{-/-}$: transplantation of $Tsp\text{-}1^{-/-}$ BM into $Tsp\text{-}1^{-/-}$ recipients.
*(Data in Figure 2.4 generated in collaboration with Dr. R. Catena. Panels **b** and **d** generated by R. Catena.)*

metastasis-incompetent tumors. To highlight the BM-derived source of Tsp-1 and exclude other non-bone marrow-derived stromal cells as possible Tsp-1 sources, we performed BMT experiments and observed that Tsp-1 protein was absent in lungs of WT mice transplanted with Tsp-1$^{-/-}$ BM, but expression was restored in Tsp-1$^{-/-}$ mice transplanted with WT BM (**Figure 2.4d**). These results strongly indicate that BM-derived cells are the main source of Tsp-1 in the lungs induced by weakly metastatic tumors.

2-2.4 Genetic deletion of Tsp-1 in the bone marrow results in increased metastasis.

We hypothesized that upregulation of Tsp-1 by Gr1^{+} cells in the lungs could generate a metastasis-refractory microenvironment. To assess this possibility, we generated Tsp-1$^{-/-}$ BMT mice, i.e. irradiated WT mice that are transplanted with Tsp-1$^{-/-}$ BM, and determined their ability to form metastases compared to WT BMT controls, i.e. irradiated WT mice receiving WT BM. As expected, after BM engraftment, Tsp-1$^{-/-}$ BMT mice lack Tsp-1 protein and mRNA in peripheral blood leukocytes (**Figure 2.5a, b**). More importantly, when we evaluated the ability of luciferase-labeled Lewis lung carcinoma (LLC) cells to colonize the lung after tail vein injection, we observed accelerated metastatic outgrowth in Tsp-1$^{-/-}$ BMT mice compared to WT BMT mice by bioluminescence imaging (BLI) (**Figure 2.5c**). Western blot analysis of whole lung lysates revealed the complete absence of Tsp-1 protein in the lungs of Tsp-1$^{-/-}$ BMT mice (**Figure 2.5d**), despite the fact that Gr1^{+} cell recruitment to the lungs is unaltered (**Figure 2.5e**), reiterating that BMDCs are the major source of Tsp-1 in lungs in this metastatic setting.

Figure 2.5. BM-derived Gr1$^+$ cells confer a metastasis-suppressive phenotype through the secretion of Tsp-1.
(a) Western blot analysis for Tsp-1 expression in peripheral blood from WT mice transplanted with WT BM (WT → WT), and WT mice transplanted with Tsp-1$^{-/-}$ BM (Tsp-1$^{-/-}$ → WT).
(b) Quantitative RT-PCR showing Tsp-1 expression levels in sorted Gr1$^+$ cells from the peripheral blood of Tsp-1$^{-/-}$, Tsp-1$^{-/-}$ BMT, and WT BMT mice. Tsp-1 expression was normalized to the internal control (GAPDH). RNA samples were pooled from 3 mice per group.
(c) Left panel, Quantitation of pulmonary metastases in WT BMT mice and Tsp-1$^{-/-}$ BMT mice (n=7 per group). BLI estimates were obtained at days 0, 5, 8, 11, 14, 19 following tail vein injections of 1x10^5 LLC cells. p=0.0013 between WT BMT and Tsp-1$^{-/-}$ BMT groups at day 19. Right panel, Representative BLI images showing metastasis suppression in WT BMT mice compared to Tsp-1$^{-/-}$ BMT mice at day 19.
(d) Western blot analysis of Tsp-1 from the lungs of WT BMT mice and Tsp-1$^{-/-}$ BMT mice. Lung sample from Tsp-1$^{-/-}$ transgenic mice was used as a control.
(e) Left panel, Representative immunofluorescence staining of Gr1$^+$ myeloid cells (white) recruited to WT BMT and Tsp-1$^{-/-}$ BMT mouse lungs. Right panel, Quantitation of recruited Gr1$^+$ myeloid cells in lungs based on immunofluorescence, depicting comparable recruitment of Gr1$^+$ cells to WT BMT and Tsp-1$^{-/-}$ BMT lungs. (n=4 mice per group).
(Data in Figure 2.5 generated in collaboration with Dr. R. Catena.)

Figure 2.5

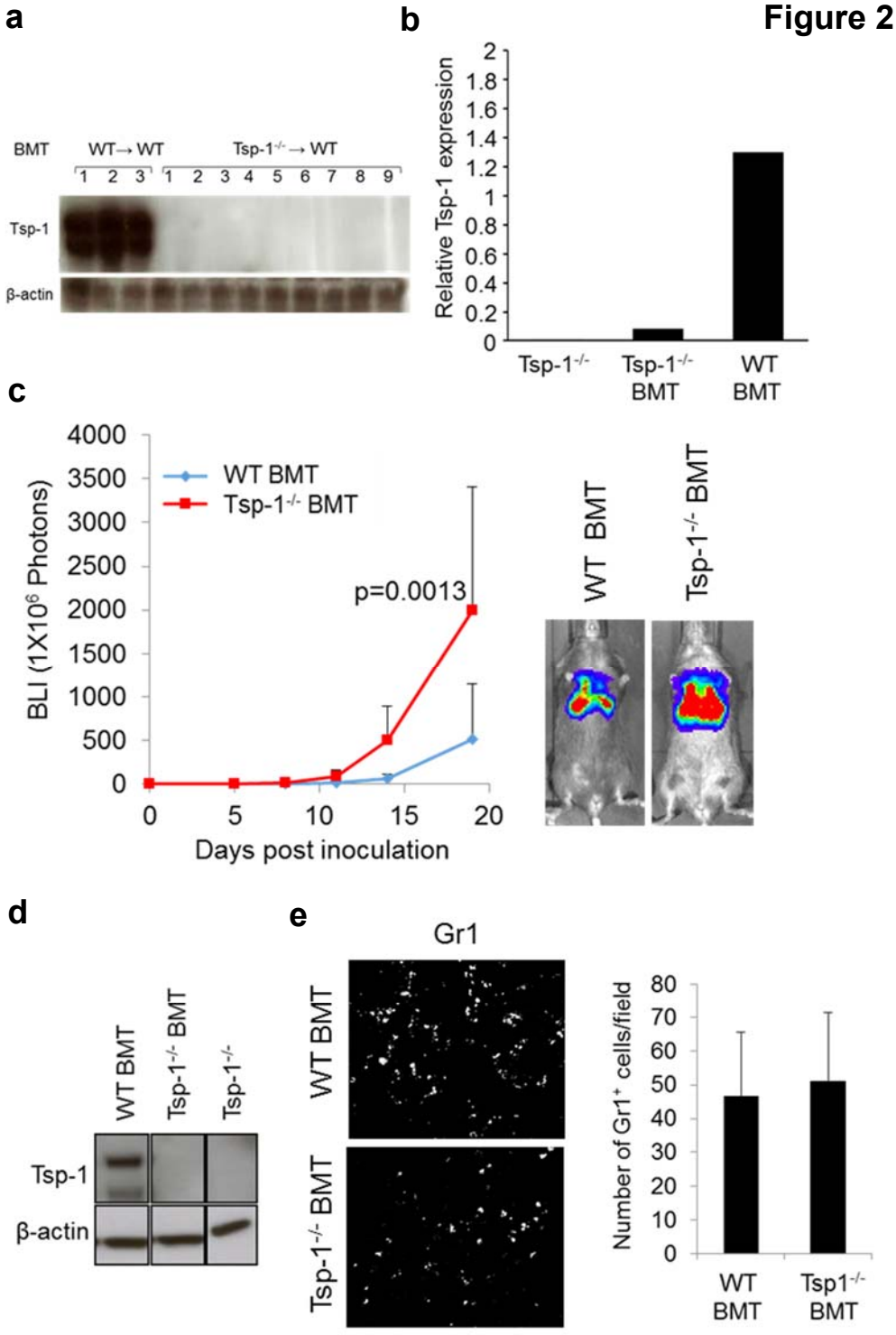
a
BMT
WT→ WT
Tsp-1-/- → WT
1 2 3 1 2 3 4 5 6 7 8 9
Tsp-1
β-actin
b
Relative Tsp-1 expression
2
1.8
1.6
1.4
1.2
1
0.8
0.6
0.4
0.2
0
Tsp-1-/-
Tsp-1-/- BMT
WT BMT
c
BLI (1X10^6 Photons)
4000
3500
3000
2500
2000
1500
1000
500
0
WT BMT
Tsp-1-/- BMT
p=0.0013
0
5
10
15
20
Days post inoculation
WT BMT
Tsp-1-/- BMT
d
WT BMT
Tsp-1-/- BMT
Tsp-1-/-
Tsp-1
β-actin
e
Gr1
WT BMT
Tsp-1-/- BMT
Number of Gr1+ cells/field
80
70
60
50
40
30
20
10
0
WT BMT
Tsp1-/- BMT

To provide further evidence that BM-derived Tsp-1 plays an anti-metastatic role, we performed the reverse BMT experiments, where we transplanted WT BM into irradiated Tsp-1$^{-/-}$ recipients, or Tsp-1$^{-/-}$ BM into irradiated Tsp-1$^{-/-}$ mice as controls. Reintroducing WT BM into Tsp-1$^{-/-}$ recipients significantly suppressed metastasis (**Figure 2.6a**), and was accompanied by an increase in the expression of Tsp-1 in the lungs of these mice (**Figure 2.4d**), with restored Tsp-1 expression in their recruited Gr1^{+} cells (**Figure 2.6b**). These results reinforce the hypothesis that induction of Tsp-1 expression in Gr1^{+} cells can inhibit metastasis, and they suggest that intervening therapeutically to upregulate Tsp-1 in the lung myeloid cells could be a viable approach for the treatment of metastatic cancer.

2-2.5. BM-derived Tsp-1 inhibits metastatic outgrowth through inhibition of tumor cell proliferation.

Tsp-1 exerts its anti-tumorigenic activity via diverse mechanisms, including inhibition of angiogenesis, suppression of cell proliferation, and induction of apoptosis in both tumor and endothelial cells (Lawler and Lawler, 2012). Tsp-1$^{-/-}$ BMT mouse lungs exhibited increased tumor cell proliferation compared to WT BMT lungs, as determined by Ki67 staining (**Figure 2.7a**), while the tumor cell apoptotic index, measured by active caspase-3 staining, was unchanged (**Figure 2.7b**). Angiogenesis was also unaffected in this model (**Figure 2.7c**), and the lack of Tsp-1 in the lung BM cells did not alter the ability of tumor cells to seed the lungs (**Figure 2.7d**). Hence, induction of Tsp-1 in recruited Gr1^{+} cells suppresses metastasis by blocking the outgrowth of seeded tumor cells.

Figure 2.6

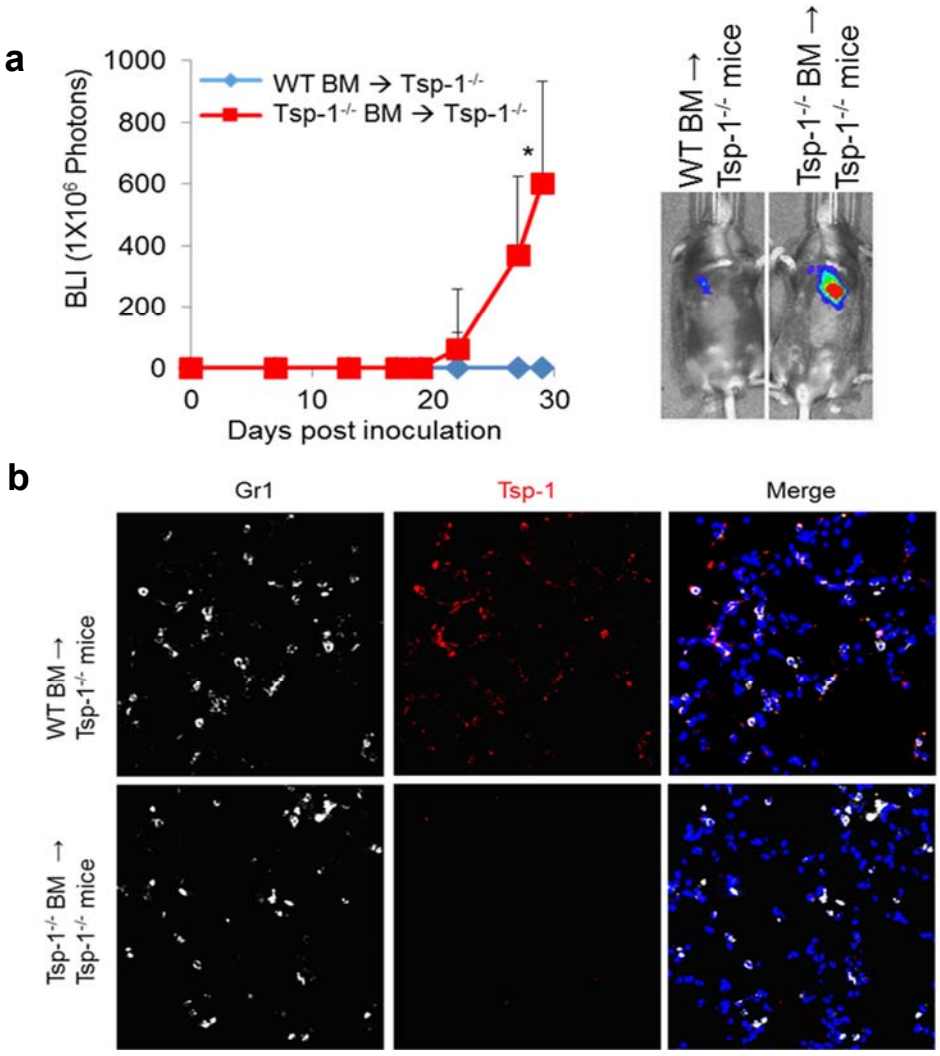

Figure 2.6. Restoring Tsp-1 in BM suppresses metastasis.
(a) Left panel, Quantitation of pulmonary metastases in Tsp-1$^{-/-}$ mice transplanted with WT BM and Tsp-1$^{-/-}$ mice transplanted with Tsp-1$^{-/-}$ BM (n=5 per group). BLI estimates were obtained following tail vein injections of 1x10^5 LLC cells. p=0.033 between the two group at day 30. Right panel, Representative bioluminescence images showing metastasis suppression in Tsp-1$^{-/-}$ mice transplanted with WT BM compared to Tsp-1$^{-/-}$ mice transplanted with Tsp-1$^{-/-}$ BM.
(b) Representative immunofluorescence stains of recruited Gr1$^+$ myeloid cells (white) and Tsp-1 (red) in WT BM → Tsp-1$^{-/-}$ and Tsp-1$^{-/-}$ BM→ Tsp-1$^{-/-}$ lungs. DAPI stains nuclei.
*(Data in Figure 2.6 generated in collaboration with Dr. R. Catena. Panel **a** generated by R. Catena.)*

Figure 2.7. Tsp-1 suppresses tumor cell proliferation in the lungs.
(a) Left panel, Representative Ki67 (magenta) immunofluorescence staining in lungs of WT BMT and Tsp-1$^{-/-}$ BMT mice. DAPI is used as a nuclear stain. Right panel, Quantitation of Ki67 staining in lungs of WT BMT and Tsp-1$^{-/-}$ BMT mice. (n=6 mice/ group). p= 0.003 (one-tailed t test).
(b) Left panel, Representative active caspase-3 (magenta) immunofluorescence staining in lungs of WT BMT and Tsp-1$^{-/-}$ BMT mice. DAPI is used as a nuclear stain. Right panel, Quantitation of active caspase-3 staining in lungs of WT BMT and Tsp-1$^{-/-}$ BMT mice. (n=6 mice/ group). p= 0.09 (one-tailed t test).
(c) Left panel, Representative immunofluorescence images showing vessel density in the metastases of WT BMT mice and Tsp1$^{-/-}$ BMT mice. Endothelial cells are CD31^{+} (green). DAPI was used to stain nuclei. Right panel, Quantitation of vessels performed by evaluating sections from 6 mice per group (p=0.1249, two-tailed t test).
(d) Left panel, Flow cytometric analysis of tumor cell seeding in WT BMT and Tsp1$^{-/-}$ BMT lungs 48 hrs following tail vein injection of mCherry-labeled LLC cells. Right panel, Flow cytometry-based quantitation of mCherry^{+} cells in lungs. (n= 4 mice per group). p=0.548 (two-tailed t-test).
*(Data in Figure 2.7 generated in collaboration with Dr. R. Catena. Panels **a ,b, d** generated by R. Catena.)*

Figure 2.7

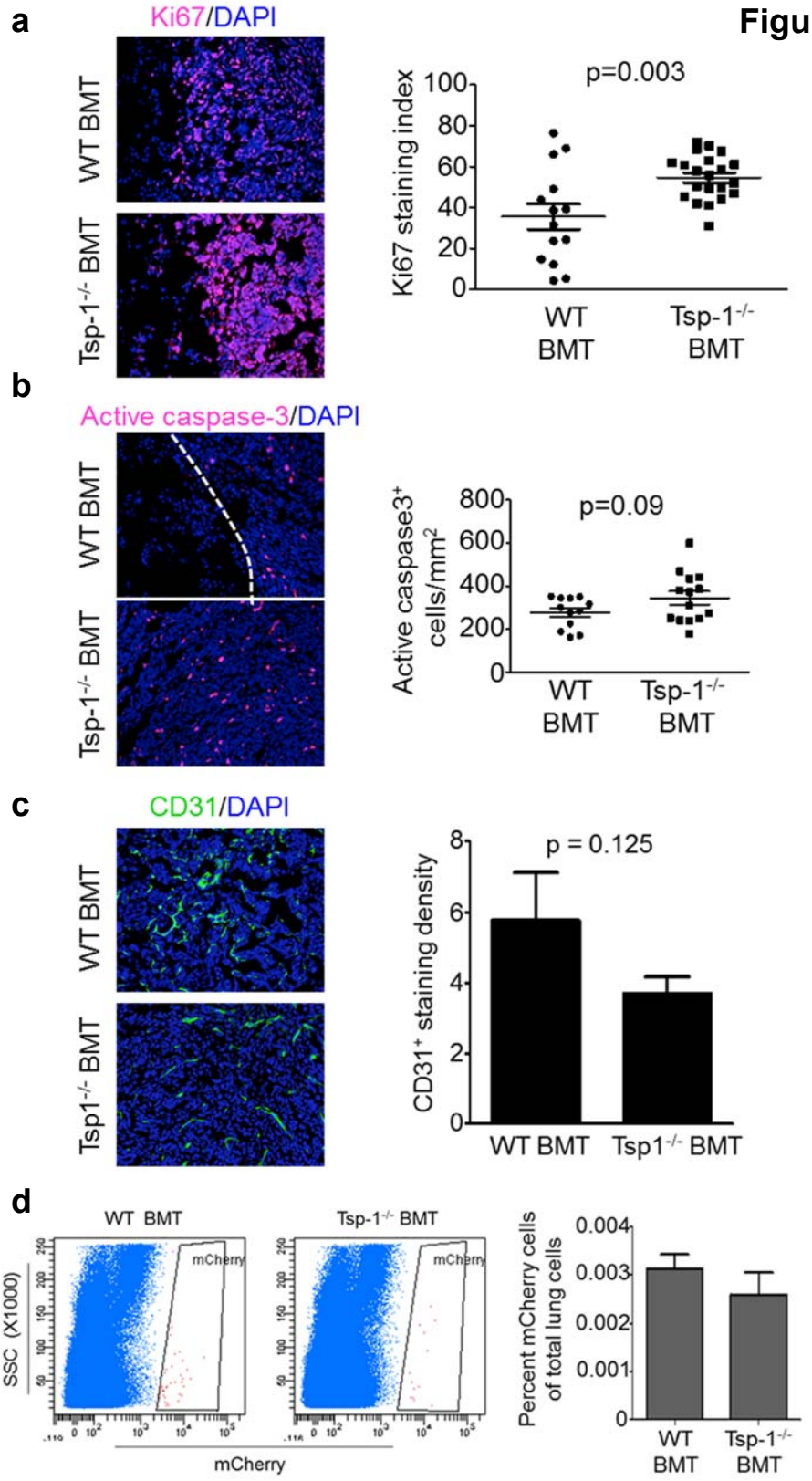
a
Ki67/DAPI
WT BMT
Tsp-1-/- BMT
p=0.003
Ki67 staining index
100
80
60
40
20
0
WT BMT
Tsp-1-/- BMT
b
Active caspase-3/DAPI
WT BMT
Tsp-1-/- BMT
p=0.09
Active caspase3+ cells/mm2
800
600
400
200
0
WT BMT
Tsp-1-/- BMT
c
CD31/DAPI
WT BMT
Tsp1-/- BMT
p = 0.125
CD31+ staining density
8
6
4
2
0
WT BMT
Tsp1-/- BMT
d
WT BMT
Tsp-1-/- BMT
mCherry
SSC (X1000)
mCherry
Percent mCherry cells of total lung cells
0.004
0.003
0.002
0.001
0
WT BMT
Tsp-1-/- BMT

2-2.6. Tumor cell-derived prosaposin systemically stimulates Tsp-1 expression in the lung microenvironment.

Based on our data, we speculated that the induction of Tsp-1 expression in the lung microenvironment could act as an anti-metastatic therapeutic approach. Previous studies have shown the antiangiogenic activity of ABT-510, a nonapeptide derived from Tsp-1 (Haviv et al., 2005); however, clinical trials have thus far not been able to prove its efficacy (Baker et al., 2008; Ebbinghaus et al., 2007; Markovic et al., 2007). This is why we believed that it would be necessary to induce full-length Tsp-1 *in vivo* to preserve all its inhibitory activity. To this end, we turned our focus to prosaposin (psap), a precursor of sphingolipid activator proteins, which was previously shown to stimulate the expression of Tsp-1 in human lung fibroblasts *in vitro* (Kang et al., 2009).

To determine whether psap can induce Tsp-1 expression in recruited $Gr1^+$ cells in mouse lungs, we utilized CM from MDA-MB-231 known to contain psap (Kang et al., 2009), and CM from MDA-MB-231 cells expressing psap-shRNA. While MDA CM treatment stimulated Tsp-1 expression in lung $Gr1^+$ cells, CM from MDA cell expressing psap-shRNA failed to induce Tsp-1 (**Figure 2.8a, b**). Furthermore, orthotopically-injected LN4 cells overexpressing psap (LN4-psap) induced robust expression of Tsp-1 in premetastatic lungs compared to LN4 tumors, which are known not to secrete high levels of psap in their CM (Kang et al., 2009) (**Figure 2.8c**). These data suggest that psap secreted by tumor cells can systemically stimulate the expression of Tsp-1 in recruited $Gr1^+$ myeloid cells in lungs.

Figure 2.8

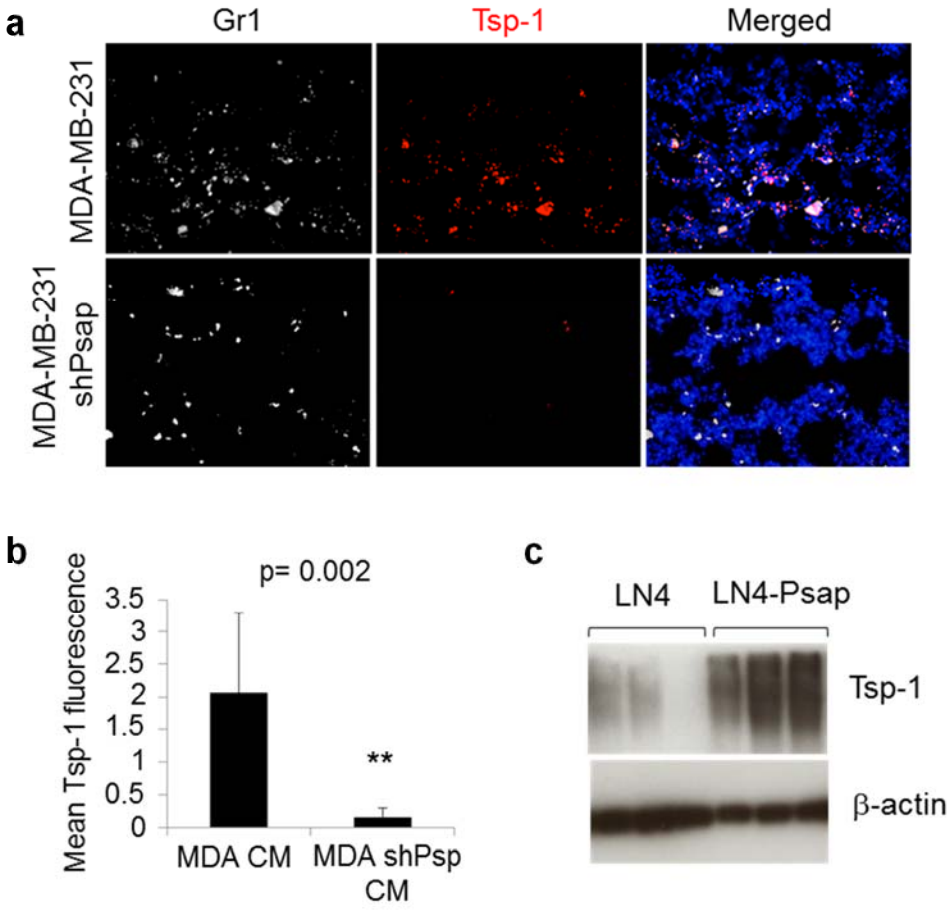

Figure 2.8. Psap in tumor CM induces Tsp-1 expression in lungs.
(a) Representative immunofluorescence staining of $Gr1^+$ cells (white) and Tsp-1 (red) in lungs of WT mice treated with MDA-MB-231 CM or CM from MDA-MB-231 expressing psap-shRNA (MDA-MB-231 shPsap). DAPI is used as a nuclear stain.
(b) Quantitation of Tsp-1 expression in stained sections from **a**. (n=3 mice/ group, 2 sections per mouse lung, 10 fields per section). Data presented as Mean ± SD. **, p= 0.002 (one-tailed t test).
(c) Western blot analysis of Tsp-1 in lungs of mice bearing LN4 or psap-overexpressing LN4 (LN4-Psap) cells orthotopically injected in the prostate gland (n=3 mice per group). β-actin is a loading control. (Tsp-1 band runs as a smudge because the protein was extracted from formaldehyde-fixed samples, after reverse-crosslinking using the Qiagen Qproteome FFPE Tissue Kit).
*(Data in Figure 2.8 generated in collaboration with Dr. R. Catena. Panel **c** generated by R. Catena.)*

2-2.7. The psap-derived pentapeptide DWLPK retains full Tsp-1-inducing activity.

To verify if psap activity could be converted into a smaller agent more amenable to therapeutic systemic delivery, we set out to pinpoint the minimum region of psap capable of stimulating Tsp-1 expression in fibroblasts *in vitro*. We generated truncation mutants of psap, containing either the saposin A domain, saposin AB, saposin ABC, or saposin BCD, and expressed them in LN4 cells. CM from these cells was tested for its Tsp-1-inducing activity on WI-38 human fibroblasts *in vitro*, and it was clear that all truncation mutants that contained the saposin A domain induced Tsp-1 expression (**Figure 2.9a**). Thus, saposin A contains the Tsp-1-stimulating activity of psap. To determine shorter regions within saposin A that harbor Tsp-1-stimulating activity, we generated 20-amino acid overlapping peptides spanning the sequence of saposin A (**Figure 2.9b)**, and observed that only the peptide spanning residues 31-50 of saposin A could induce Tsp-1 expression (**Figure 2.9c**). Based on the crystal structure of saposin A, the peptide lies in the hairpin region between helices 2 and 3 (Ahn et al., 2006). Hence, we tested a 13-amino acid cyclic peptide corresponding to residues 35-47, constrained by a disulfide bond at each end of the peptide. The cyclic peptide stimulated Tsp-1 (**Figure 2.9d**). We then tested a 6-amino acid peptide, CDWLPK, corresponding to the first six residues of the cyclic peptide and found that it also was able to stimulate Tsp-1 (**Figure 2.9f**). Finally, we tested six peptides from within the 6-amino acid sequence of CDWLPK and found that both a 5-amino acid peptide (DWLPK) and a 4-amino acid peptide (DWLP) were able to stimulate Tsp-1 expression to an even greater extent than CDWLPK (**Figure 2.9f**). Finally, we assessed the 5-amino acid peptide *in vivo* by administering it

Figure 2.9. Deriving a peptide that retains the Tsp-1-inducing activity of Psap.
(a) Schematic of Psap and its 4 saposin domains.
(b) Western blot analysis of Tsp-1 induction in WI-38 human fibroblasts treated with CM from control LN4 cells (-), LN4 cells expressing an empty pLNCX vector (V), or LN4 expressing saposin domains A, AB, ABC, or BCD.
(c) Amino acid sequence of human saposin A. The stem and hairpin regions are depicted above the sequence. The six conserved cysteines are in green. The boxed region represents the 20-amino acid peptide spanning residues 31-50 of saposin A, capable of stimulating the expression of Tsp-1.
(d) Western blot analysis of Tsp-1 expression in fibroblasts cultured with 7 overlapping 20-amino acid peptides (1-20, 10-30, 21-40, 31-50, 41-60, 51-70 and 61-81) spanning the length of saposin A.
(e) Western blot analysis of Tsp-1 in WI-38 fibroblasts which were untreated (-) or treated with a cyclic 13-amino acid peptide corresponding to residues 35-47 of saposin A.
(f) Western blot analysis of Tsp-1 expression in WI-38 fibroblasts which were untreated (-) or treated with peptides derived from amino acids 35-40 of saposin A ranging from 3-6 amino acids in length (1=CDWLPK, 2=CDWLP, 3=DWLPK, 4=DWLP, 5=CDW, 6=DWL).
(g) Western blot showing Tsp-1 levels in mouse lung tissue following administration of media alone (-), LN4 CM (CM), or LN4 CM with 30 mg/kg/day psap peptide (DWLPK) for 6 days.
(Data in Figure 2.9 was generated in the lab of Dr. Randolph Watnick at Children's Hospital in Boston).

Figure 2.9

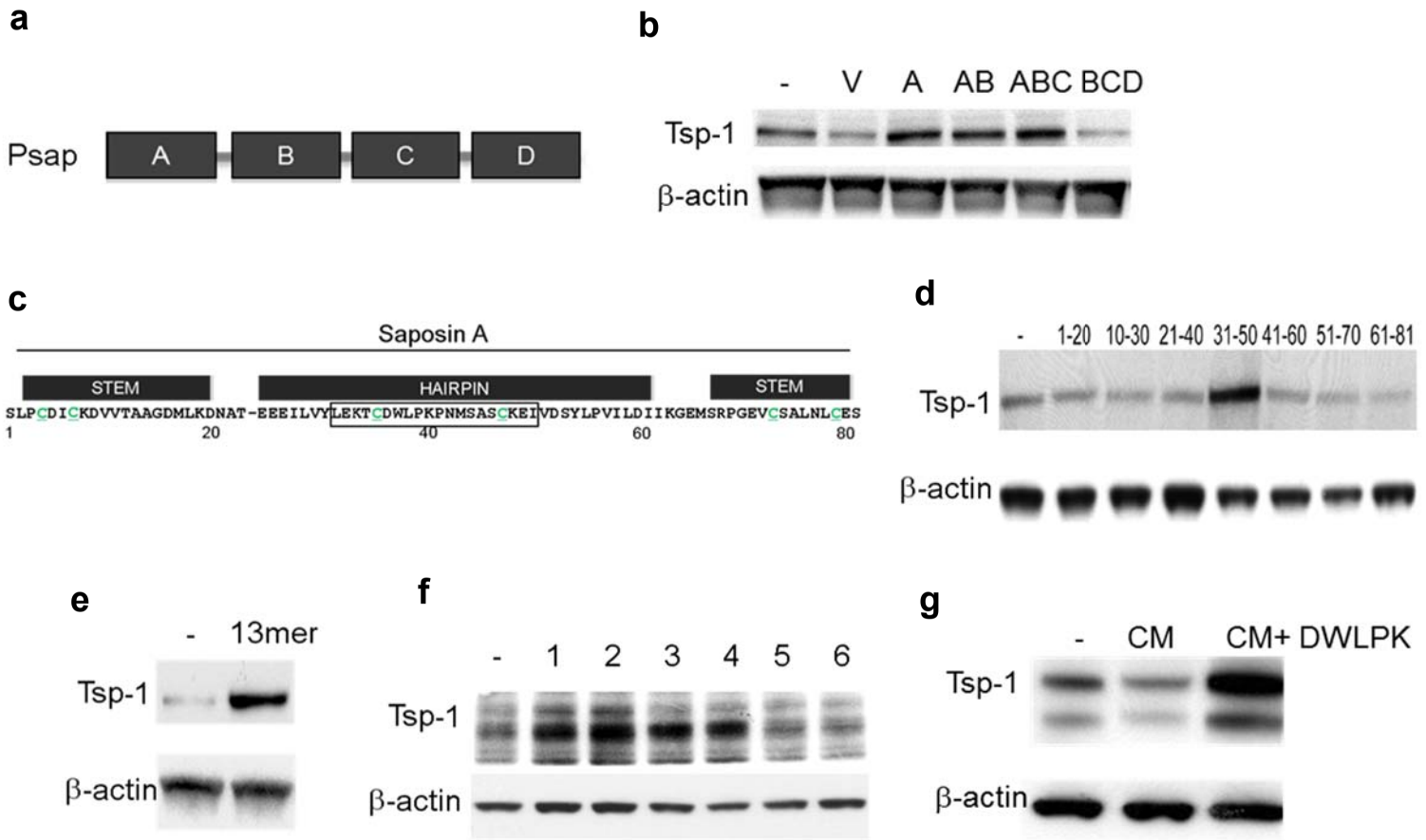
a
Psap
A
B
C
D
b
-
V
A
AB
ABC
BCD
Tsp-1
β-actin
c
Saposin A
STEM
HAIRPIN
STEM
SLPCDICKDVVTAAGDMLKDNAT-EEEILVYLEKTCDWLPKPNMSASCKEIVDSYLPVILDIIKGEMSRPGEVCSALNLCES
1
20
40
60
80
d
-
1-20
10-30
21-40
31-50
41-60
51-70
61-81
Tsp-1
β-actin
e
-
13mer
Tsp-1
β-actin
f
-
1
2
3
4
5
6
Tsp-1
β-actin
g
-
CM
CM+ DWLPK
Tsp-1
β-actin

to mice in combination with LN4 CM and observed that it was able to stimulate Tsp-1 in the lungs of these mice (**Figure 2.9g**).

2-2.8. DWLPK stimulates Tsp-1 expression in lung $Gr1^+$ cells.

After demonstrating that DWLPK retains Tsp-1-inducing activity of full-length psap *in vitro* and *in vivo*, we evaluated if it could equally influence $Gr1^+$ cells in the lungs. To do that, we treated mice with LN4 CM to stimulate BMDC recruitment to the lungs, either alone or in combination with the DWLPK peptide (30 mg/kg). Treatments were administered daily via the intraperitoneal route, for 6 days. As expected, $Gr1^+$ cell recruitment was comparable in both cases (**Figure 2.10a, b**); however, DWLPK induced significant expression of Tsp-1 in the recruited $Gr1^+$ cells, as opposed to a peptide composed of the same amino acids in the scrambled sequence LPKDW (scrambled peptide) (**Figure 2.10a, c**). These results suggest that DWLPK peptide, by virtue of stimulating Tsp-1 in recruited $Gr1^+$ cells in lungs, could generate a metastasis-suppressive microenvironment.

2-2.9. DWLPK inhibits metastasis through stimulation of Tsp-1 in $Gr1^+$ cells.

To evaluate if DWLPK-mediated Tsp-1 induction in lung $Gr1^+$ myeloid cells can confer metastasis resistance, we introduced luciferase-labeled LLC cells via the tail vein into mice treated with either DWLPK peptide or scrambled control. Strikingly, treatment with DWLPK peptide dramatically reduced lung metastasis compared to the scrambled peptide, as measured by bioluminescence imaging (**Figure 2.11a**). Consistent with our previous observations, qRT-PCR analysis of different cell populations sorted from lungs

Figure 2.10

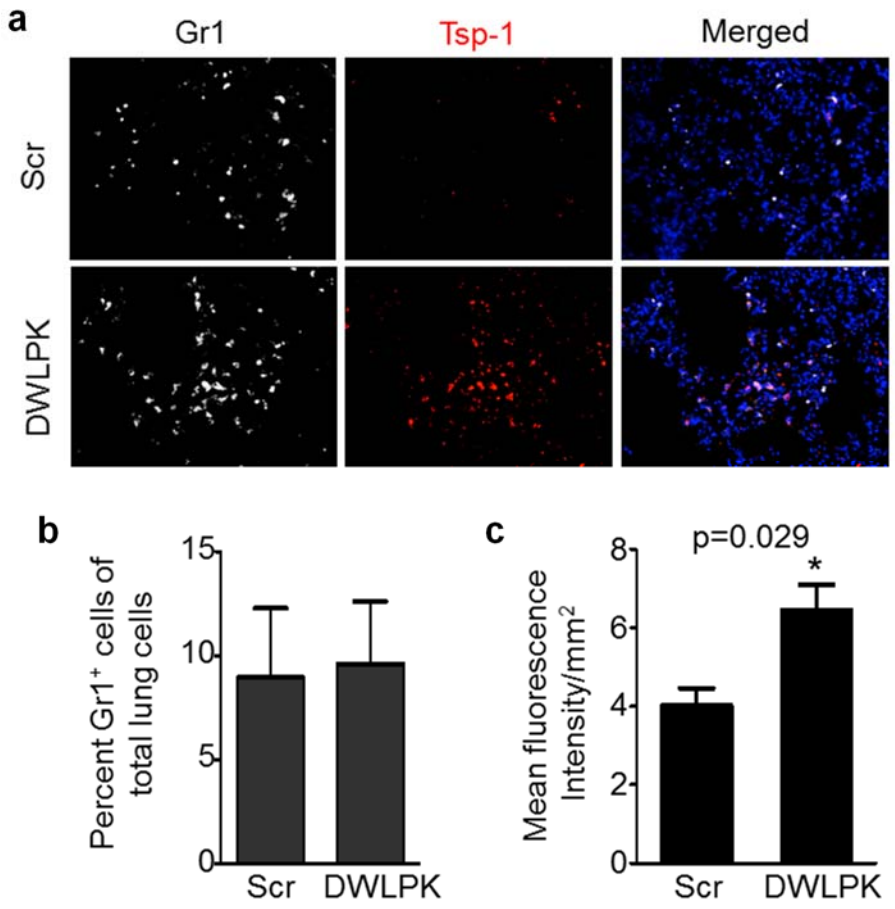

Figure 2.10. Psap-derived DWLPK peptide induces Tsp-1 in Gr1$^+$ myeloid cells recruited to the lungs.
(a) Representative immunofluorescence staining of Gr1$^+$ myeloid cells (white) and Tsp-1 (red) in lungs of mice treated intraperitoneally with LN4 CM in combination with the scrambled-sequence peptide LPKDW (scr) or LN4 CM with the Psap-derived peptide DWLPK for 6 days.
(b) Flow cytometry-based quantitation of Gr1$^+$ cells in lungs of mice from the cohorts in **a**. (n= 3 mice/ group).
(c) Immunofluorescence-based quantitation of Tsp-1 expression in stained lung sections from Scr-treated or DWLPK-treated mice. (n= 3 mice /group, 4 sections/ mouse, 7-12 fields/ section). *, p=0.029 (one-tailed t-test).
Mice were treated for 6 days with daily intraperitoneal injections of 30 mg/kg peptide + LN4 CM.
(Data in Figure 2.10 generated in collaboration with Dr. R. Catena).

Figure 2.11

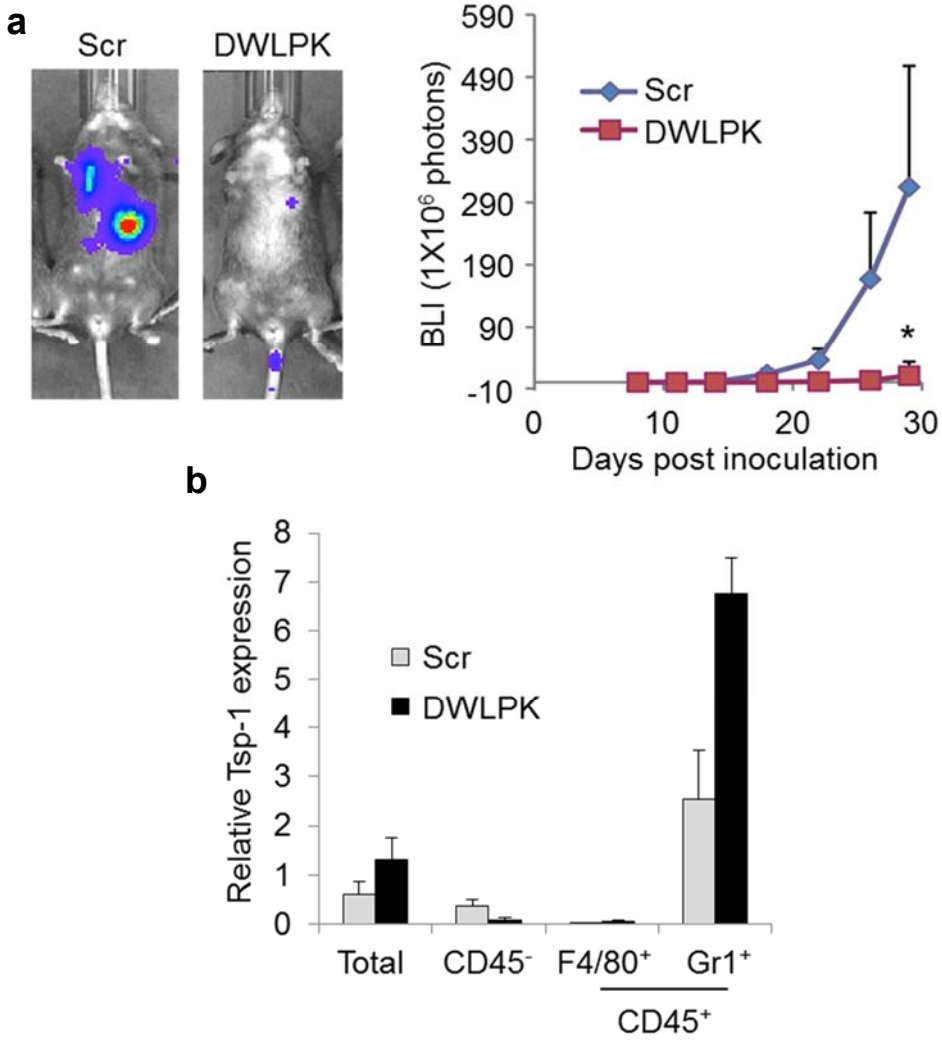

Figure 2.11. DWLPK suppresses metastasis and induces Tsp-1 in Gr1$^+$ myeloid cells recruited to the lungs.
(a) Left Panel, Representative bioluminescence images showing pulmonary metastases, at day 29-post tumor inoculation, of WT mice treated with scrambled peptide (Scr) or DWLPK, and tail vein-injected with luciferase-labeled LLCs. Right panel, Quantitation of pulmonary metastases. BLI measurements were obtained at days 7, 11, 14, 18, 22, 26, and 29 after inoculation of LLC cells. The relative BLI values show total photon count over time. (n=5 per group). *, p=0.032 between Scr and DWLPK peptide-treated groups at day 29. Identical results were obtained in repeat experiments.
(b) Quantitative RT-PCR of Tsp-1 expression in cells sorted from lungs of Scr or DWLPK-treated mice. Total: total lung cells; CD45$^-$: non-hematopoietic cells; CD45$^+$: hematopoietic cells; F4/80$^+$: macrophages; Gr1$^+$: myeloid cells.
(Data in Figure 2.11 generated in collaboration with Dr. R. Catena).

revealed that Tsp-1 induction in response to DWLPK treatment was confined to $Gr1^+$ myeloid cells and not $Gr1^-$ cells (**Figure 2.11b**).

To confirm that the DWLPK-induced Tsp-1 expression in the BM compartment was responsible for the metastasis-suppressive phenotype observed, we generated Tsp-1 deletion in the bone marrow by transplanting $Tsp\text{-}1^{-/-}$ BM into WT mice, and used WT BMT mice as controls. Then both groups were treated with DWLPK and challenged with luciferase-labeled LLC cells via the tail vein. Notably, DWLPK treatment failed to suppress metastasis in $Tsp\text{-}1^{-/-}$ BMT mice, while it efficiently suppressed metastasis in WT BMT mice (**Figure 2.12**). Taken together, these data indicate that DWLPK peptide could have a therapeutic application for treating metastatic cancer via Tsp-1 induction in myeloid cells recruited to the lung microenvironment.

2-2.10. Mechanism of psap-mediated Tsp-1 induction in $Gr1^+$ cells

Having established that psap and the psap-derived peptide DWLPK can induce Tsp-1 in $Gr1^+$ myeloid cells in the lung microenvironment, we sought to determine the receptor via which psap signals in this context.

The most commonly cited prosaposin receptor is the low density lipoprotein receptor-related protein 1 (LRP1). It is an endocytic receptor known to internalize secreted full-length psap, delivering it to the lysosome, where psap is processed into the individual saposins (Hiesberger et al., 1998). Despite the fact that no cytosolic signaling has been reported as a consequence of psap binding the LRP1 receptor, save the activation of the endocytic pathway, several reports have described signaling downstream of LRP1 in other contexts (Lillis et al., 2008).

Figure 2.12

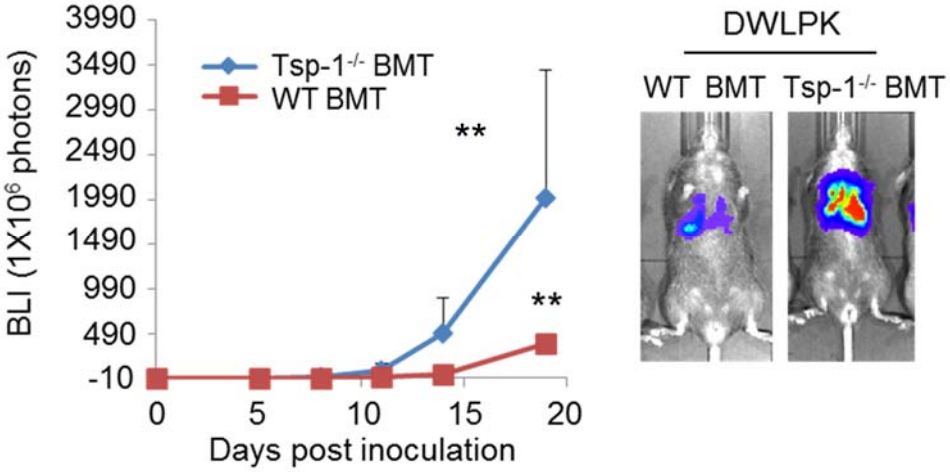

Figure 2.12. Metastasis suppression by DWLPK requires bone marrow-derived Tsp-1. Left Panel, Quantitation of pulmonary metastases in DWLPK peptide-treated WT BMT mice and Tsp-$1^{-/-}$ BMT mice (n=7 per group). BLI measurements were obtained at days 0, 5, 8, 14, and 19 following tail vein injections of $1x10^5$ LLC cells. p-values between WT BMT and Tsp-$1^{-/-}$ BMT groups are p=0.0049 and p=0.0084 at days 14 and 19, respectively (one-tailed t-test). Right panel, Representative bioluminescence images showing pulmonary metastases, at day 19 post-tumor inoculation, of DWLPK peptide-treated WT BMT mice and Tsp-$1^{-/-}$ BMT mice tail vein-injected with luciferase-labeled LLCs.
(Data in Figure 2.12 generated in collaboration with Dr. R. Catena).

To evaluate the role of LRP1 in our model, we first deleted LRP1 in the myeloid cell compartment by making use of two transgenic mouse lines: the $LRP1^{flox/flox}$ mouse line, which has exons 1 and 2 of LRP1 flanked by LoxP sites (Rohlmann et al., 1996), and the LysM-Cre mouse line, which expresses Cre recombinase enzyme under the control of the myeloid-specific promoter of lysozyme M (LysM) (Clausen et al., 1999). Breeding these mouse lines generated two genotypes of interest to our study, both of which had $LRP1^{f/f}$ in the homozygous state, but had LysM-Cre either in the heterozygous state or the homozygous state. Flow cytometry analysis of LRP1 surface expression in peripheral blood $Gr1^+$ cells revealed that around 20% of $Gr1^+$ cells in WT mice expressed LRP1 receptor on their surface, whereas $LRP1^{f/f}$ LysM-Cre mice showed significant reduction in LRP1 expression on $Gr1^+$ myeloid cells (**Figure 2.13a, b**). Notably, $LRP1^{f/f}$ mice homozygous for LysM-Cre (LysM-$Cre^{+/+}$) exhibited a more complete deletion of LRP1 on $Gr1^+$ myeloid cells, compared to those with LysM-Cre in the heterozygous state (LysM-$Cre^{+/-}$) (**Figure 2.13a**), prompting us to conduct all subsequent experiments using $LRP1^{f/f}$ LysM-$Cre^{+/+}$ mice. Notably, $LRP1^{f/f}$ LysM-$Cre^{+/+}$ mice and WT mice had a comparable composition of the major hematopoietic cell subpopulations in their peripheral blood (**Figure 2.13c**).

2-2.11. LRP1 receptor is required for psap-mediated Tsp-1 induction in lung $Gr1^+$ cells.

To determine whether the LRP1 receptor is required for psap-mediated Tsp-1 induction *in vivo*, we treated WT and $LRP1^{f/f}$ LysM-$Cre^{+/+}$ mice with psap-containing PC3 CM intraperitoneally for six days, then analyze the lungs for Tsp-1 protein expression. Immunofluorescence staining revealed that, as

Figure 2.13

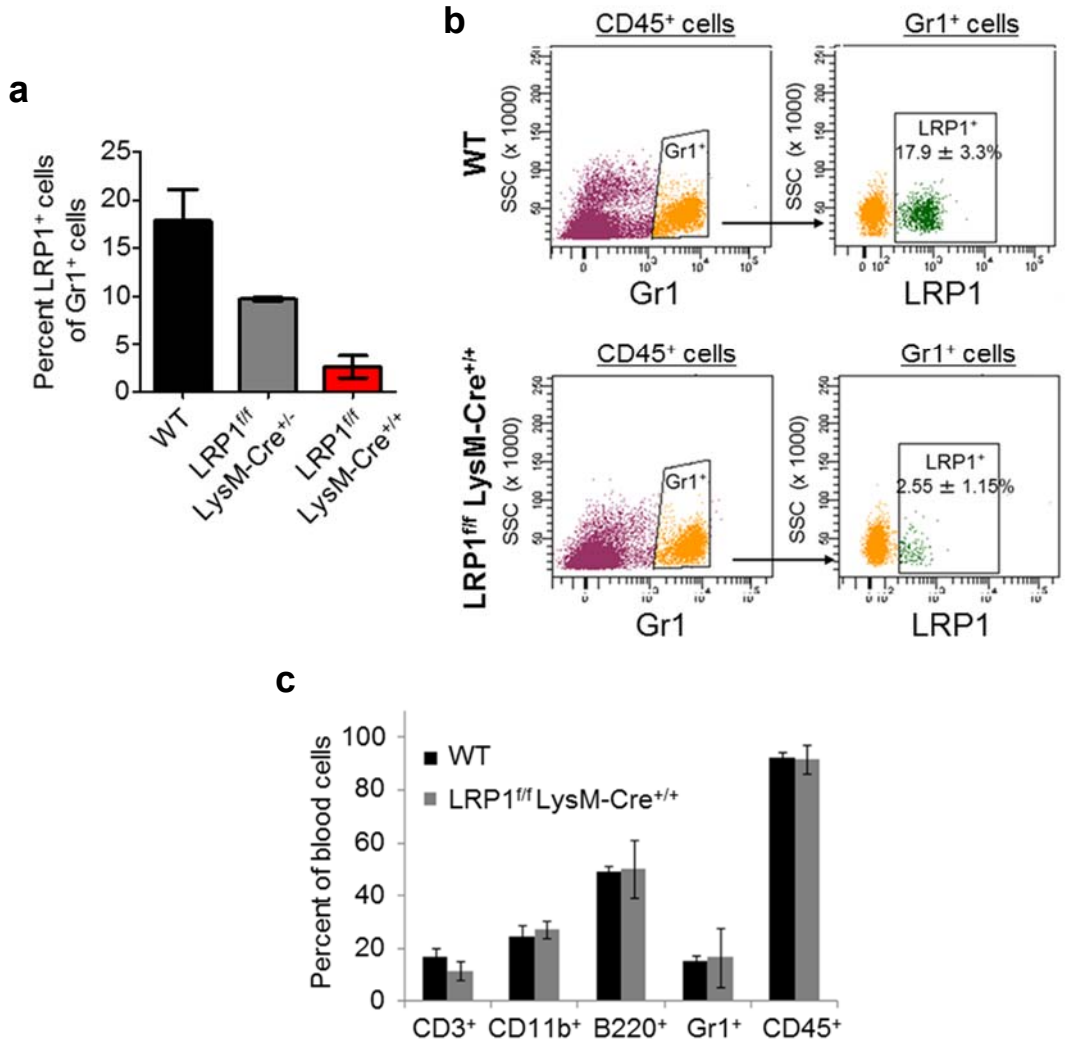

Figure 2.13. Myeloid-specific inducible knockout of LRP1.
(a) Flow cytometry-based quantitation of the percentage of LRP1^{+} cells within the Gr1^{+} cell population, in peripheral blood from WT, LRP1$^{f/f}$ LysM-Cre$^{+/-}$, and LRP1$^{f/f}$ LysM-Cre$^{+/+}$ mice. (n= 3 mice/ group). Data presented as Mean ± SD.
(b) Representative flow cytometry plots depicting the percentage of LRP1^{+} cells within the Gr1^{+} cell population in peripheral blood from WT and LRP1$^{f/f}$ LysM-Cre$^{+/+}$ mice. We first gated Gr1^{+} myeloid cells within the total CD45^{+} hematopoietic cell population in the blood, followed by gating LRP1^{+} cells within the Gr1^{+} cell population. Blood samples from 3 mice per genotype were analyzed. Results are presented as Mean ± SD.
(c) Flow cytometry-based quantitation of hematopoietic cell composition in peripheral blood of WT and LRP1$^{f/f}$ LysM-Cre$^{+/+}$ mice. CD3^{+}: T cells; CD11b^{+}: myeloid cells; B220^{+}: B cells; Gr1^{+}: myeloid cells; CD45^{+}: total hematopoietic cells.

expected, LRP1$^{f/f}$ LysM-Cre$^{+/+}$ lungs lacked LRP1 expression in Gr1^{+} myeloid cells (**Figure 2.14a**). More importantly, LRP1$^{f/f}$ LysM-Cre$^{+/+}$ lungs showed significantly lower induction of Tsp-1 in response to psap-containing medium compared to WT lungs, by immunofluorescence staining, despite the comparable recruitment of Gr1^{+} myeloid cells to these lungs (**Figure 2.14a, b**). Similarly, LRP1$^{f/f}$ LysM-Cre$^{+/+}$ mice treated with DWLPK peptide exhibited lower levels of Tsp-1 protein in their whole lung lysates compared to WT mice (**Figure 2.14c**). These results suggest that LRP1 receptor on Gr1^{+} myeloid cells responds to psap/DWLPK and relays signals leading to Tsp-1 induction.

2-3. DISCUSSION

Our study demonstrates, for the first time, the ability of metastasis-incompetent primary tumors to systemically reprogram BM-derived myeloid cells in the lung microenvironment, inhibiting metastasis. Prior to our study, research on metastasis suppression had been focused on tumor cell intrinsic suppressors of metastasis, such as KISS1, MKK4, p38, and MKK7 (Cook et al., 2011; Shevde and Welch, 2003). Here, we have identified a mechanism whereby metastasis-incompetent primary tumors, by virtue of secreting prosaposin, systemically alter the microenvironment at the distal organ, rendering it metastasis-suppressive (**Figure 2.15**).

Though initially surprising, we demonstrated that tumors with low metastatic potential are as efficient as highly metastatic tumors at generating a premetastatic niche, composed primarily of recruited BM-derived CD11b^{+} Gr1^{+} myeloid cells (**Figure 2.1a, b**). More interesting was the fact that the niches

Figure 2.14

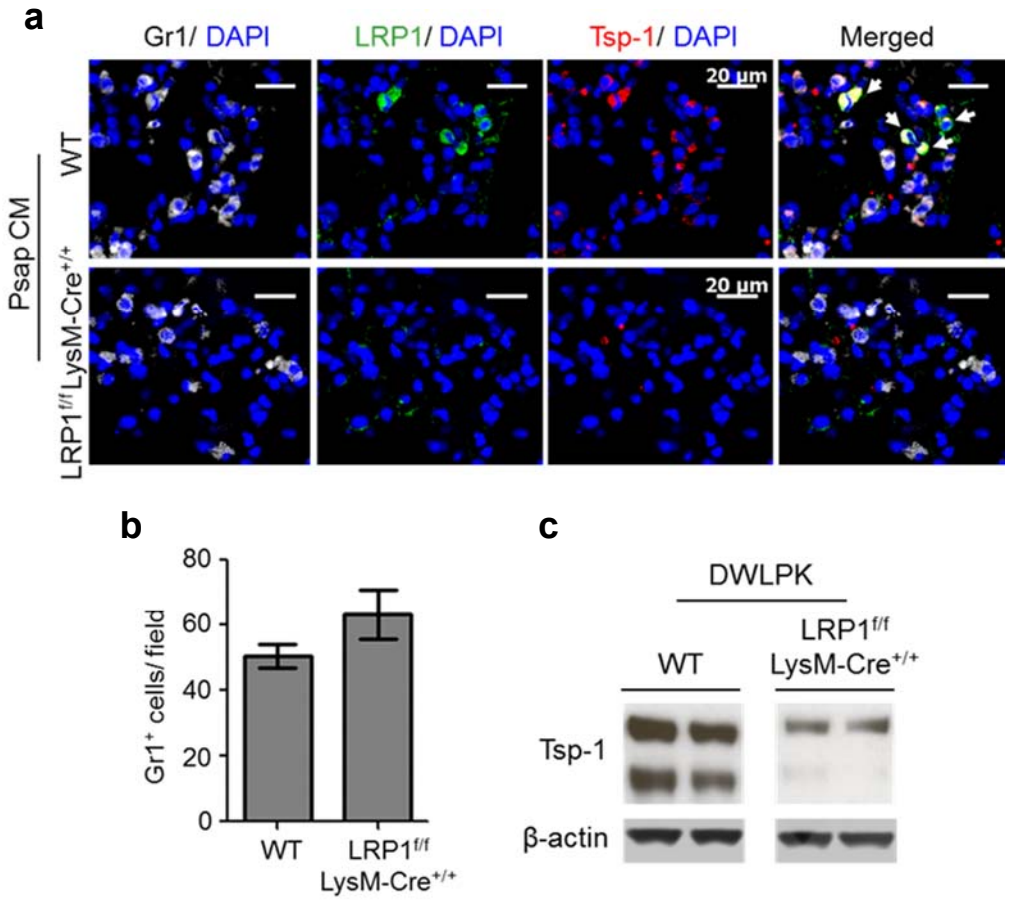

Figure 2.14. Myeloid-specific knockout of LRP1 blocks Psap-mediated Tsp-1 induction in Gr1$^+$ myeloid cells.
(a) Representative immunofluorescence staining of Gr1$^+$ myeloid cells (white) and the expression of LRP1 (green) and Tsp-1 (red) in the lungs of WT and LRP1$^{f/f}$ LysM-Cre$^{+/+}$ mice treated with Psap-containing PC3 CM for 6 days. DAPI stains nuclei. White arrows point to cells that show colocalization of Gr1, LRP1, and Tsp-1.
(b) Immunofluorescence staining-based quantification of Gr1$^+$ cells recruited to lungs of WT and LRP1$^{f/f}$ LysM-Cre$^{+/+}$ mice treated with PC3 CM (n= 3 mice per group, 1 section per mouse, 7-8 fields per sections). p=0.198 (two-tailed t test). **(c)** Western blot analysis of Tsp-1 in lungs of WT and LRP1$^{f/f}$ LysM-Cre$^{+/+}$ mice treated with DWLPK for 6 days. β-actin is a loading control.

Figure 2.15

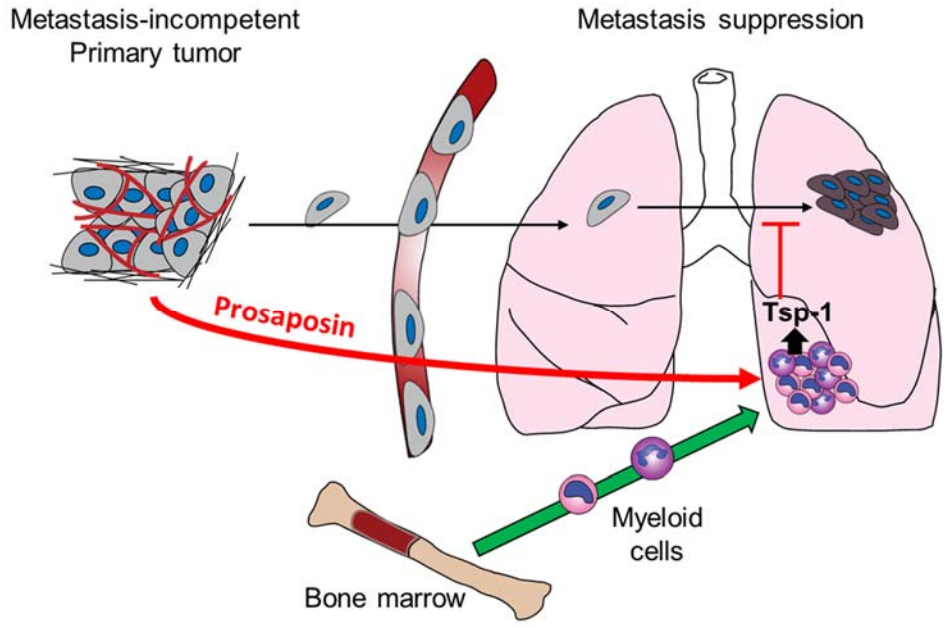

Figure 2.15. Proposed model. Metastasis-incompetent primary tumors secrete prosaposin, which systemically acts on bone marrow-derived myeloid cells recruited to the lungs, inducing their expression of the anti-tumorigenic factor Tsp-1. This suppresses metastasis by blocking tumor cell proliferation.

generated in each case were molecularly different, with metastasis-incompetent tumors systemically upregulating the expression of the anti-tumorigenic factor Tsp-1 in the recruited myeloid cells (**Figure 2.2**). This is especially significant since BM-derived myeloid cells in the premetastatic niche are known to promote metastasis by supporting angiogenesis, enhancing tumor proliferation, and driving mesenchymal-to-epithelial transition (Gao et al., 2008, 2012; Shojaei et al., 2007). However, under conditions in which the primary tumor is poorly metastatic, the same myeloid cells are converted into metastasis-inhibitory cells by virtue of their Tsp-1 expression. This scenario underscores the plasticity of BM-derived cells and the large impact that tumor-derived systemic factors have on shaping the distant organ microenvironment depending on different contexts.

Moreover, the fact that metastasis suppression was abrogated in Tsp-1$^{-/-}$ BMT mice highlights the requirement for Tsp-1 expression in recruited BM-derived Gr1^{+} myeloid cells. In addition, we have uncovered a novel mechanism in which Gr1^{+} cells in the lungs are the major source of Tsp-1, leading to metastasis inhibition.

Based on a previous study conducted by our collaborators identifying the tumor-secreted factor prosaposin with anti-metastatic activity (Kang et al., 2009), we derived the pentapeptide DWLPK. This allowed us to test its potential use as a therapeutic agent to suppress metastasis. DWLPK exhibited significant anti-metastatic activity, and it induced Tsp-1 expression in Gr1^{+} cells in the lung microenvironment.

Another therapeutic, the Tsp-1-derived nonapeptide, ABT-510, is currently in phase II clinical trials for the treatment of advanced metastatic tumors.

Although ABT-510 is derived from the second type-1 repeat of Tsp-1, with known antiangiogenic activity, and it exhibits antiangiogenic activity *in vitro* (Haviv et al., 2005), it has failed to enhance patient outcomes in clinical trials (Baker et al., 2008; Ebbinghaus et al., 2007; Markovic et al., 2007). We believe that DWLPK will be a more successful anti-metastatic therapeutic agent than ABT-510 because, contrary to ABT-510, DWLPK can induce the expression of full-length Tsp-1 with all its domains and functions intact. The next step for optimizing DWLPK function as a therapeutic agent for advanced metastatic cancer will be to chemically modify it to increase its half-life in circulation, increase its bioavailability, and reduce the rate of its clearance. This will be further discussed in Chapter Four.

Based on data generated with myeloid-specific LRP1 knockout mice, psap signals via the LRP1 receptor on myeloid cells to induce Tsp-1 expression. These results, for the first time, describe a signaling event involving psap and LRP1, where LRP1 does not merely act as an endocytic receptor for psap. Signaling events described downstream of LRP1 have been sparse, but have included activation by PDGF-BB in conjunction with PDGFR-β, intracellular signaling following Tsp-1-calreticulin binding leading to focal adhesion disassembly, and possible transcriptional regulation via the cleaved LRP1 intracellular domain (Kinoshita et al., 2003; May et al., 2002). Studies are underway to determine the domains within LRP1 that are required for Tsp-1 induction in response to psap, as well as the downstream signaling cascade activated. In addition, it would be interesting to evaluate whether psap or DWLPK signaling downstream of LRP1 can also suppress metastasis. This is discussed in greater detail in Chapter Four.

In conclusion, we have established the novel mechanism whereby tumors with low metastatic potential systemically impinge upon the distant organ microenvironment, rendering it less conducive to metastatic outgrowth. Our study further highlights the plasticity of myeloid cells in the lung microenvironment and their ability to respond to primary tumor-derived factors, shaping the outcome of metastatic progression.

2-4. MATERIALS AND METHODS

2-4.1. Mice and cell lines

All animal work was conducted in accordance with a protocol approved by the Institutional Animal Care and Use Committee. Wild type C57BL/6J, GFP transgenic C57BL/6-Tg (CAG-EGFP) 1Osb/J, LRP1$^{f/f}$ transgenic B6;129S7-Lrp1^{tm2Her}/J, and LysM-Cre transgenic B6.129P2-Lyz2$^{tm1(cre)Ifo}$/J mice were obtained from The Jackson Laboratory (Bar Harbor, Maine). CB-17 SCID mice were obtained from Charles River (Wilmington, MA). Tsp-1 knockout mice in the C57BL/6J background, a kind gift from Dr. Shahin Rafii (Weill Cornell Medical College, NY) were bred in the lab and genotyped according to standard protocols.

The human prostate cancer cell lines PC3 and PC3M-LN4 are previously described (Kang et al., 2009). The human breast cancer cell lines MDA-MB-231 and MDA-MB-LM2 are described previously (Ryu et al., 2011). The murine Lewis lung carcinoma cell line LLCs/D122 (provided by Lea Eisenbach, Wiesmann Institute of Science, Rehovot, Israel) stably expressing RFP and firefly luciferase (Gao et al., 2008) was cultured in DMEM supplemented with 10% fetal bovine serum (FBS). PC3, LN4, and MDA-MB-231 cell lines were obtained from ATCC and cultured in RPMI supplemented with 10% FBS.

2-4.2. Bone marrow isolation and transplantation

BM transplantation was performed by injecting $1x10^7$ total BM cells into the retro-orbital sinus (Yardeni et al., 2011) of lethally irradiated (900 rads) 8-week old C57BL/6 female mice. BM cells were harvested by flushing femurs and tibias of donor animals, including C57BL/6 Tg (ACTB-EGFP) 1Osb/J GFP transgenic, C57BL/6 Wild-type, or C57BL/6 Tsp-$1^{-/-}$ mice, using 1X phosphate buffer saline (PBS). After 4 weeks of BM engraftment, reconstitution efficiency was monitored by flow cytometry of hematopoietic cell populations in the peripheral blood, as well as Western blot analysis of peripheral blood for absence of Tsp-1 protein in mice transplanted with Tsp-$1^{-/-}$ BM.

2-4.3. Conditioned medium (CM) experiments

PC3 or PC3M-LN4 cells were cultured in RPMI with 10% FBS. $5x10^6$ cells were then subcultured in 7 mL of serum-free medium in 10 cm plates for 24 hours in order to generate CM. Harvested media was centrifuged and filtered through 0.22 μm pore-size filters to remove any cells or cell debris.
Wild-type BMT and Tsp-$1^{-/-}$ BMT C57BL/6J mice were pretreated with 200 μL serum-free CM from PC3 or LN4 cells or serum-free RPMI media daily for 6 days via intraperitoneal (i.p.) injection.

2-4.4. Peptide generation and administration

Prosaposin truncation mutants were created by cloning the regions of prosaposin generated by PCR amplification using the following strategy: Saposin A, Saposin AB, and Saposin ABC were all created using the same 5' primer: ggcggcgtcgacATGTACGCCCTCTTCCTCC and the following 3' primers: saposin A: ggcgcctctagaAGAGACTCGCAGAGGTTGAG; saposin

AB: ggcgcctctagaACCTCATCACAGAACCC; saposin ABC: ggcgcctctagaGCCAGAGCAGAGGTGCAGC. The PCR products were then cleaved with Xba1 and Sal1 and cloned into pCMVneo.

The psap truncation constructs were then used to transfect PC3M-LN4 using the Fugene6 transfection reagent and protocol (Roche). CM of transfected cells was harvested 48 hours after transfection and used to treat WI-38 lung fibroblasts for 16 hours. After CM treatment, fibroblasts were harvested and lysed, and Tsp-1 protein expression analyzed by Western blot as previously described (Kang et al., 2009).

The seven 20-amino acid peptides spanning the length of saposin A were comprised of the following sequences:

1-20- SLPCDICKDVVTAAGDMLKD; 11-30- VTAAGDMLKDNATEEEILVY; 21-40- NATEEEILVYLEKTCDWLPK; 31-50- LEKTCDWLPKPNMSASCKEI; 41-60- PNMSASCKEIVDSYLPVILD; 51-70- VDSYLPVILDIIKGEMSRPG; 61-81- IIKGEMSRPGEVCSALNLCES. All peptides were synthesized by Anaspec, Inc (Fremont, CA). The 13 amino acid cyclic peptide was comprised of the following sequence: CDWLPKPNMSASC.

For *in vitro* analysis of peptide activity, WI-38 lung fibroblasts were treated with peptide for 16 hours at a concentration of 5 µg/mL. The cells were then harvested and lysed for Tsp-1 Western blot analysis as previously described (Kang et al., 2009).

The *in vivo* analysis of peptide activity was performed by treating 8-week old C57BL/6 mice with either 300 µL of PC3M-LN4 CM alone or in combination with peptide, diluted in PBS, at a dose of 30 mg/kg/day via intraperitoneal

injection for six days. After six days the mice were euthanized by cervical dislocation under isofluorane anesthetic. The lungs were harvested, lysed, and analyzed for protein expression.

For metastasis experiments, the psap peptide DWLPK and a scrambled peptide LPKDW were synthesized by AnaSpec (Fremont, CA). Peptide diluted in saline was administered to mice (30 mg/kg) via intraperitoneal injection on a daily basis for six days before LLC tumor cell tail vein injection and until the end of the metastasis assays.

2-4.5. Metastasis assay, bioluminescence imaging, and analysis

For experimental metastasis, 8-week old C57BL/6 mice were injected via tail vein with 1 x 10^5 luciferase-labeled LLC cells. Pulmonary metastases were monitored by live animal bioluminescence imaging (Xenogen) once per week. For *in vivo* determination of the metastatic burden of luciferase-labeled LLCs, mice were anaesthetized and injected intraperitoneally with 75 mg/kg of D-luciferin (100 µL of 30 mg/mL in PBS). Metastatic growth was monitored over time using bioluminescence imaging performed with mice in a supine position 5 min after D-luciferin injection with a Xenogen IVIS system coupled to Living Image acquisition and analysis software (Xenogen). For BLI plots, photon flux was calculated for each mouse by using the same circular region of interest encompassing the thorax of the mouse.

For orthotopic prostate cancer cell injections, 2 x 10^6 viable LN4 or LN4-psap cells were injected into the prostate gland of CB-17 SCID mice. Primary tumor size was monitored using a caliper. When tumor size reached 1 cm^3, lungs were collected to determine Tsp-1 protein levels.

2-4.6. Immunofluorescence and microscopy

Animals were euthanized at the end of experiments, and lungs were quickly perfused by injecting 5 mL of cold PBS through the right ventricle of the heart. One part of the lung from each animal was fixed in 3.7% formalin and the other part was sorted by flow cytometry for RNA extraction or used for protein extraction.

For microscopy, following formalin fixation, tissues were cryoembedded in Tissue-Tek O.C.T. embedding compound (Electron Microscopy Sciences). Sections (10 μm) were washed 3 times in PBS and incubated in blocking/permeabilization buffer (PBS, 5% BSA, 0.25% Triton X-100). Sections were then incubated with labeled primary antibodies against Gr1 (Clone RB6-8C5, BD Pharmingen), CD11b (Clone M1/70, BD Pharmingen), Ki-67 (abcam), Tsp-1 (Ab-4 or Ab-11 from LabVision), Active-Caspase-3 (BD Pharmingen), and LRP1 (clone EPR3724, abcam) for 2 hours at room temperature. Typically primary antibodies were either commercially conjugated to fluorescent dyes, or manually conjugated to Alexa Fluor dyes (Alexa 488, Alexa 568, Alexa 647 and Alexa 750) using antibody-labeling kits (Invitrogen) performed as per manufacturer's instructions and purified over BioSpin P30 Gel (Biorad). Primary antibodies were diluted in blocking/permeabilization buffer at a dilution of 1:100. After primary antibody incubation, sections were rinsed 5 times with PBS, counter-stained with DAPI and mounted in Prolong Gold-antifade reagent for epifluorescence microscopy analysis. For LRP1 staining, after primary antibody incubation, secondary anti-rabbit antibody conjugated to Alexa Fluor-488 was used at a dilution of 1:100 for 1 hour.

Lung sections were also stained with hematoxylin and eosin for morphometric determinations. GFP positive cells were detected by their intrinsic fluorescence.

Fluorescence images were obtained using a computerized Zeiss fluorescence microscope (Axiovert 200M), fitted with an apotome and a HRM camera. Images were analyzed using Axiovision 4.8 software (Carl Zeiss Inc.).

2-4.7. Flow cytometry and cell sorting

To obtain single cell suspensions, lungs were minced and then digested in collagenase/DNase mix (Roche) for 30 min at 37ºC. Cells were washed, strained and resuspended in FACS staining buffer (PBS + 2 mM EDTA, 1% BSA). For analysis of peripheral blood, blood was collected from the tails of mice in anti-coagulant buffer (PBS with 5 mM EDTA). Red blood cells were eliminated by incubation in RBC Lysis Buffer (5 Prime) for 10 min on ice. Cell suspensions were pre-blocked in FACS buffer plus Fc block (CD16/CD32, 1:100, BD Biosciences Pharmingen) and then incubated with the following primary antibodies: rat IgG2ακ and IgG2αβ isotype control (BD Pharmingen), Ly6G (Clone 1A8, BD Pharmingen), Ly6C (Clone HK1.4), Gr1 (Clone RB6-8C5, Biolegend), CD11b (clone M1/70, BD Pharmingen), CD45 (Clone 30-F1, Biolegend), CD3 (Clone 17A2, Biolegend), and B220 (Clone RA3-6B2, Biolegend). LRP1 antibody (clone 5A6, abcam) was conjugated to Alexa Fluor-488 dye. SYTOX blue (Invitrogen) was added and incubated for 5 minutes at room temperature in each cell staining tube to facilitate the elimination of dead cells by flow cytometry.

Labeled cell populations were measured by LSRII flow cytometer coupled with FACSDiva software (BD Bioscience). Flow cytometry analysis was performed

using a variety of controls including isotype antibodies, single color control samples, and unstained samples for determining appropriate gates, voltages, and compensations required in multivariate flow cytometry. For sorting, targeted cell populations were gated within FACSDiva software and sorted by Aria II sorter (BD Bioscience). For sorting, SYTOX blue-negative was utilized to remove dead cells. $CD45^-$, $CD45^+$ $Ly6C^{high}$, $CD45^+$ $Ly6G^+$, $CD45^+$ $Gr1^+$, $CD45^+$ $Gr1^-$, $CD45^+$ $F4/80^+$, and $CD45^+$ $CD3^+$ subsets were isolated. Cells were quickly processed for RNA isolation using PicoPure RNA isolation kit (Arcturus).

2-4.8. Quantitative RT-PCR analysis

Total RNA from flow cytometry sorted cells was extracted using the PicoPure RNA extraction kit (Arcturus) following the manufacturer's protocol. RNA was converted to cDNA using qScript™ cDNA supermix (Quanta Biosciences). Q-PCR was performed with primers and iQTM SYBER Green master mix (Biorad, Hercule, CA). Each sample was duplicated to minimize pipetting error. A standard protocol of initial denaturing at 95°C for 10 min, 40 cycles of 95°C for 10 sec, 60°C for 30 sec, and 72°C for 30 sec, followed by final extension at 72°C for 5 min and melt curve analysis was applied on a BioRad CFX96 Real Time System (BioRad) coupled with Bio-Rad-CFX Manager software. The relative abundance of each transcript compared with the control was calculated utilizing the delta-Ct method.

The primer sequences used for RT-PCR were:

Mus-GAPDH-for: CATGGCCTTCCGTGTTCCTA

Mus-GAPDH-rev: GCGGCACGTCAGATCCA

Mus-Tsp-1-for: CTTGAGGCAGATGAAGAAGACC

Mus-Tsp-1-rev: ACTGACACCACTTGTTGCTTCC

2-4.9. Western blot analysis

Cells were homogenized in lysis buffer (BioRad) containing protease inhibitors (Roche Applied Science). Samples were boiled in 1x SDS sampling buffer with 10% β-mercaptoethanol, and loaded onto 4-12% gradient Bis-Tris NuPAGE gels (Invitrogen). Western blotting was performed using antibodies specific for Tsp-1, (clones Ab-4 and Ab-11, Labvision), LRP1 (clone EPR3724, abcam), and β-actin (Sigma-Aldrich).

2-4.10. Gene expression profiling

Mice were administered intraperitoneally with 200 µL of PC3-CM or LN4-CM daily for 8 days. Lungs were collected at day 9 and used for harvesting RNA. RNA quality and integrity was assessed by a bioanalyzer (Agilent). RNA was converted to biotinylated cDNA, and hybridized to Mouse Exon Affymetrix Gene ST 1.0 chips (Affymetrix, Santa Clara, CA) for gene expression analysis. Microarray data was processed using Affymetrix Expression Console™ software (Affymetrix, CA) with RMA (Robust Multi-array Analysis) normalization. The data was normalized by Z-score calculations using standard deviation, and hierarchical clustering was performed on 1846 genes with gene ontology annotation describing them as being extracellular (secreted), using software from Spotfire. The files for this experiment are available at the NCBI´s public microarray repository under the link: http://www.ncbi.nlm.nih.gov/geo/query/acc.cgi?acc=GSE44459

2-4.11. Statistical Analysis

Results were expressed as mean ± SEM depicted by error bars, unless otherwise noted. Analyses of different treatment groups were performed using the Mann-Whitney U or Student t tests using the GraphPad Prism statistics software. p values < 0.05 were considered significant.

CHAPTER THREE
LUNG INFLAMMATION PROMOTES METASTASIS VIA TSP-1 DEGRADATION.

3-1. INTRODUCTION

Clinical and animal model studies have suggested a strong interplay between inflammation and primary tumor progression (Ben-Neriah and Karin, 2011). However, less is known about the contribution of inflammation to metastatic outgrowth in distant organs. Accumulating evidence has demonstrated that primary tumors generate metastasis-promoting premetastatic niches in distant metastatic organs that exhibit features of inflammation. For instance, primary tumors systemically induce elevated levels of the chemoattractants S100A8 and S100A9 in the lungs, which in turn stimulate the expression of serum amyloid A (SAA) 3, leading to further recruitment of myeloid cells and the activation of NF-κB signaling through TLR4, resulting in the amplification of inflammatory responses (Hiratsuka et al., 2006, 2008). Identifying mechanisms by which primary tumor-derived premetastatic niches contribute to tumor outgrowth is an area of active investigation; however, little is known about the mechanisms by which external inflammation in the lungs can impact metastasis of extapulmonary neoplasms.

The lung, which is susceptible to inflammatory insults, is a frequent site of metastasis from a variety of extrapulmonary neoplasms. For example, in a mouse model of autoimmune arthritis, increased recruitment of inflammatory neutrophils and macrophages in the lungs was associated with increased breast cancer metastasis to the lungs (Das Roy et al., 2009). Similarly,

external insults, including smoke-inhalation and bacterial infections induced metastasis-conducive microenvironments in the lung (Murin et al., 2004; Smith and Kang, 2013). The mechanisms by which inflammation contributes to tumor outgrowth in distant metastatic organs have remained underexplored.

We hypothesized that externally-induced lung inflammation could function in a manner similar to that of a premetastatic niche and predispose the lungs to enhanced metastasis. In this chapter, we have explored mechanisms of inflammation-driven metastatic progression. We demonstrate that lung-specific inflammation was associated with recruitment of neutrophils, which degranulated to release the serine proteases, neutrophil elastase (NE) and cathepsin G (CG). Importantly, NE and CG degraded the anti-tumorigenic factor thrombospondin-1 (Tsp-1), rendering the lung microenvironment conducive to metastatic outgrowth. Genetic and pharmacological inhibition of both proteases suppressed inflammation-mediated metastatic outgrowth, providing further evidence that neutrophil-derived proteases are responsible for generating a tumor-promoting microenvironment, and demonstrating a novel mechanism of Tsp-1 regulation in the metastatic organ.

3-1.1. Common forms of lung inflammation in humans

1- Acute lung injury (ALI)

Acute lung injury (ALI) as a result of sepsis is a major cause of mortality (Kao et al., 2007). ALI, and its more severe manifestation, acute respiratory distress syndrome (ARDS), are characterized by a significant infiltration of neutrophils into the lungs, accompanied by the expression of pro-inflammatory cytokines and damage to the lungs (Goodman et al., 1996). More specifically, ALI is

characterized by an acute inflammatory phase followed by a chronic fibroproliferative phase. The acute phase consists of increased epithelial and vascular permeability, as well as impaired clearance of the excess alveolar fluid, leading to an increase in extravascular lung fluid and edema. This is also accompanied by pronounced neutrophil infiltration, protease activation, and an increased expression of pro-inflammatory cytokines. At later stages, a fibrotic response occurs, characterized by the deposition of collagen types I and III and marked fibroblast proliferation, accompanied by the destruction of the alveolar basement membrane (Matute-Bello et al., 2008; Pittet et al., 1997).

Bacterial lipopolysaccharide (LPS) is the main component of sepsis-caused ALI (Brigham and Meyrick, 1986). LPS causes damage to the lung epithelium and endothelium, associated with increased neutrophil influx to lungs and increase in free oxygen radicals (Brigham and Meyrick, 1986; Güngör et al., 2010a; Haegens et al., 2009; Jeyaseelan et al., 2004). LPS induced elevated levels of nitric oxide (NO), inducible nitric oxide synthase (iNOS), and the pro-inflammatory cytokines tumor necrosis factor α (TNFα) and interleukin-1β (IL-1β), as well as a neutrophil chemoattractants CXCL1, MIP-1α, MIP-2, and CXCL5 (Haegens et al., 2009; Jeyaseelan et al., 2004; Su et al., 2012; Wang et al., 1999). Furthermore, inhibition of iNOS attenuated the release of NO and cytokines, and inhibited the damage causing ALI (Su et al., 2007, 2012).

2- COPD and emphysema

One manifestation of chronic inflammation in lungs is chronic obstructive pulmonary disorder (COPD). COPD is characterized by an elevated and persistent inflammatory infiltrate, composed of neutrophils, macrophages, and

lymphocytes in the airways and parenchyma, increased deposition of collagen in airway walls characteristic of fibrosis, disruption of elastin fibers, finally leading to loss of alveolar septa, resulting in emphysema (Jeffery, 1998). The pro-inflammatory cytokine IL-1β is significantly elevated in the lungs of patients with COPD, along with TNFα, IL-6, and IL-8 (Chung, 2001). Using transgenic mice that expressed IL-1β in the lung epithelium in an inducible manner, the effects of IL-1β-driven lung inflammation were determined. IL-1β expression in lung epithelium caused infiltration of neutrophils and macrophages, enlargement of alveoli reminiscent of emphysema, fibrosis in airway walls characterized by collagen deposition, and upregulation of neutrophil chemoattractants CXCL1 and CXCL2, as well as the proteases MMP9 and MMP12 (Lappalainen et al., 2005). These observations suggest that IL-1β expression in the lung epithelium was sufficient to generate a state similar to human COPD.

IL-1 pro-inflammatory cytokine is involved in initiating inflammation and maintaining it. Activation of TLR signaling, leading to NF-κB signaling, induces the expression and synthesis of inactive pro-IL-1β that gets activated upon cleavage by the IL-1β-converting enzyme (ICE), also known as caspase-1 (Dinarello, 1996; Takeuchi and Akira, 2010), or by MMP9 (Schönbeck et al., 1998). IL-1β is produced by monocytes and macrophages primarily, and also by neutrophils, T cells, fibroblasts, and epithelial cells (Dinarello, 1996). It contributes to the mobilization of neutrophils from the bone marrow, and it promotes the synthesis of other cytokines, including TNFα, IL-6, IL-8, and granulocyte monocyte colony-stimulating factor (GM-CSF) (Chung, 2001). Furthermore, IL-1β induces the expression of intercellular adhesion molecule -

1 (ICAM-1) and vascular cell adhesion molecule -1 (VCAM-1) on endothelial cells, allowing the adhesion of neutrophils to endothelial cells during inflammation (Chung, 2001).

3-1.2. Pattern recognition receptors and LPS signaling

1- Pattern recognition receptors

Pattern recognition receptors (PRRs) on the surface of immune cells allow the response to microbial pathogens or damaged host cells. They do that by recognizing pathogen-associated molecular patterns (PAMPs), conserved molecular structures on different microbial species, and damage-associated molecular patterns (DAMPs), which are endogenous molecules released by damaged host cells. Signaling downstream of PAMP- or DAMP-activated PRRs leads to the induction of pro-inflammatory mediators, such as IL-1β, TNFα, IL-6, and type I interferons (IFNs) (Takeuchi and Akira, 2010).

The best characterized PRR family is the TLR family. It consists of 10 members identified in humans and 12 in mice. TLRs sense pathogens outside the cell, as well as inside endosomes and lysosomes (Akira et al., 2006). Different TLRs can recognize different pathogen-derived and self-derived molecular patterns. For instance, TLR1, TLR2, and TLR6 recognize lipids, while TLR7, TLR8, TLR9 recognize nucleic acids. Interestingly, TLR4 is the only receptor that can recognize a diverse array of structurally unrelated ligands, including LPS, some self-derived heat shock proteins, and some viral antigens. TLR expression is regulated in response to pathogens, other environmental stressors, or cytokines, and TLRs are expressed on a number

of immune cells, including macrophages, dendritic cells, neutrophils, B cells, and some T cells (Akira et al., 2006).

2- Bacterial lipopolysaccharide (LPS) signals through TLR4.

LPS, also called endotoxin, is a component of the outer membrane of Gram-negative bacteria, and is a known cause of septic shock. LPS is structurally composed of polysaccharides of the O-antigen and the core domain, and an amphipathic lipid A (Raetz and Whitfield, 2002). Lipid A is the immunogenic domain of LPS. An important determinant of LPS inflammatory activity is the number of lipid chains constituting lipid A, where lipid A with six lipid chains has optimal immunogenic activity, and one with five lipid chains is ~ 100-fold less active (Teghanemt et al., 2005). LPS is recognized by TLR4 in a complex with myeloid differentiation protein 2 (MD-2) on immune cells. LPS aggregates on Gram-negative bacterial outer membranes are bound by lipopolysaccharide binding protein (LBP), which catalyzes their extraction and binding to CD14 (Yu et al., 1997). CD14 delivers LPS to TLR4-MD2 complexes. The structural interaction between LPS, TLR4, and MD2 has been determined at a 3.1 Å resolution (Park et al., 2009). Binding of LPS to TLR4-MD2 leads to heterodimerization with another TLR4-MD2-LPS complex, in a symmetrical fashion (Park et al., 2009).

TLR4 triggers both myeloid differentiation primary response 88 (MyD88)-dependent and TIR domain-containing adaptor inducing IFN-β (TRIF)-dependent signaling cascades. MyD88 is bridged to TLR4. It interacts with the serine/threonine kinase IL-1R-associated kinase (IRAK)-4, which activates IRAK-1 and IRAK-2. These IRAKs dissociate from MyD88 and bind TNFR-

associated factor 6 (TRAF6), which acts as an E3 ubiquitin protein ligase. Together with an E2 ligase, TRAF6 forms a polyubiquitin chain that activates a complex of TGFβ-activated kinase 1 (TAK1) and TAK1-binding proteins (TABs) that phosphorylates IKK-β. This leads the IKK complex to phosphorylate the NF-κB inhibitor IκB, causing its degradation, releasing NF-κB to translocate to the nucleus and activate expression of pro-inflammatory cytokine genes. Simultaneously, TAK1 activates MAP kinase cascades leading to the activation of the transcription factor AP-1, which also induces cytokine genes (Takeuchi and Akira, 2010) (**Figure 3.1**).

LPS also induces translocation of TLR4 to the endosome together with the TRIF-related adaptor molecule (TRAM). This triggers TRIF-dependent signaling. Downstream of TRIF, TRAF6 and receptor-interacting protein (RIP1) activate NF-kB, leading to proinflammatory cytokine expression, whereas TRAF3 induces TANK-binding kinase 1 (TBK1) and IKK-i-mediated phosphorylation of interferon regulatory factor 3 (IRF3). Phosphorylated IRF3 translocates into the nucleus, activating the expression of type I IFN genes (Takeuchi and Akira, 2010) (**Figure 3.1**).

TLR signaling leads to the expression of proinflammatory cytokines such as IL-1β, TNFα, and IL-6. These cytokines orchestrate the immune response by regulating inflammatory cell survival, vascular permeability, and leukocyte recruitment (Takeuchi and Akira, 2010).

Figure 3.1

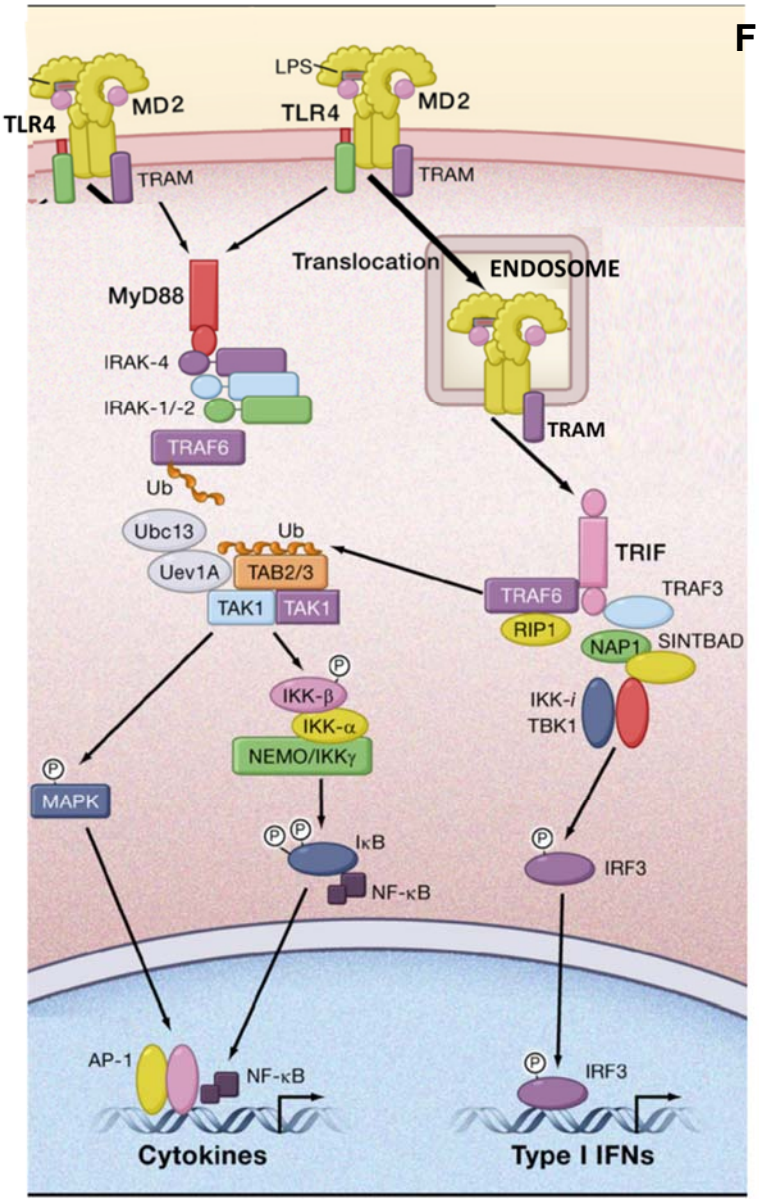

Figure 3.1. LPS signaling via TLR4. LPS is recognized by TLR4/MD2 heterodimer. This recruits MyD88 to the receptor and a complex of IRAKs and TRAF6 is formed. TRAF6 catalyzes the formation of a polyubiquitin chain on TAK1/ TABs complex, activating it, and resulting in the phosphorylation and activation of an IKK complex. This phosphorylated IκB, leading to its degradation and the release of NF-κB to the nucleus, where it drives cytokine expression. TAK1 also phosphorylates MAPK, leading to AP-1 activation and cytokine expression. LPS causes translocation of TLR4 to the endosome, together with TRAM. This activates TRIF signaling, leading to NF-κB and IRF activation, resulting in cytokine and IFN expression. *(Modified from Takeuchi and Akira, 2010*).

3-1.3. Neutrophils and their proteases in inflammation

Neutrophils account for about 70% of circulating immune cells, and as components of the innate immune system, they are the primary responders to infection. In order to accomplish that role, neutrophils express TLRs to detect pathogens and tailor the response to the pathogen detected. In addition to responding to pathogens, neutrophils have the ability to detect and respond to DAMPs, which can be released due to tissue damage and inflammation, further fueling the inflammatory response. Neutrophils express most TLRs, except two of the intracellular ones, TLR3 and TLR7 (Prince et al., 2011).

Neutrophils are short-lived cells, and this functions as an anti-inflammatory mechanism in healthy tissues. Under normal conditions, circulating neutrophils have a half-life of around 7 hours. However, in response to a pathogenic insult, neutrophils recruited to the site of infection can survive up to 4 days (Doerschuk, 2001). For instance, LPS has been shown to act as a mediator of neutrophil survival (Hachiya et al., 1995). LPS *in vitro* enhanced the short term survival of neutrophils by signaling via TLR4 and both signaling arms downstream of TLR4: MyD88 and TRIF (Dick et al., 2009). Longer term enhancement of neutrophil survival in response to LPS is suggested to be dependent upon monocytes (Sabroe et al., 2002).

1- Neutrophil granules

Neutrophils carry four types of granules: azurophilic (also called primary), specific (secondary), gelatinase (tertiary), and secretory granules. The granules form sequentially during neutrophil differentiation in the bone marrow, with azurophilic granules forming early during the promyelocyte stage,

followed by specific, gelatinase, and finally secretory granules in later stages. Proteins synthesized at same stage during neutrophil differentiation are sorted into the same granules (Gullberg et al., 1997; Pham, 2006). The granules are also classified based on their ability to be exocytosed after neutrophil activation. By decreasing order of degranulation, the secretory granules are the most highly exocytosed, followed by gelatinase granules, specific granules, and finally the azurophilic granules (Pham, 2006). Azurophilic granules undergo limited exocytosis, and their activity is mostly intracellular, where they degrade pathogens in the phagolysosome (Korkmaz et al., 2008; Pham, 2006). Azurophilic granules carry high levels of myeloperoxidase (MPO), defensins, as well as the serine proteases neutrophil elastase (NE), cathepsin G (CG), and proteinase 3. The level of serine protease mRNAs is the highest during the promyelocytic stage of neutrophil differentiation in the bone marrow, and is later downregulated (Garwicz et al., 2005; Gullberg et al., 1997), explaining why serine proteases are only found in early-forming azurophilic granules and excluded from later-forming granules.

2- Neutrophil serine proteases

Neutrophil serine proteases are 30-35 kDa enzymes, with an active site characterized by a serine residue. They contain a conserved catalytic triad composed of histidine, aspartic acid, and serine residues, which are spatially separated in the primary sequence but are brought together in the tertiary structures (Korkmaz et al., 2008; Pham, 2006).

Neutrophil serine proteases are synthesized as inactive zymogens and require two cleavage steps at the amino-terminal to become active. First the signal peptide is cleaved, followed by cleavage of a dipeptide sequence by cathepsin

C before or during transport to granules (Adkison et al., 2002). C-terminal processing has been shown to be important for the localization of NE to granules (Horwitz et al., 2004), but this remains unclear for CG and proteinase 3.

Released serine proteases are active in the neutral extracellular milieu. They can degrade ECM proteins and have overlapping substrates, like elastin, fibronectin, laminin, collagen, and proteoglycans (Korkmaz et al., 2008; Pham, 2006). Neutrophil serine proteases play a role in ECM remodeling. Purified neutrophil elastase can cleave soluble type I collagen, as well as type I collagen fibrils (Kafienah et al., 1998; Zhu et al., 2001) and can increase fibroblast-mediated contraction of type I collagen, leading to ECM rearrangement (Sköld et al., 1999). Moreover, increased cathepsin G was shown to correlate with increased expression of type I and type III collagen in stenotic valves (Helske et al., 2006).

Serine proteases are inhibited by serpins (serine protease inhibitors) found in the ECM. For instance, α1-antitrypsin (also called α1-protease inhibitor (α1-PI) inhibits the activity of neutrophil elastase, cathepsin G, and proteinase 3 (Korkmaz et al., 2010). Some studies suggest that neutrophil serine proteases, once released extracellularly, bind to the plasma membrane of neutrophils, where they are active and simultaneously protected from the inhibitory effect of serpins (Owen and Campbell, 1999; Owen et al., 1995). However, the nature of this binding is still debated.

The serine proteases also play a role in regulating inflammation by modulating various chemokines. Proteinase 3 can truncate the N-terminal of CXC-

chemokine ligand 8 (CXCL8; also known as IL-8) (Padrines et al., 1994), and CG can truncate that of CXCL5 (Nufer et al., 1999), increasing their neutrophil chemotactic activity. CG also N-terminally truncates CC-chemokine ligand 15 (CCL15) increasing its monocyte chemotactic activity (Berahovich et al., 2005). Interestingly, NE can activate TLR4 through an unknown mechanism, leading to the expression of CXCL8 (Devaney et al., 2003).

3- Neutrophils in lung inflammation

Neutrophils cause lung damage by releasing proteases and reactive oxygen species in response to inflammatory signals. Neutrophil elastase is the major protease released by neutrophils in ALI. Elastase expression in neutrophils was found to be elevated in lungs of patients with ALI (Weiland et al., 1986), as well as in their bronchoalveolar lavage (BAL) (Suter et al., 1992). Collagenase (MMP8), stored in secondary granules of neutrophils can degrade collagen types I, II, and III. MMP8 activity is upregulated in lungs of patients with ALI (Christner et al., 1985). MMP2 and MMP9, the gelatinases stored in gelatinase granules of neutrophils, can degrade collagen type IV, which makes up basement membranes, as well as gelatin. MMP9 levels were found to be elevated in the BAL of patients in the early stages of ARDS (Delclaux et al., 1997).

Finally, neutrophils produce reactive oxygen species, such as hydrogen peroxide and superoxides. Moreover, myeloperoxidase (MPO) stored in primary granules can catalyze the release of oxidants like hypochlorous acid (HOCl), which introduces pro-mutagenic DNA adducts (Güngör et al., 2010b). Patients with ALI have elevated levels of MPO in their BAL.

3-1.4. The role of inflammation in metastasis

Recent reports demonstrate a positive association between lung inflammation and metastasis to the lungs. For instance, in a mouse model of autoimmune arthritis (AA), characterized by upregulated bone and lung inflammation, arthritic mice showed increased lung metastasis of mammary fat pad-injected 4T1 cells, accompanied by a high degree of neutrophil infiltration in the lungs and high levels of MMP9, IL-17, and monocyte colony-stimulating factor (M-CSF) in the BAL fluid. Interestingly, metastasis in AA mice was significantly suppressed by blocking inflammation, using anti- IL-17, either alone or with the Cox-2 inhibitor celecoxib (Das Roy et al., 2009).

Another study tested the effect of surgery, and specifically endotoxin contamination during surgery, on metastasis. 4T1 mouse breast cancer cells were injected intravenously, followed by laparoscopic surgery (with air sufflation), laparatomy (midline incision), or LPS intraperitoneal injection. Both surgery and LPS challenge increased metastatic burden in lungs, accompanied by increased proliferation and decreased apoptosis in nodules (Pidgeon et al., 1999). Increased levels of LPS in circulation as a result of surgery or LPS challenge strongly correlated with increased circulating VEGF levels, indicating that LPS in the circulation enhances metastasis by increasing tumor proliferation, reducing tumor apoptosis, and promoting the production of VEGF (Pidgeon et al., 1999). Furthermore, LPS induced vascular permeability in mouse lungs and increased protein levels of inducible nitric oxide synthase (iNOS) and MMP2 in lung nodules, increasing extravasation of 4T1 tumor cells via a NOS-dependent mechanism (Harmey et al., 2002).

Moreover, bacterial- or LPS-induced lung inflammation through intranasal instillation enhanced lung metastasis of intravenously injected tumor cell lines, including B16-F10 melanoma, 4T1 breast cancer, RM-9 prostate cancer, and LLC lung cancer, as well as the metastasis of 4T1 orthotopic breast tumors to the lungs. This was mediated by increased extracellular ubiquitin levels in inflamed lungs, inducing migration via the CXCR4 receptor on the surface of tumor cells (Yan et al., 2013). Furthermore, E-selectin, an inflammation-inducible endothelial cell adhesion molecule, mediated lung metastasis of intravenously injected 4T1 cells in response to systemic LPS, and this could be attributed to increased adhesion of tumor cells to lung endothelial cells (Jiang et al., 2014). E-selectin binds a molecule on leukocytes and tumor cells called sialyl Lewis x (sLex), which allows cells to be tethered to endothelial cells and to extravasate (Gout et al., 2008). E-selectin expression on endothelial cells is induced in response to pro-inflammatory mediators, like TNFα, IL-1β, VEGF, and LPS (Stannard et al., 2007; Vestweber and Blanks, 1999). Moreover, intraperitoneal LPS treatment enhanced the lung metastatic growth of CT26 colon cancer and 4T1 breast cancer cell lines injected intravenously into mice, via a mechanism that involves LPS-driven induction of TNFα in host cells, leading to the paracrine activation of NF-κB signaling in tumor cells, upregulating proliferation and suppressing apoptosis (Luo et al., 2004).

In a different model of lung inflammation, lung epithelial activation of NF-kB by intratracheal instillation of an adenoviral vector expressing the active molecule of NF-κB, RelA (Ad-RelA), also known as p65, led to an initial influx of neutrophils, followed by recruitment and accumulation of macrophages, which

were the main effector cells promoting LLC tumor cell metastatic outgrowth in the lungs (Stathopoulos et al., 2008).

Despite the above studies describing the link between inflammation and metastasis, the underlying mechanisms governing the contribution of the inflammatory distal microenvironment to enhanced metastasis are not fully understood.

3-1.5. Tsp-1 as a mediator of pulmonary homeostasis

Tsp-1 mRNA expression can be detected in the mouse lung at embryonic day 14 and persists to embryonic day 18 (Iruela-Arispe et al., 1993). It is expressed in the bronchi by columnar epithelial cells, and the protein localizes to the basement membrane of the nascent bronchi in the mouse embryo (O'Shea and Dixit, 1988). Tsp-1 protein can also be detected in the basement membrane in the adult lungs (O'Shea and Dixit, 1988; Wight et al., 1985).

In Tsp-1-deficient mice, signs of lung inflammation are visible starting 4 weeks of age, and consist of neutrophil and macrophage infiltration, followed by collagen and elastin deposition, and airway epithelial thickening due to epithelial hyperplasia (Lawler et al., 1998). Furthermore, recruited macrophages become laden with the iron storage complex hemosiderin, an indicator of alveolar hemorrhage, subsequent to tissue damage (Lawler et al., 1998).

These studies suggest that Tsp-1 is a mediator of lung homeostasis, at least partly through the regulation of the inflammatory response. Tsp-1 deficiency results in longer inflammation and confers worse lung fibrosis in response to bleomycin treatment (Ezzie et al., 2011; Lamy et al., 2007).

Based on the extensive literature describing the intricate connection between inflammatory components, the premetastatic niche, and metastasis, we undertook a comprehensive mechanistic approach to determine the direct impact of pre-existing lung inflammation, caused by external insults, on metastasis progression.

3-2. RESULTS

3-2.1. Lung inflammation enhances metastatic outgrowth.

To determine the contribution of the inflammatory microenvironment to the outgrowth of metastasis, we experimentally induced an inflammatory state in mouse lungs through intranasal instillation of LPS. We used LPS, as it is a well-known inducer of inflammation, previously used to study colon cancer and breast cancer metastasis to the lung (Jiang et al., 2014; Luo et al., 2004; Yan et al., 2013). Importantly, mechanisms of LPS-mediated inflammation are well described. Both systemic or intranasal administration of LPS has been reported to induce neutrophil influx to the lungs (Jiang et al., 2014; Luo et al., 2004; Yan et al., 2013). Furthermore, the binding of LPS to TLR4 on immune cells leads to activation of NF-κB, promoting the expression of pro-inflammatory cytokines, including IL-1β, TNFα, and IL-6 (Takeuchi and Akira, 2010). In addition to acute lung injury (ALI), whose major causative factor is LPS (Brigham and Meyrick, 1986), other lung inflammatory conditions are marked with increased neutrophil influx and upregulation of the mentioned pro-inflammatory cytokines, including severe asthma (Fahy, 2009), COPD (Chung, 2001; Jeffery, 1998), and pneumonia (Craig et al., 2009; Yamamoto et al., 2014). With respect to the route of LPS administration, intranasal delivery was used to generate lung-specific inflammation, since our goal was to determine

the impact of pulmonary inflammation on promoting metastasis to the lung. As expected, intranasal LPS administration resulted in recruitment of neutrophils, determined by myeloperoxidase staining, specifically to the lungs and not to other organs, including the liver and kidneys, indicating the absence of systemic inflammation (**Figure 3.2a).** Administration of luciferase-labeled Lewis lung carcinoma (LLC) cells that are metastatic to the lungs (Gao et al., 2008; Kim et al., 2009) via tail vein resulted in significantly increased metastatic burden in the LPS-challenged lungs compared to controls (**Figure 3.2b**). Similarly, the tail vein-injected B16-BL6 melanoma cell line that is metastatic to lungs (Nakamura et al., 2002) showed increased metastatic lesions following LPS challenge (**Figure 3.2c**), suggesting that the contribution of inflammation to metastasis is relevant across tumor types. Next, we determined if LPS-mediated inflammation in the lungs would enhance melanoma metastasis from the orthotopic site. To this end, B16-BL6 melanoma cells were implanted subcutaneously in the flank and allowed to form primary tumors for three weeks. Mice were then challenged with LPS for a week, after which primary tumors were resected and metastasis was allowed to proceed for another three weeks. At the time of lung harvest, LPS-challenged lungs showed enhanced metastasis from subcutaneous B16-BL6 primary melanoma tumors (**Figure 3.3a**). These results suggest that inflammation in distant organs can accelerate the rate of metastasis of primary tumors.

Figure 3.2. LPS-driven lung inflammation enhances metastatic outgrowth of tail vein-injected tumor cell lines.
(a) Representative IHC of myeloperoxidase (MPO) in lungs, livers, and kidneys of mice challenged intranasally with 12.5 µg of LPS or the equivalent volume of PBS (Ctrl). Insets show magnified areas of lung.
(b) Top panel, Quantitation of pulmonary metastasis by bioluminescence imaging of mice challenged with PBS (Ctrl) or LPS, followed by tail-vein injection of $1x10^5$ luciferase-labeled LLC cells, 3 days after last PBS/LPS dose. BLI estimates were obtained at day 15 following tail vein injections and are represented as means ± SEM (n= 5 mice/ group). *, p=0.048 (one-tailed Mann-Whitney U test). Bottom panel, Representative BLI showing increased metastatic burden in intranasal LPS-treated mice.
(c) Top panel, Quantitation of B16-BL6 melanoma lung metastases in mice following intranasal administration of PBS (Ctrl), or LPS. Stereological measurements were obtained 18 days following tail vein injection of $2x10^5$ B16-BL6 cells. Data are plotted as the means ± SEM (n=10/ group). **, p=0.002 (one-tailed t test with Welch's correction). Bottom panel, Representative H&E stains showing increased metastatic burden in LPS-challenged mice.
*(Data in Figure 3.2 generated in collaboration with Dr. R. Catena. Panels **a** and **b** generated by R. Catena.)*

Figure 3.2

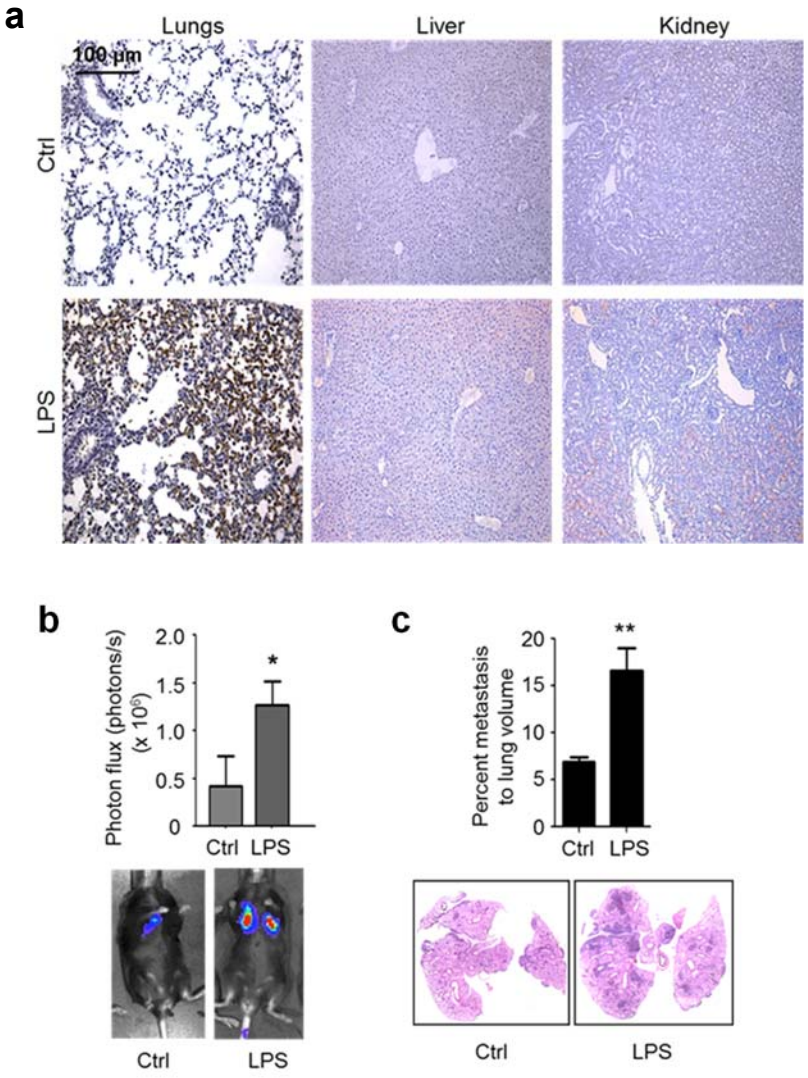
a
Lungs
Liver
Kidney
100 μm
Ctrl
LPS
b
Photon flux (photons/s) (x 10^6)
2.0
1.5
1.0
0.5
0
*
Ctrl
LPS
Ctrl
LPS
c
Percent metastasis to lung volume
20
15
10
5
0
**
Ctrl
LPS
Ctrl
LPS

Figure 3.3. LPS-driven lung inflammation enhances metastatic outgrowth of orthotopically implanted melanoma.
(a) Left panel, Quantitation of metastasis in lungs of PBS- (Ctrl) or LPS-challenged mice, 6 weeks post primary tumor inoculation. Data represented as mean ± SD. (n=3 Ctrl mice and 4 LPS mice. 5-8 sections per lung were analyzed stereologically. p= 0.025, one-tailed Mann-Whitney U test). Right panel, Representative H&E staining of PBS- (Ctrl) and LPS-challenged lungs, 6 weeks post primary tumor inoculation.
(b) Top panel, Immunofluorescence-based quantitation of neutrophil recruitment to lungs, 3 days after the last intranasal administration of PBS (Ctrl) or LPS. Data represented as mean ± SEM. (n= 3 mice per group, 2 sections per lung, 8 fields per section). $p<0.0001$, one-tailed Mann-Whitney U. Bottom panel, Representative immunofluorescence micrographs of neutrophils in lungs. Ly6G in green, DAPI in blue. Scale bar = 20 μm.
(c) Immunofluorescence-based quantitation of $CD45^+$ cell recruitment to lungs of non-tumor-bearing (Ctrl) mice, or tumor-bearing PBS-treated (Tum-Ctrl) or LPS-treated (Tum-LPS). Data represented as mean ± SEM. (n= 3 mice per group, 2 sections per lung, 9 fields per section). $p<0.0001$, one-tailed t test for comparisons between Ctrl and Tum-Ctrl, as well as Ctrl and Tum-LPS.

Figure 3.3

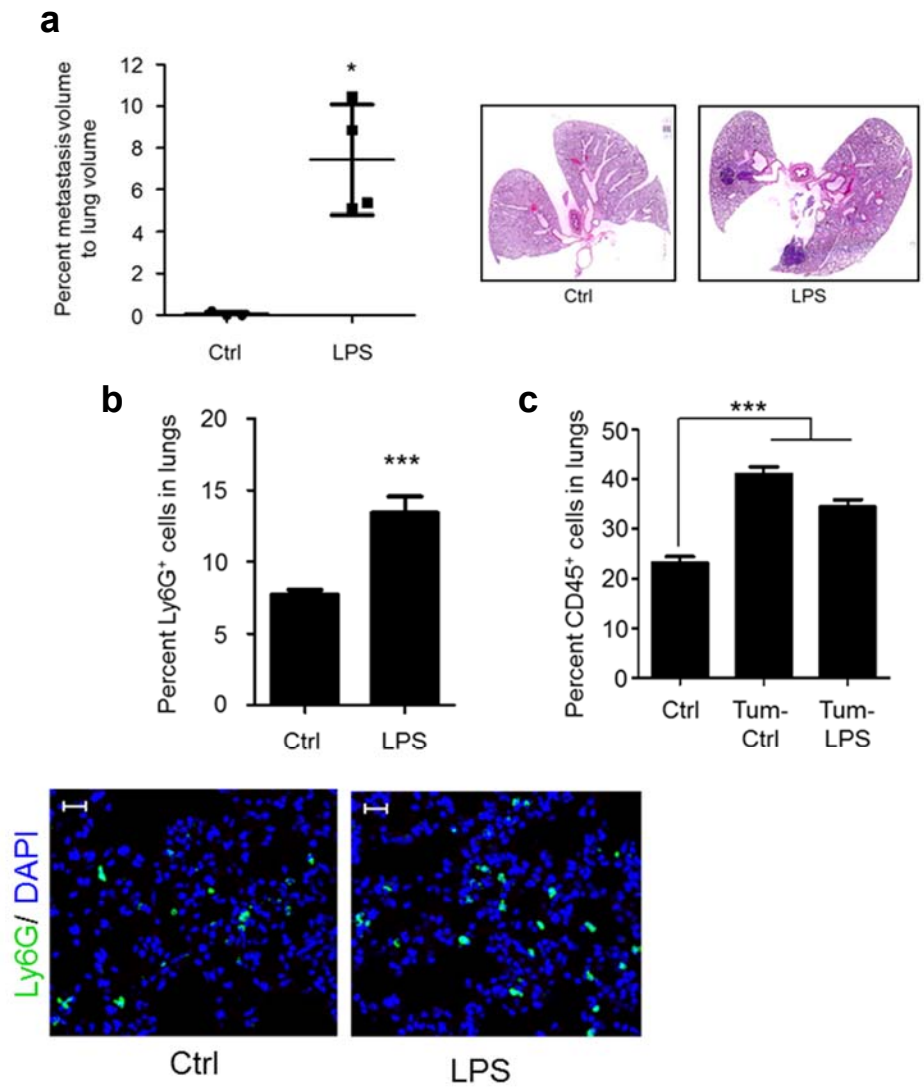
a
Percent metastasis volume to lung volume
12
10
8
6
4
2
0
*
Ctrl
LPS
Ctrl
LPS
b
Percent Ly6G+ cells in lungs
20
15
10
5
0
***
Ctrl
LPS
c
Percent CD45+ cells in lungs
50
40
30
20
10
0
***
Ctrl
Tum-Ctrl
Tum-LPS
Ly6G/ DAPI
Ctrl
LPS

3-2.2. Inflamed lungs show enhanced neutrophil recruitment that promotes metastatic outgrowth, and upregulation of cytokines.

To further understand this phenomenon of enhanced metastasis, we evaluated the cellular composition of inflammatory cells in tumor-free LPS-challenged lungs. Flow cytometry analysis revealed significantly increased recruitment (>7-folds) of bone marrow (BM)-derived $CD45^+$ $CD11b^+$ $Ly6G^+$ neutrophils in LPS-challenged lungs compared to control lungs (**Figure 3.4a**). Increased recruitment of $CD11b^+$ $Ly6G^+$ cells in LPS-challenged lungs was corroborated by immunofluorescence staining (**Figure 3.4b**). Interestingly, increased recruitment of $Ly6G^+$ neutrophils was also observed in the lungs of primary melanoma-bearing mice, after LPS challenge, while total $CD45^+$ cells recruited remained unchanged (**Figure 3.3b, c**).

On the molecular level, elevated expression of inflammatory mediators, including interleukin-1 beta (IL-1β), tumor necrosis factor alpha (TNFα), interleukin-6 (IL-6), and Cox-2, was detected in the LPS-challenged lungs and in $Ly6G^+$ cells sorted from these lungs (**Figure 3.4c, d**). These results suggested that neutrophil–mediated inflammation in the lungs contributes to the enhanced metastasis. To evaluate this hypothesis, neutrophils were depleted by using anti-Ly6G neutralizing antibody (Daley et al., 2008), and metastasis of tail vein-injected LLC cells was monitored following LPS challenge. The efficiency of neutrophil depletion was assayed in peripheral blood, where the circulating neutrophil population was seen to be significantly depleted (**Figure 3.5b**). Notably, neutrophil depletion resulted in diminished metastatic burden (**Figure 3.5a),** which further confirmed the contribution of neutrophils to metastasis.

Figure 3.4. LPS challenge upregulates neutrophil recruitment and pro-inflammatory mediator expression in the lungs.
(a) Flow cytometry-based quantitation of bone marrow-derived cells in lungs of PBS- (Ctrl) or LPS-challenged lungs 3 days after the last treatment. Fold increase depicted as percentage of each cell population in LPS-treated lungs compared to that in control lungs. Red dotted line represents a fold increase of 1. (n=3 mice/ group). CD45: hematopoietic cells; CD11b: myeloid cells; CD3: T cells; CD25: lymphocytes; B220: B cells; VEGFR1: hematopoietic progenitor cells; F4/80: macrophages; Gr1: myeloid cells; Ly6G: granulocytes (neutrophils); Ly6C: monocytes; c-Kit: hematopoietic progenitor cells; CD49b: natural killer (NK) cells; CD11c: dendritic cells.
(b) Representative immunofluorescence staining of $CD11b^+$ and $Ly6G^+$ cells in lungs from PBS- (Ctrl) and LPS-treated mice. Magnified panel shows colocalization CD11b and Ly6G markers (white arrows, n=5 mice, 4 sections per mouse, 7-10 fields per section).
(c) Representative quantitative RT-PCR depicting the normalized fold expression of the pro-inflammatory cytokines IL-1β, IL-6, and TNFα in LPS-challenged lungs compared to control PBS-challenged lungs.
(d) Representative quantitative RT-PCR depicting the normalized fold expression of the pro-inflammatory cytokines IL-1β, IL-6, TNFα, and Cox-2 in $Ly6G^+$ cells sorted from LPS-challenged lungs compared to control PBS-challenged lungs. Control expression levels are set to 1. Numbers signify fold expression relative to controls. (n=3 mice per group. Experiment was repeated 3 times with comparable results).
*(Data in Figure 3.4 generated in collaboration with Dr. R. Catena. Panels **a** and **b** generated by R. Catena.)*

Figure 3.4

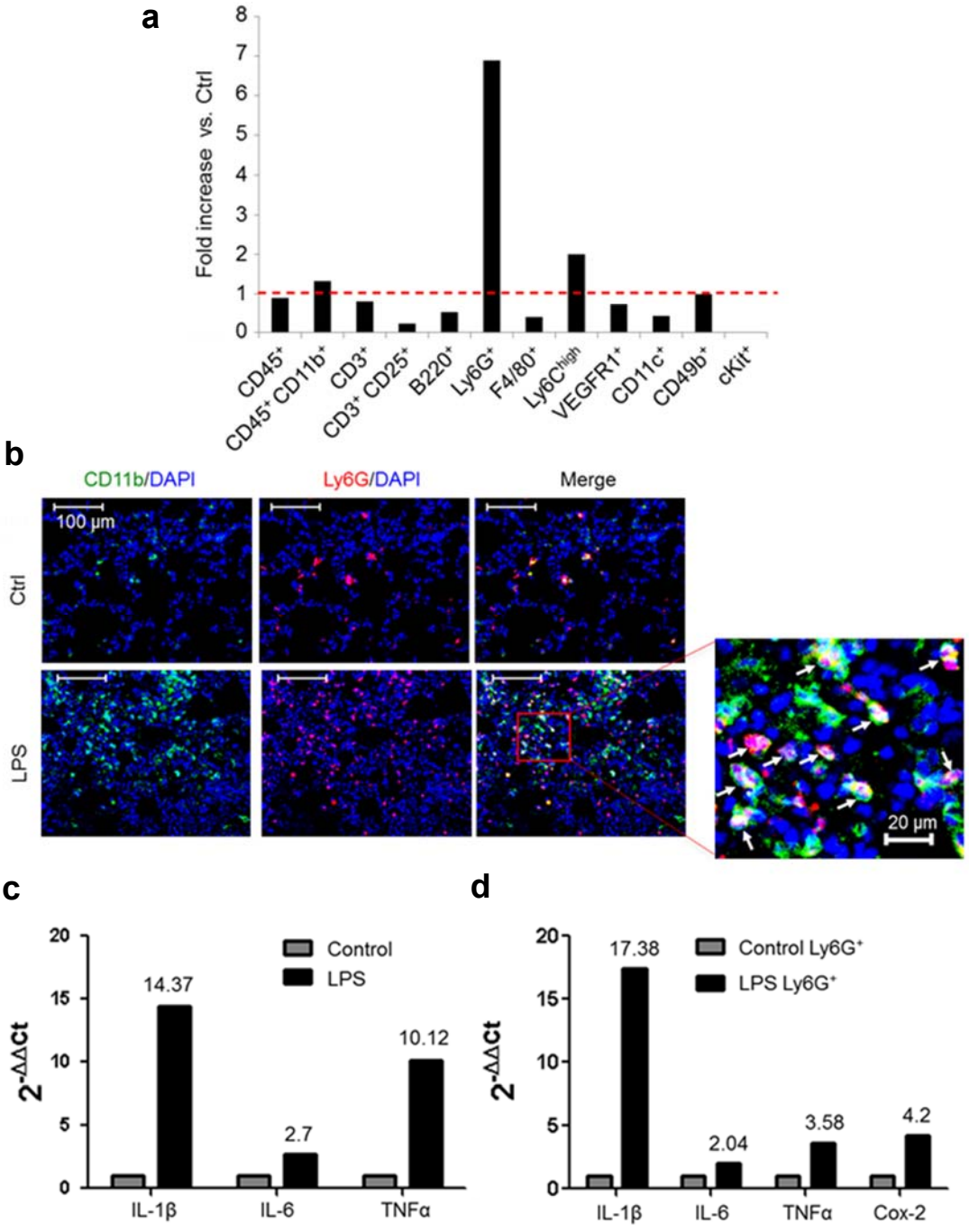
a
Fold increase vs. Ctrl
CD45+
CD45+ CD11b+
CD3+
CD3+ CD25+
B220+
Ly6G+
F4/80+
Ly6Chigh
VEGFR1+
CD11c+
CD49b+
cKit+
b
CD11b/DAPI
Ly6G/DAPI
Merge
100 μm
Ctrl
LPS
20 μm
c
Control
LPS
14.37
2.7
10.12
2-ΔΔCt
IL-1β
IL-6
TNFα
d
Control Ly6G+
LPS Ly6G+
17.38
2.04
3.58
4.2
IL-1β
IL-6
TNFα
Cox-2

Figure 3.5

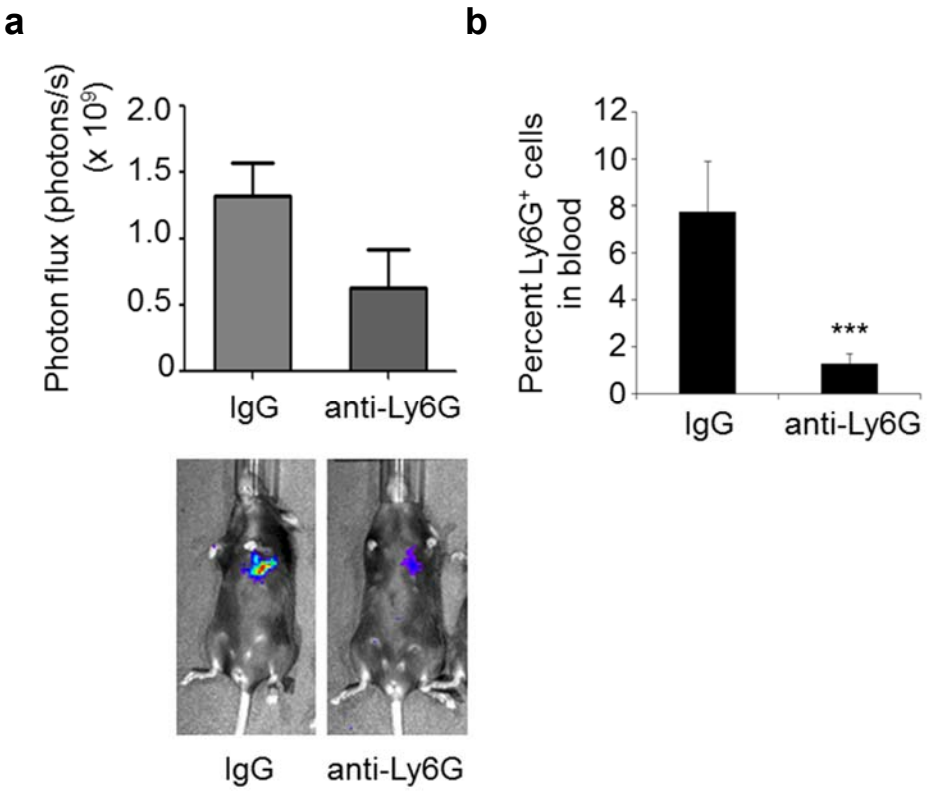

Figure 3.5. Depletion of Ly6G$^+$ neutrophils reduces metastatic outgrowth of tail vein-injected LLCs following LPS challenge.
(a) Top panel, Quantification of pulmonary metastases using BLI at day 21 in mice administered with IgG isotype antibody or anti-Ly6G neutralizing antibody, followed by tail vein injection of luciferase-labeled LLC cells (n=5 per group). Bottom panel, Representative BLI images.
(b) Flow cytometry-based quantification of Ly6G$^+$ cells in the peripheral blood of isotype-treated and anti-Ly6G-treated mice (n=3 per group). $p < 0.001$ (one-tailed Mann-Whitney U test).
*(Data in Figure 3.5 generated in collaboration with Dr. R. Catena. Panels **a** and **b** generated by R. Catena.)*

3-2.3. Inflamed lungs exhibit loss of Tsp-1 and upregulation of neutrophil serine protease activity.

To elucidate the mechanisms by which neutrophils in the inflamed lungs promote metastasis, we focused on thrombospondin-1 (Tsp-1), a secreted protein, present transiently in the extracellular matrix, which is critical for normal lung homeostasis and inflammation (Ezzie et al., 2011; Lamy et al., 2007; Lawler et al., 1998; Lopez-Dee et al., 2011). More importantly, we had previously demonstrated that myeloid-derived Tsp-1 in lungs is required for metastasis suppression (Catena et al., 2013). Strikingly, Western blot analysis showed almost complete loss of Tsp-1 protein in LPS-inflamed lungs compared to control lungs (**Figure 3.6a**). This observation is novel, as previous studies have described other mechanisms of Tsp-1 cleavage, leading to the generation of cleavage products with their own anti-angiogenic activities (Lawler, 1986; Lee et al., 2006b; Taraboletti et al., 1997) (see discussion). Functionally, Tsp-1 is a potent inhibitor of tumor angiogenesis and growth (Good et al., 1990; Lawler, 1986) suggesting that decreased Tsp-1 protein levels in the inflamed lungs may be the cause of enhanced metastasis. However, given that $Ly6G^+$ neutrophils are a main source of Tsp-1 in the lungs (**Figure 2.4c**) (Catena et al., 2013), it was surprising to observe the dramatic loss of Tsp-1 protein in inflamed lungs, despite the increased influx of $Ly6G^+$ cells. When we analyzed $Ly6G^+$ neutrophils more closely, we discovered that the loss of Tsp-1 protein was not due to a reduction in Tsp-1 mRNA levels within $Ly6G^+$ neutrophils (**Figure 3.6b**), suggesting post-translational regulation of Tsp-1 protein.

Specifically, we hypothesized that Tsp-1 in inflamed lungs may have been subjected to proteolytic degradation. In this context, $Ly6G^+$ neutrophils carry a

Figure 3.6. LPS challenge is associated with loss of Tsp-1 protein and increased neutrophil protease activity in lungs.
(a) Western blot analysis of Tsp-1 levels in the lungs of WT mice challenged with PBS (Control, n=3 mice) or LPS (n=4 mice). β-actin is a loading control. Experiment was reproduced 3 times with comparable results.
(b) Quantitative RT-PCR analysis of Tsp-1 in flow cytometry-sorted $Ly6G^+$ cells from the lungs of PBS- (Ctrl) or LPS-challenged mice. Samples were normalized based on equal $Ly6G^+$ cell numbers, and normalized to GAPDH mRNA. Data are plotted as the means ± SEM (n=3 mice per group, in duplicates). PBS group used as control for relative expression ($2^{-\Delta\Delta Ct}$).
(c) Flow cytometry analysis of CD63 median fluorescence intensity in the $CD11b^+$ $Ly6G^+$ population in lungs of PBS- (Ctrl) and LPS-challenged mice. Data are plotted as the means ± SEM (n=4/ group). *, p=0.029 (one-tailed Mann-Whitney U test). Experiment was reproduced twice with comparable results.
(d) Neutrophil elastase activity (Left panel) and cathepsin G activity (Right panel) in lungs of PBS-treated (Ctrl) and LPS-treated mice. Activity presented as relative fluorescence unit per minute (RFU/min) and plotted as the means ± SEM (n=4 per group). *, p= 0.018 and 0.029 for elastase activity and cathepsin G activity, respectively (one-tailed Mann-Whitney U test).
*(Data in Figure 3.6 generated in collaboration with Dr. R. Catena. Panel **d** generated by R. Catena.)*

Figure 3.6

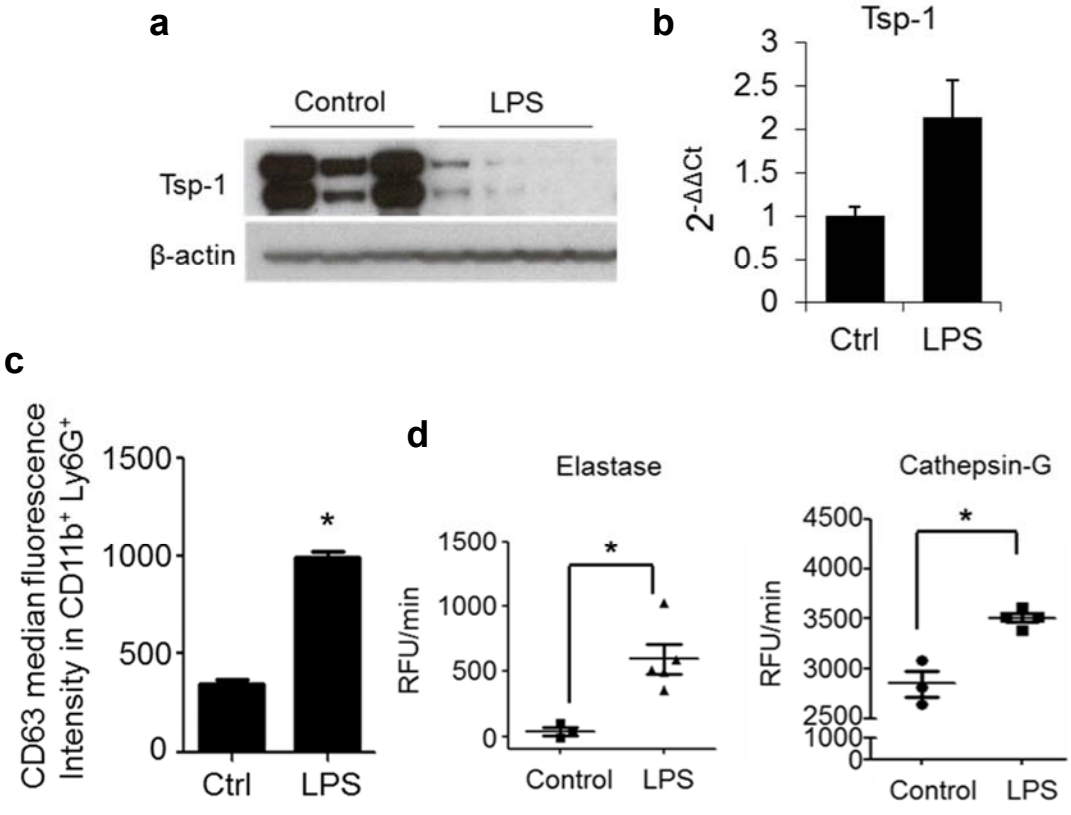
a
Control
LPS
Tsp-1
β-actin
b
Tsp-1
$2^{-\Delta\Delta Ct}$
3
2.5
2
1.5
1
0.5
0
Ctrl
LPS
c
CD63 median fluorescence Intensity in CD11b+ Ly6G+
1500
1000
500
0
*
Ctrl
LPS
d
Elastase
RFU/min
1500
1000
500
0
*
Control
LPS
Cathepsin-G
RFU/min
4500
4000
3500
3000
2500
1000
0
*
Control
LPS

variety of granules which are stores for specific proteases, among which two serine proteases, neutrophil elastase (NE) and cathepsin G (CG), have been shown to possess high binding affinities for Tsp-1 (Hogg et al., 1994). Given that NE and CG are stored in specialized azurophilic granules, and inflammation is a major trigger of neutrophil degranulation (Faurschou and Borregaard, 2003; Korkmaz et al., 2010), we speculated that degranulating neutrophils in the inflamed lungs, by virtue of secreting NE and CG, may have resulted in Tsp-1 proteolysis. Indeed, increased neutrophil degranulation was detected in LPS-challenged inflamed lungs compared to controls (**Figure 3.6c**), as determined by increased cell surface presentation of the azurophilic granule membrane molecule, CD63, on $Ly6G^+$ neutrophils (Kuijpers et al., 1991; Simard et al., 2010). CD63 is exclusively expressed on the membrane of azurophilic granules of resting neutrophils, and is a marker of azurophilic granule fusion with the neutrophil plasma membrane during degranulation (Kuijpers et al., 1991). Increased neutrophil degranulation was associated with enhanced activity of both NE and CG proteases in LPS-inflamed lungs compared to controls (**Figure 3.6d**).

3-2.4. A genetic model of inflammation captures key events observed in LPS-driven inflammation.

To evaluate whether the observations derived from the LPS model of inflammation are generalizable to other models of inflammation, we used a genetic model of inflammation. In the CCSP-rtTA;tetO-IL-1β bitransgenic mouse model of inflammation, the potent inflammatory cytokine IL-1β is conditionally expressed in the lung epithelium, under the Clara cell secretory protein (CCSP) promoter, when mice are administered with doxycycline

(Lappalainen et al., 2005). In this model, induction of IL-1β causes a significant increase in neutrophils in the BAL of mice, and causes pulmonary inflammation in the adult murine lung (Lappalainen et al., 2005). Consistent with the LPS model, lungs from IL-1β bitransgenic mice fed with doxycycline showed significantly increased recruitment of $Ly6G^+$ neutrophils, and elevated levels of pro-inflammatory mediators, including IL-1β, TNFα, and Cox-2, compared to their littermates (**Figure 3.7a, b**). Notably, there was a significant increase in NE and CG activity, associated with degradation of Tsp-1 protein in the lungs (**Figure 3.7c, d**). These results demonstrate that the observed loss of Tsp-1 protein is an effect of lung inflammation rather than an artifact of LPS challenge. Taken together, these data suggest that NE and CG are likely candidates causing proteolytic degradation of Tsp-1.

3-2.5. NE and CG degrade Tsp-1 *in vitro.*

To demonstrate that NE and CG actually possess Tsp-1 proteolysis activity, we performed *in vitro* proteolysis assays, in which recombinant Tsp-1 protein was incubated with either recombinant NE or CG proteins for different time intervals, followed by a Western blot to detect Tsp-1 protein levels. Both NE and CG resulted in the degradation of Tsp-1, and this degradation was blocked in the presence of protease-specific inhibitors (**Figure 3.8a, b)**. We also tested Sivelestat (ONO-5046), a pharmacological inhibitor of NE (IC_{50} = 44 nM, Ki = 0.2 μM), that has been shown to prevent acute lung injury in animal models (Hagio et al., 2004, 2005) and is currently in Phase III clinical trials for ALI associated with systemic inflammatory response syndrome (SIRS) (Iwata et al., 2010). As expected, Sivelestat inhibited NE-mediated

Figure 3.7. Ectopic expression of IL-1β in lungs promotes neutrophil recruitment and Tsp-1 degradation.
(a) Left panel, Representative scatter plots depicting flow cytometry analysis of $Ly6G^+$ cells in lungs of CCSP-rtTA; tetO-IL-1β or age-matched control littermates (WT or CCSP-rtTA single transgenic) fed with doxycycline for 10 days (n=5 controls and 7 CCSP-rtTA; tetO-IL-1β). Right panel, Flow cytometry-based quantification of $Ly6G^+$ cells in lungs of CCSP-rtTA; tetO-IL-1β mice or controls fed with doxycycline for 10 days. Data are plotted as means ± SEM (n=5 controls and 7 CCSP-rtTA; tetO-IL-1β). *, p= 0.006 (one-tailed t test).
(b) Representative quantitative RT-PCR depicting the normalized expression of the pro-inflammatory mediators IL-1β, TNFα, and Cox-2 in lungs of CCSP-rtTA; tetO-IL-1β mice and controls fed with doxycycline for 10 days. (n=5 controls and 7 CCSP-rtTA; tetO-IL-1β, in duplicates). Means ± SEM are shown. p=0.005, p=0.025, and p=0.01 for IL-1β, TNFα, and Cox-2, respectively (one-tailed t test for IL-1β and TNFα; one-tailed Mann-Whitney U test for Cox-2).
(c) Neutrophil elastase (Left panel) and cathepsin G (Right panel) activity in lungs of CCSP-rtTA; tetO-IL-1β mice and controls fed with doxycycline for 10 days. (n=5 controls and 7 CCSP-rtTA; tetO-IL-1β). Activity represented as relative fluorescence unit per minute (RFU/min). Means ± SEM are shown. *, p= 0.038 for elastase activity (one-tailed t test), and p= 0.013 for cathepsin G activity (one-tailed t test).
(d) Western blot analysis of Tsp-1 in pooled lungs of bitransgenic mice or littermates fed with doxycycline for 10 days. (n=5 controls and 7 CCSP-rtTA; tetO-IL-1β). β-actin is used as loading control.

Figure 3.7

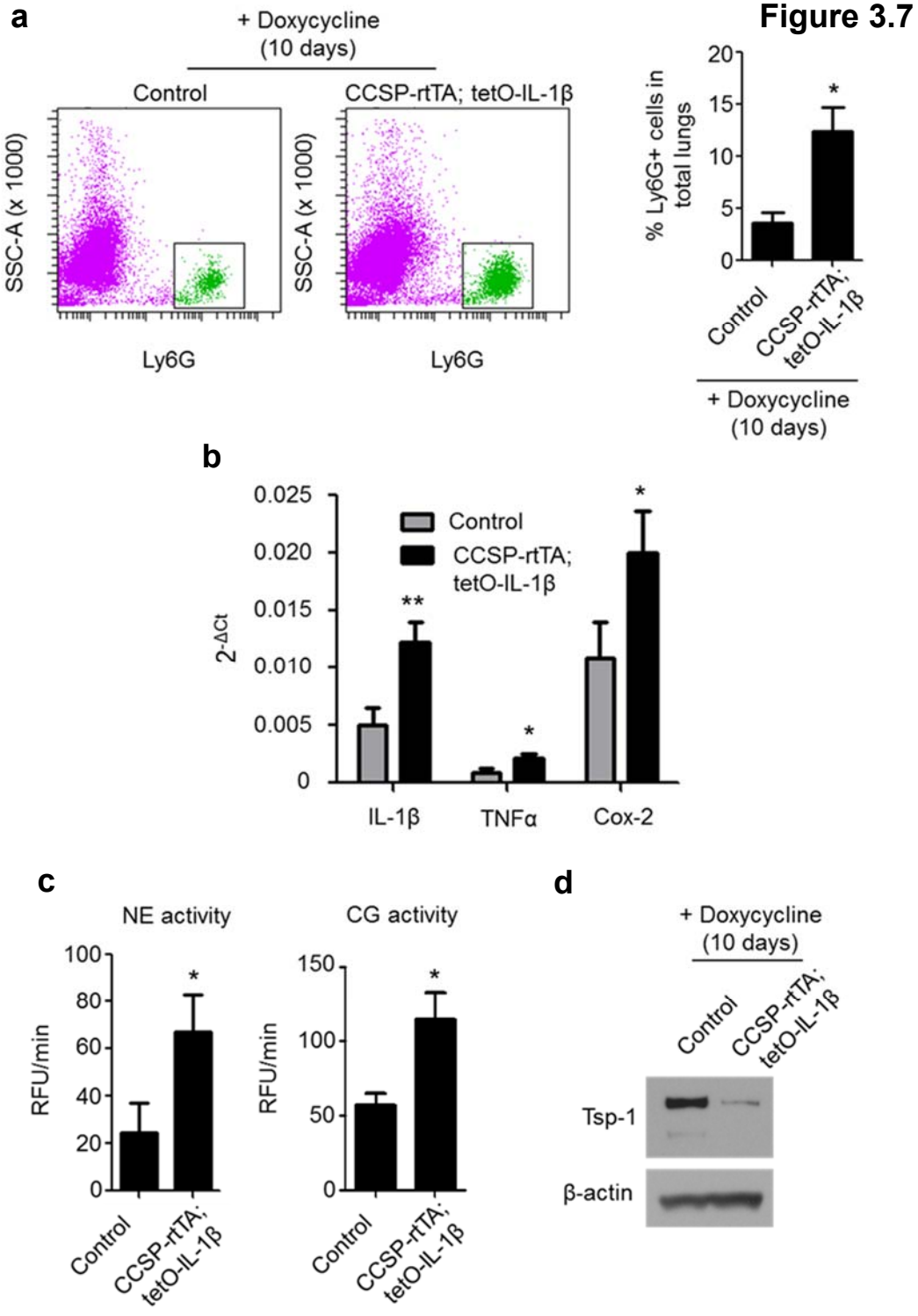
a
+ Doxycycline
(10 days)
Control
CCSP-rtTA; tetO-IL-1β
SSC-A (x 1000)
Ly6G
% Ly6G+ cells in total lungs
Control
CCSP-rtTA; tetO-IL-1β
b
Control
CCSP-rtTA; tetO-IL-1β
2-ΔCt
IL-1β
TNFα
Cox-2
c
NE activity
CG activity
RFU/min
d
Tsp-1
β-actin

Figure 3.8. Neutrophil-derived proteases elastase (NE) and cathepsin G (CG) degrade Tsp-1.
(a, b) *In vitro* degradation assays of recombinant Tsp-1 with recombinant NE and CG proteases, alone, or in combination with the specific inhibitors of NE (N-(Methoxysuccinyl)-Ala-Ala-Pro-Val-chloromethyl ketone) or CG (Z-Gly-Leu-Phe-CMK), and Sivelestat. Recombinant protein incubations were followed by Western blot analysis for Tsp-1 levels. Experiments repeated 3 times with similar results.
(c) Representative flow cytometry analysis of degranulation marker CD63, in $CD11b^+$ $Ly6G^+$ cells cultured *in vitro* with 0.01% DMSO (Ctrl, solid grey histogram), 20 nM TPA (TPA, empty blue histogram), or 20 nM TPA + 0.05 µg/µl Sivelestat (TPA + Siv, solid red histogram).
(d) Representative protease activity assays for elastase (Left panel) and cathepsin G (Right panel) in conditioned media of $Ly6G^+$ cells cultured *in vitro* with 20 nM TPA or 20 nM TPA + 0.05 µg/µl Sivelestat. Activities represented as relative fluorescence units (RFU) as a function of time.
(e) Western blot analysis of Tsp-1 in conditioned media of $Ly6G^+$ cells cultured in the presence of TPA or TPA + Siv at time 0, 30, 60, and 120 min. Ponceau S staining shows equal protein loading.

Figure 3.8

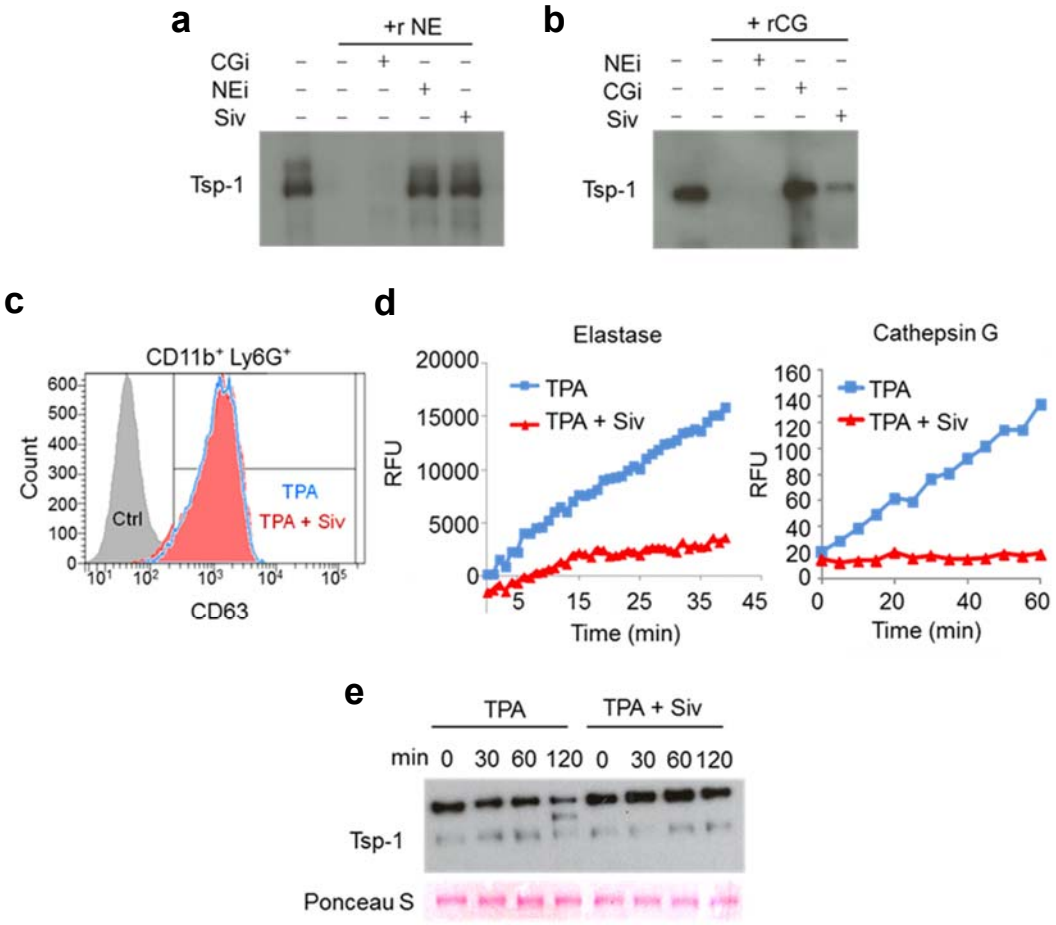
a
+r NE
CGi
NEi
Siv
Tsp-1
b
+ rCG
NEi
CGi
Siv
Tsp-1
c
CD11b⁺ Ly6G⁺
Count
Ctrl
TPA
TPA + Siv
CD63
d
Elastase
RFU
TPA
TPA + Siv
Time (min)
Cathepsin G
RFU
TPA
TPA + Siv
Time (min)
e
TPA
TPA + Siv
min 0 30 60 120 0 30 60 120
Tsp-1
Ponceau S

Tsp-1 proteolysis (**Figure 3.8a**). Strikingly, Sivelestat also reduced CG-mediated Tsp-1 proteolysis (**Figure 3.8b**), thereby exhibiting dual protease inhibitor activity. This is a novel finding, and it could be explained by the fact that NE and CG show high structural similarity and display a root mean square deviation (RMSD) of 1.03 Å when 201 of their α-carbons are superimposed (Averhoff et al., 2008). Furthermore, NE and CG share the same catalytic triad composed of histidine, aspartate, and serine residues at identical positions (His^{57}, Asp^{102} and Ser^{195}) in both enzymes (Korkmaz et al., 2008).

To expand upon the role of neutrophils in Tsp-1 proteolysis through degranulation of proteases, we isolated neutrophils and induced their degranulation using the phorbol ester tetradecanoyl phorbol acetate (TPA), widely used in the literature to study neutrophil activity (Jones et al., 2002; Manara et al., 1991; Xu and Håkansson, 2002). TPA-induced neutrophil degranulation was confirmed by the membrane presentation of CD63 quantified by flow cytometry (**Figure 3.8c**). Conditioned media (CM) from TPA-treated neutrophils showed an increase in NE and CG protease activity (**Figure 3.8d**). TPA-treated neutrophil CM also exhibited proteolysis of endogenous neutrophil-secreted Tsp-1, as determined by time course analysis (**Figure 3.8e**). Notably, Sivelestat concurrently blocked NE and CG protease activity in the CM and protected Tsp-1 from proteolysis (**Figure 3.8d, e**), without inhibiting TPA-mediated neutrophil degranulation (**Figure 3.8c**). These results demonstrate that both NE and CG can degrade Tsp-1. Furthermore, Sivelestat acts as a dual protease inhibitor, protecting Tsp-1 from degradation.

3-2.6. NE and CG degrade Tsp-1 *in vivo*

Our *in vitro* data suggest that Tsp-1 degradation observed in inflamed lungs may be mediated by the activity of the degranulated neutrophil proteases NE and CG. However, to address the causal relationship between increased protease activity and Tsp-1 degradation, we made use of NE and CG double knockout ($NE^{-/-}$ $CG^{-/-}$) mice, which we generated in the lab by breeding $NE^{-/-}$ mice to $CG^{-/-}$ mice (**Figure 3.9a**). We determined that $Ly6G^{+}$ neutrophils harvested from the BM of $NE^{-/-}$ $CG^{-/-}$ mice showed similar degrees of degranulation *in vitro* as neutrophils harvested from the BM of wild type mice following treatment with TPA (**Figure 3.9b**). As expected, neutrophils harvested from $NE^{-/-}$ $CG^{-/-}$ mice lacked significant NE and CG activity (**Figure 3.9c**), and more importantly, failed to induce Tsp-1 degradation, compared to wild type controls *in vitro* (**Figure 3.9d**).

Next, we challenged these mice with LPS to induce lung inflammation. As expected, lungs of wild type control mice showed Tsp-1 degradation; however, lungs of $NE^{-/-}$ $CG^{-/-}$ mice showed protection of Tsp-1 from proteolysis (**Figure 3.10a**). This was not due to degranulation defects, since comparable degranulation of neutrophils was observed in the lungs in both groups, assayed by flow cytometry of CD63 cell surface expression in $Ly6G^{+}$ neutrophils (**Figure 3.10b**).

Taken together, these data suggest that the neutrophil proteases NE and CG mediate Tsp-1 proteolysis both *in vitro* and *in vivo*. Moreover, in contrast to previous studies, where specific Tsp-1 cleavage was shown to contribute to Tsp-1 function (Lawler, 1986; Lee et al., 2006b; Taraboletti et al., 1997), in our study, none of these cleavage products appear in the inflamed lungs of mice

Figure 3.9. $NE^{-/-}$ $CG^{-/-}$ neutrophils don't degrade Tsp-1.
(a) Top panel, Genotyping PCR of $NE^{-/-}$ $CG^{-/-}$ mice compared to $CG^{+/-}$ (het) and $CG^{-/-}$ mice, using CG primers. WT band is 475 bp and mutant band is 330 bp. Bottom panel, Genotyping PCR of $NE^{-/-}$ $CG^{-/-}$ mice compared to WT and $NE^{-/-}$ mice, using NE primers. WT band is 230 bp and mutant band is 310 bp.
(b) Representative flow cytometry analysis of the degranulation marker CD63 in $Ly6G^{+}$ cells isolated from WT (solid purple histogram) or $NE^{-/-}$ $CG^{-/-}$ (empty green histogram) mice and cultured *in vitro* with 20 nM TPA.
(c) Neutrophil elastase activity (Left panel) and cathepsin G activity (Right panel) in conditioned media of $Ly6G^{+}$ cells isolated from WT and $NE^{-/-}$ $CG^{-/-}$ mouse bone marrows and cultured with 20 nM TPA for 30 min. Data are plotted as the means ± SEM (n=3/ group). ***, $p< 0.001$ for NE activity and for CG activity (Analysis of Covariance, ANCOVA, comparing activity curves).
(d) Representative Western blot analysis of Tsp-1 in conditioned media from $Ly6G^{+}$ cells isolated from WT and $NE^{-/-}$ $CG^{-/-}$ mouse bone marrows and cultured with 20nM TPA for t= 0, 2 hours, or 4 hours. Ponceau S stain is used as loading control. Repeated twice with similar results.

Figure 3.9

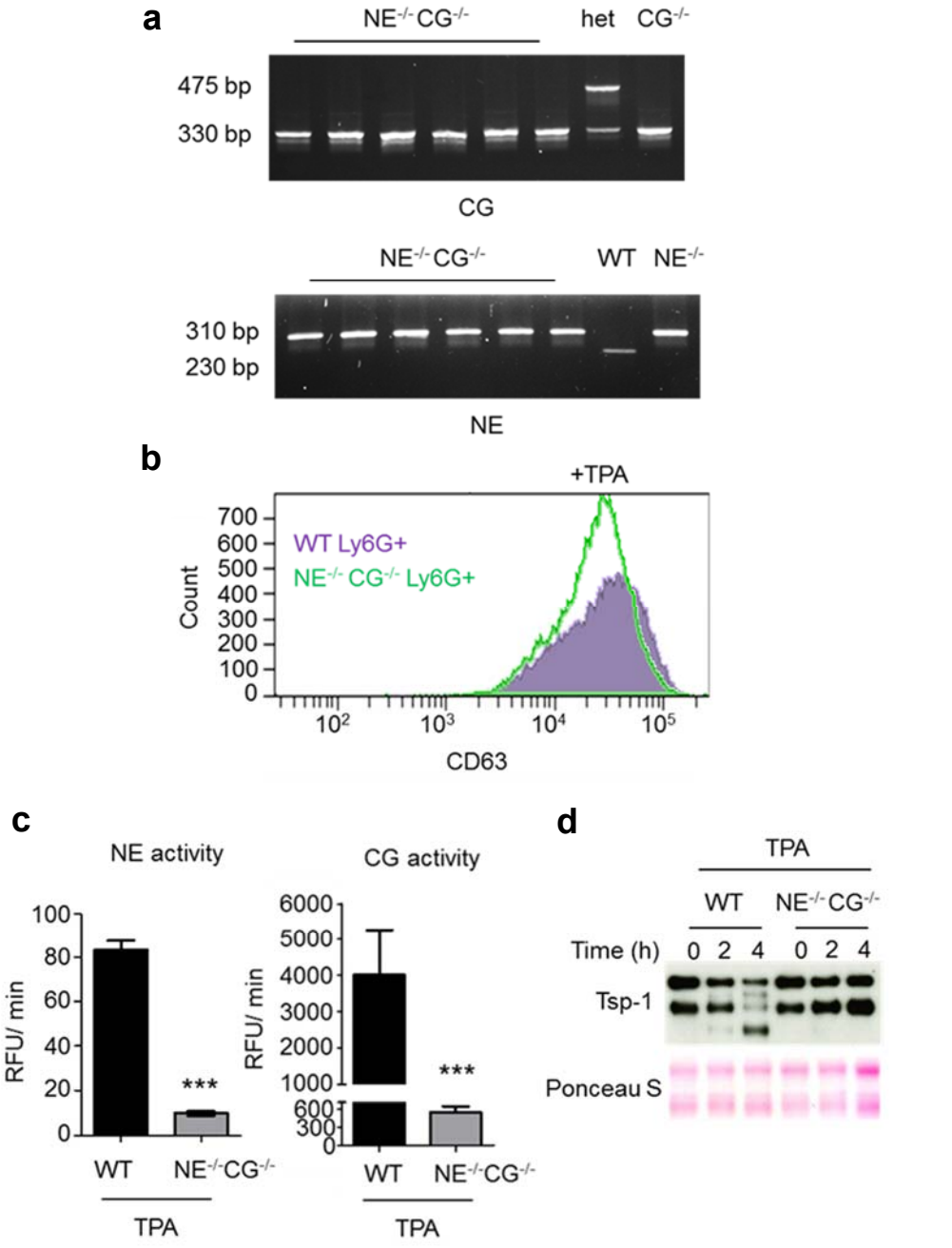
a
NE-/- CG-/-
het
CG-/-
475 bp
330 bp
CG
NE-/- CG-/-
WT
NE-/-
310 bp
230 bp
NE
b
+TPA
WT Ly6G+
NE-/- CG-/- Ly6G+
Count
700
600
500
400
300
200
100
0
10^2
10^3
10^4
10^5
CD63
c
NE activity
CG activity
RFU/ min
100
80
60
40
20
0
6000
5000
4000
3000
2000
1000
600
300
0
***
***
WT
NE-/-CG-/-
TPA
d
TPA
WT
NE-/- CG-/-
Time (h)
0 2 4 0 2 4
Tsp-1
Ponceau S

Figure 3.10

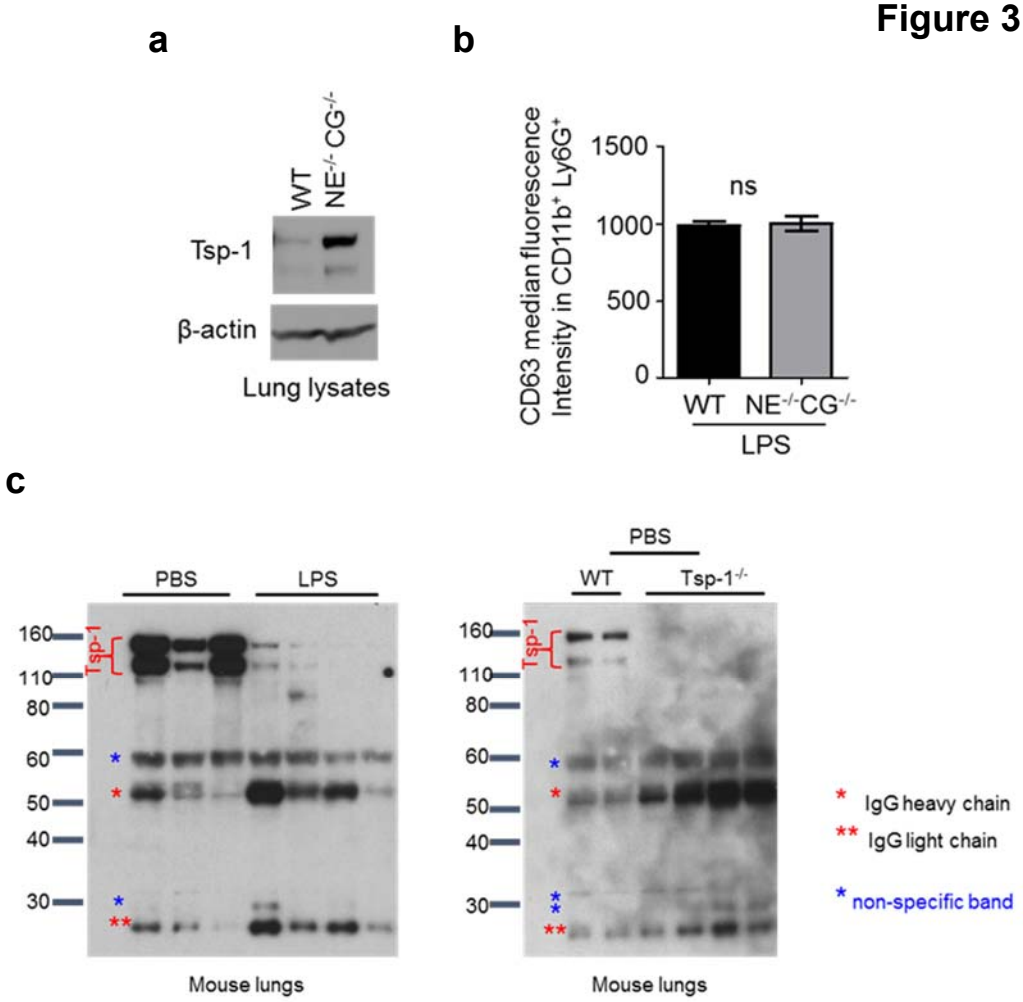

Figure 3.10. Neutrophil-derived NE and CG degrade Tsp-1 *in vivo*.
(a) Western blot analysis of Tsp-1 protein in lungs of WT and $NE^{-/-}$ $CG^{-/-}$ mice (n=4 per group) treated with LPS. Protein samples are pooled from 4 mice per group. β-actin serves as a loading control.
(b) Flow cytometry analysis of the median fluorescence intensity of the degranulation marker CD63 in $CD11b^{+}$ $Ly6G^{+}$ cells in lungs of WT and $NE^{-/-}$ $CG^{-/-}$ mice treated with LPS. Data are plotted as means ± SEM (n= 4 lungs per group). ns: not significant (two-tailed Mann-Whitney U test).
(c) Left panel, Western blot analysis of Tsp-1 in lungs from mice challenged intranasally with PBS or LPS. Full-length Tsp-1 runs as double band between 110 kDa and 170 kDa. Right panel, Western blot analysis of Tsp-1 in lungs from WT and $Tsp\text{-}1^{-/-}$ mice challenged intranasally with PBS. Protein from $Tsp\text{-}1^{-/-}$ mice is used to determine non-specific bands, which appear as a result of using a mouse-derived Tsp-1 antibody on mouse lungs, and having to use an anti-mouse secondary antibody for detection. Of note: The Tsp-1 antibody clone we use is the Ab-11 clone, which has the ability to recognize the N-terminal heparin-binding domain, the calcium-binding domain, and the collagen type V-binding domain of Tsp-1.

(**Figure 3.10c**), suggesting a novel mechanism of Tsp-1 regulation by combined proteolytic activity of NE and CG.

3-2.7.NE- and CG-mediated Tsp-1 degradation is required for inflammation-enhanced metastasis.

To determine the impact of inflammation-driven protease activity on metastasis and the contribution of NE/CG-Tsp-1 axis in promoting metastasis in LPS-inflamed lungs, we generated NE and CG deficiency in the BM. Initially, we generated single deletions in NE or CG separately in the BM by transplanting $NE^{-/-}$ BM or $CG^{-/-}$ BM into irradiated syngeneic WT mice, to generate cohorts of $NE^{-/-}$ BMT or $CG^{-/-}$ BMT mice. As controls, BM from WT mice was transplanted into irradiated WT mice to generate a cohort of WT BMT mice. NE or CG deficiency in the BM did not affect hematopoietic cell composition (**Figure 3.11a**). More importantly, deficiency in only one of the proteases in the BM only partially impaired metastatic outgrowth of tail vein-injected LLC cells after LPS challenge in $NE^{-/-}$ BMT and $CG^{-/-}$ BMT mice compared to WT BMT mice, as determined by BLI analysis (**Figure 3.11b**). This suggests that the activity of both proteases could be necessary to enhance metastasis. To evaluate this hypothesis, we generated $NE^{-/-}$ $CG^{-/-}$ double knockout mice, harvested their BM cells, and transplanted them into irradiated syngeneic wild type mice to generate a cohort of $NE^{-/-}$ $CG^{-/-}$ BMT mice. Importantly, combined NE and CG deficiency in BM cells in $NE^{-/-}$ $CG^{-/-}$ BMT mice did not perturb the mobilization of $Ly6G^{+}$ neutrophils in the peripheral blood, their recruitment to the lung microenvironment, or their degranulation in lungs after LPS treatment (**Figure 3.12a-c**). Furthermore, deficiency of NE and CG in the BM did not disrupt the composition of

Figure 3.11

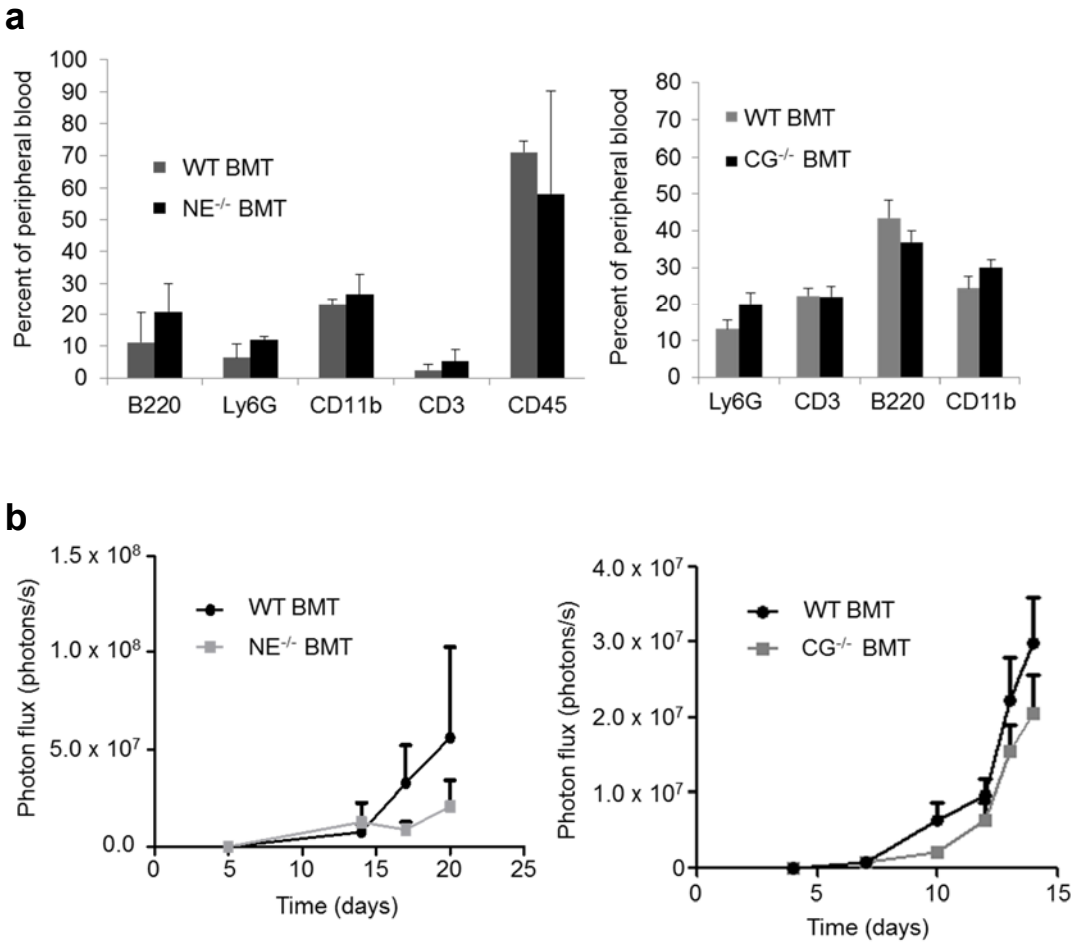

Figure 3.11. Single NE$^{-/-}$ or CG$^{-/-}$ does not significantly impair LPS-mediated metastasis enhancement.
(a) Flow cytometry-based quantitation of hematopoietic cell subsets in blood of WT BMT and NE$^{-/-}$ BMT mice (Left panel) or WT BMT and CG$^{-/-}$ BMT mice (Right panel).
(b) Analysis of bioluminescence imaging showing luciferase-labeled LLC cell outgrowth in lungs of WT BMT and NE$^{-/-}$ BMT mice (Left panel, n= 8 mice/group; p= 0.4796, one-tailed Mann-Whitney U test) or CG$^{-/-}$ BMT mice (Right panel, n= 8 mice/group).
*(Data in Figure 3.11 generated in collaboration with Dr. R. Catena. Panels **a** and **b** generated by R. Catena.)*

Figure 3.12. NE and CG deficiency in the bone marrow compartment does not impact neutrophil recruitment to lungs, their degranulation, or hematopoietic reconstitution.
(a) Flow cytometry-based quantitation of $CD11b^+$ $Ly6G^+$ cells in blood of PBS-treated WT BMT, and LPS-treated WT BMT or $NE^{-/-}$ $CG^{-/-}$ BMT mice. (n= 4 mice per group, p= 0.044 between WT BMT and WT BMT + LPS, and p= 0.016 between WT BMT and $NE^{-/-}$ $CG^{-/-}$ BMT + LPS. Two-tailed t test).
(b) Flow cytometry-based quantitation of $CD45^+$ hematopoietic cells and $Ly6G^+$ neutrophils recruited to lungs of WT BMT and $NE^{-/-}$ $CG^{-/-}$ BMT mice treated with LPS (n= 4 mice per group, Differences are not statistically significant, as determined by two-tailed Mann-Whitney U test). Lungs were collected 3 days after LPS treatment.
(c) Flow cytometry-based quantitation of CD63 mean fluorescence intensity (MFI) of $Ly6G^+$ cells in lungs of WT BMT and $NE^{-/-}$ $CG^{-/-}$ BMT mice treated with LPS (n=4 per group,
p= 0.305 as determined by two-tailed unpaired t test).
(d) Flow cytometry-based quantitation of hematopoietic cell subsets in blood of WT BMT and $NE^{-/-}$ $CG^{-/-}$ BMT mice (p= 0.1 for $CD45^+$ cells; p= 0.4 for $CD11b^+$ cells; p=0.4 for $Ly6G^+$ cells; p= 0.475 for $CD3^+$ cells and p= 0.628 for $B220^+$ cells). Statistical analysis used is two-tailed Mann-Whitney U test.

Figure 3.12

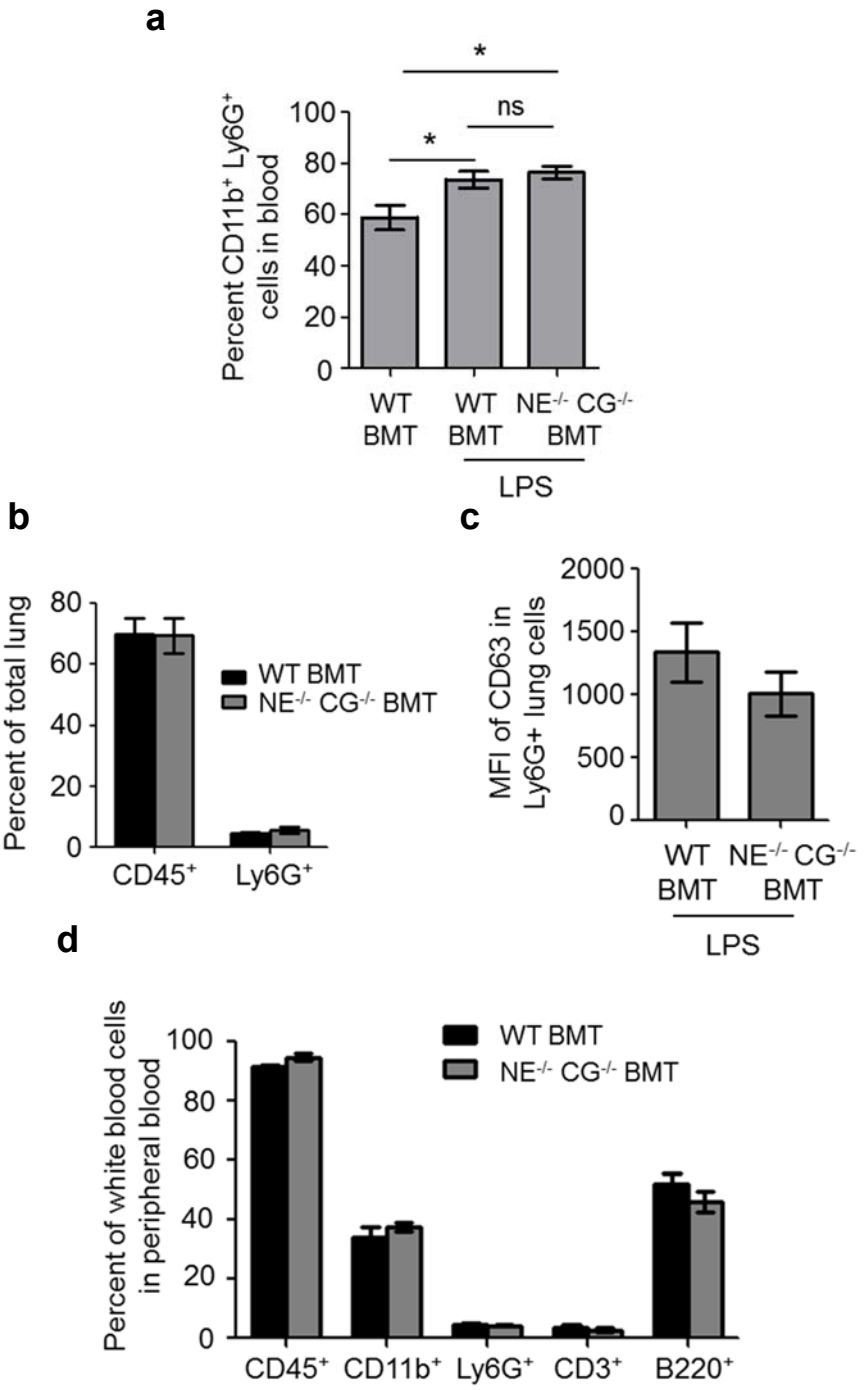
a
*
ns
*
Percent CD11b+ Ly6G+ cells in blood
100
80
60
40
20
0
WT BMT
WT BMT
NE-/- CG-/- BMT
LPS
b
Percent of total lung
80
60
40
20
0
WT BMT
NE-/- CG-/- BMT
CD45+
Ly6G+
c
MFI of CD63 in Ly6G+ lung cells
2000
1500
1000
500
0
WT BMT
NE-/- CG-/- BMT
LPS
d
Percent of white blood cells in peripheral blood
100
80
60
40
20
0
WT BMT
NE-/- CG-/- BMT
CD45+
CD11b+
Ly6G+
CD3+
B220+

hematopoietic cell subsets (**Figure 3.12d**). After having characterized these critical parameters in the $NE^{-/-}$ $CG^{-/-}$ BMT mice, we determined the impact of NE and CG deficiency in the lung microenvironment on metastasis, following inflammation. Strikingly, we observed impaired metastatic outgrowth of tail vein-injected LLC cells after LPS challenge in $NE^{-/-}$ $CG^{-/-}$ BMT mice compared to WT BMT mice, as determined by BLI and analysis of lungs by H&E (**Figure 3.13a**). Western blot analysis of total lung lysates showed protection of Tsp-1 from proteolysis in $NE^{-/-}$ $CG^{-/-}$ BMT mice compared to wild type controls (**Figure 3.13b**). Together, these results demonstrate that both proteases are needed to enhance metastasis in response to inflammation, and the neutrophil NE/CG-Tsp-1 axis is a major contributor to metastasis.

3-2.8. Pharmacological blockade of NE and CG suppresses metastasis.

To determine the clinical feasibility of blocking neutrophil proteases as a potential anti-metastasis strategy, we used a pharmacological approach to inhibit the activity of both proteases. Our finding that Sivelestat inhibits both NE and CG activities (**Figure 3.8**) allowed us to test its therapeutic efficacy in blocking metastasis *in vivo*. Treatment of tumor-bearing mice daily with Sivelestat dramatically blocked metastasis (**Figure 3.14a, b**). Sivelestat did not significantly impact the recruitment of neutrophils to the lungs or influence their degranulation potential (**Figure 3.14c, d**), suggesting that protease inhibition is the main cause of impaired metastasis. It is to be noted that the metastasis experiments with Sivelestat were performed in the absence of LPS challenge. Perhaps, neutrophils recruited by metastasis-initiating nodules were

Figure 3.13

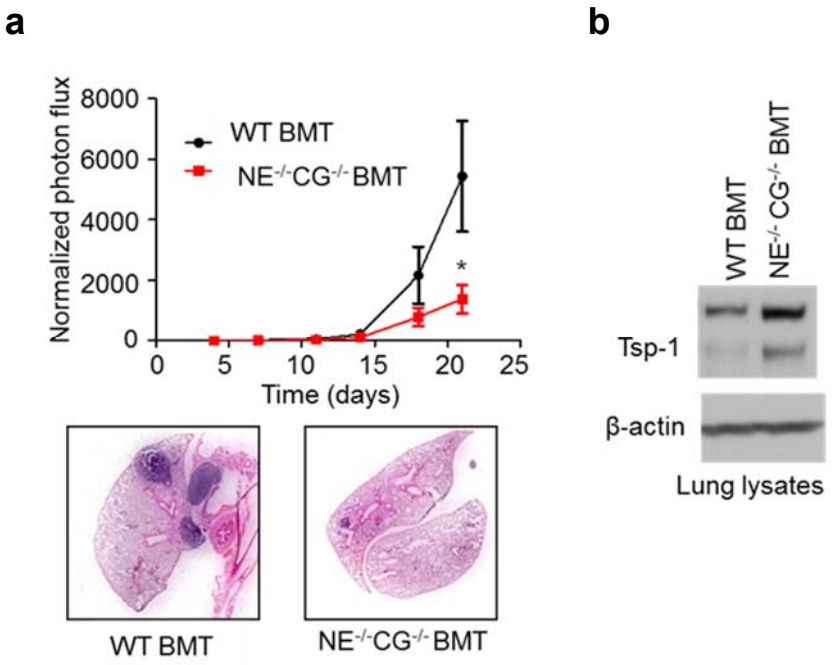

Figure 3.13. Neutrophil-derived NE and CG enhance metastasis.
(a) Top panel, Quantification of metastatic burden via bioluminescence imaging in WT BMT and NE$^{-/-}$ CG$^{-/-}$ BMT mice treated with LPS and tail vein-injected with LLC tumor cells. Signals were normalized to the readings obtained at day 4 for each individual animal. Data at each time point is plotted as means ± SEM (n= 8 mice per group). *, p= 0.038 at day 21 (one-tailed t test with Welch's correction). Bottom panel, Representative H&E stains of lungs collected at day 21 from WT and NE$^{-/-}$ CG$^{-/-}$ BMT mice treated with LPS (n= 8 mice per group).
(b) Western blot analysis of Tsp-1 in lung samples from WT BMT and NE$^{-/-}$ CG$^{-/-}$ BMT mice treated with LPS. Samples are pooled from 3 mice per group. β-actin serves as a loading control**.**

Figure 3.14. Pharmacological inhibition of the proteases using Sivelestat suppresses metastasis.
(a) Quantitation of metastatic burden via bioluminescence imaging in PBS-treated (Ctrl) and Sivelestat-treated (Siv) WT mice tail vein-injected with luciferase-labeled LLC cells. Signals were normalized to the readings obtained at day 5 for each individual animal. (n=7 per group, p= 0.0224 at day 23 as determined by two-tailed t test with Welch's correction). Data are represented as mean ± SEM.
(b) Quantitation of mean lung metastasis area in PBS-treated (Ctrl) and Sivelestat-treated (Siv) mice. (n= 6 per group, p= 0.043 as determined by one-tailed t test). Data are represented as mean ± SEM.
(c) Flow cytometry-based quantitation of $CD11b^+$ $Ly6G^+$ cells in the lungs of control mice (Ctrl, n= 3 mice), LPS-treated mice (n= 4 mice), or LPS and Sivelestat-treated mice (LPS+ Siv, n= 4 mice). p= 0.005 between Ctrl and LPS groups (two-tailed t test with Welch's correction). p= 0.03 between Ctrl and LPS +Siv groups (two-tailed t test with Welch's correction). p= 0.133 between LPS and LPS + Siv groups (two-tailed t test).
(d) Flow cytometry-based quantitation of CD63 median fluorescence intensity in $CD11b^+$ $Ly6G^+$ cells in lungs of PBS-treated (Ctrl), LPS-treated mice (n= 4 mice), or LPS and Sivelestat-treated mice (LPS+ Siv, n= 4 mice). $p < 0.0001$ between Ctrl and LPS groups (two-tailed t test). $p < 0.0001$ between Ctrl and LPS +Siv groups (two-tailed t test). p= 0.08 between LPS and LPS + Siv groups (two-tailed t test).
*(Data in Figure 3.14 generated in collaboration with Dr. R. Catena. Panel **a** generated by R. Catena.)*

Figure 3.14

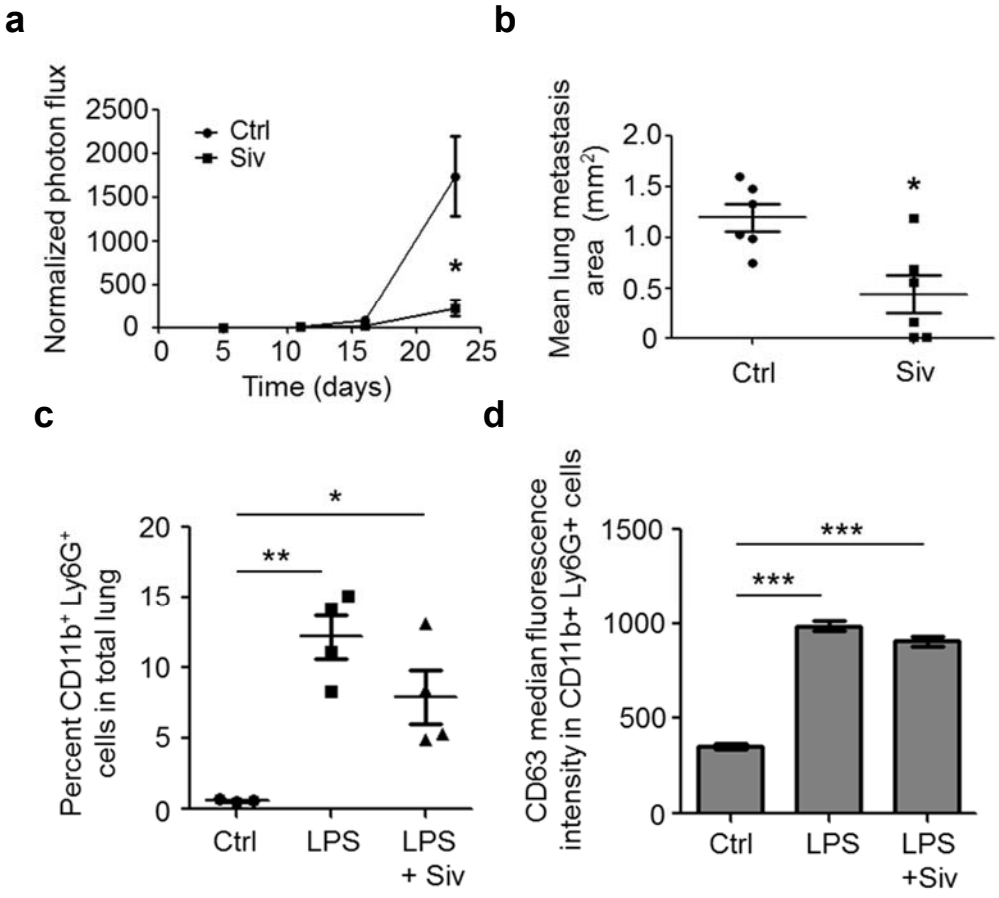
a
b
c
d
Normalized photon flux
2500
2000
1500
1000
500
0
Ctrl
Siv
*
0
5
10
15
20
25
Time (days)
Mean lung metastasis area (mm2)
2.0
1.5
1.0
0.5
0
*
Ctrl
Siv
Percent CD11b+ Ly6G+ cells in total lung
20
15
10
5
0
*
**
Ctrl
LPS
LPS + Siv
CD63 median fluorescence intensity in CD11b+ Ly6G+ cells
1500
1000
500
0
***
***
Ctrl
LPS
LPS +Siv

targeted by Sivelestat to yield significant anti-metastatic phenotypes.
To confirm that the effect of Sivelestat on metastasis was mediated via Tsp-1, we used Tsp-1$^{-/-}$ mice. Notably, Sivelestat was unable to mediate its metastasis-suppressive effects in Tsp-1$^{-/-}$ mice (**Figure 3.15a**). Moreover, in the Tsp-1$^{-/-}$ mice, neutrophil recruitment and degranulation remained unaffected (**Figure 3.15b, c**). Taken together, these data further validate results obtained from genetic ablation of NE and GG, showing that neutrophil protease-mediated degradation of Tsp-1 is necessary for metastasis. Furthermore, they provide a potential pharmacological strategy for targeting metastasis.

3-3. DISCUSSION

We have established that lung inflammation induced by external insults enhances metastatic progression. We have further deciphered the mechanism responsible for this phenotype, and we reveal the novel finding that Ly6G^{+} neutrophils recruited to inflamed lungs degrade Tsp-1 through the action of their serine proteases, NE and CG (**Figure 3.16**).

The metastatic potential of cancer cells has generally been attributed to cell intrinsic properties. However, recent studies have brought to light the intricate involvement of premetastatic niche components in supporting metastasis (Gao et al., 2008, 2012; Kaplan et al., 2005; Kim et al., 2009). While evidence has emerged on the interplay between tumor-derived factors and the formation of a premetastatic niche with a significant inflammatory component, little is known about the role of external inflammation in distant organs on metastasis.

Figure 3.15. Sivelestat suppresses metastasis via a Tsp-1-dependent mechanism.
(a) Quantitation of metastatic burden via bioluminescence imaging in PBS-treated (Ctrl) and Sivelestat-treated (Siv) Tsp-$1^{-/-}$ mice injected with luciferase-labeled LLC cells. Signals were normalized to the readings obtained at day 4 for each individual animal. (n= 5 mice per group, p=1.0 at day 18 as determined by two-tailed Mann-Whitney U test). Data are represented as mean ± SEM.
(b) Western blot analysis of Tsp-1 protein in lungs of WT PBS-treated (Ctrl) lungs (n=2) and Tsp-$1^{-/-}$ lungs treated with PBS (Ctrl) (n=4) or Sivelestat (Siv) (n=4). β-actin serves as a loading control.
(c) Flow cytometry-based quantitation of $Ly6G^+$ cells in Tsp-$1^{-/-}$ lungs treated with PBS (Ctrl) or Sivelestat (Siv). (n=4 per group, p= 0.371, as determine by two-tailed unpaired t test).
(d) Flow cytometry-based quantitation of CD63 mean fluorescence intensity (MFI) in $Ly6G^+$ cells in lungs of Tsp-$1^{-/-}$ mice treated with PBS (Ctrl) or Sivelestat (Siv) (n=4 per group, p= 0.653 as determined by two-tailed unpaired t test).
(Data in Figure 3.15 generated in collaboration with Dr. R. Catena.)

Figure 3.15

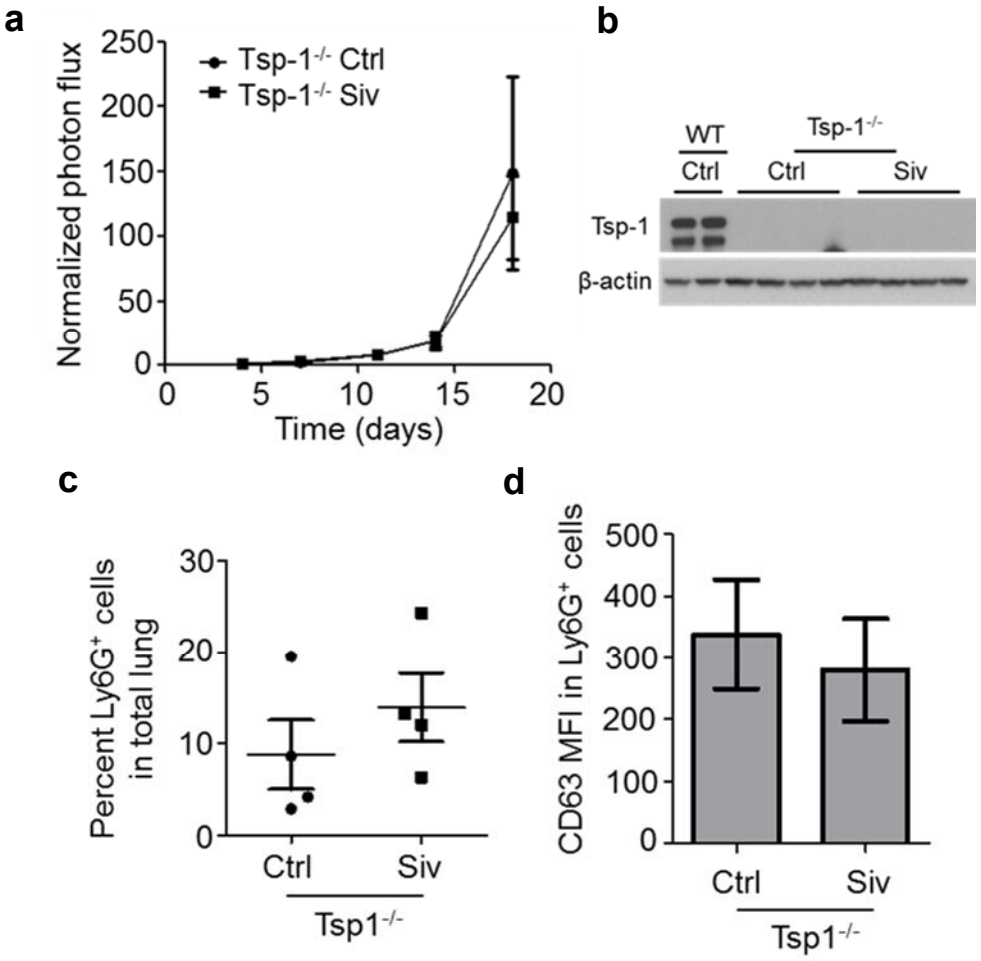
a
Normalized photon flux
250
200
150
100
50
0
0
5
10
15
20
Time (days)
Tsp-1-/- Ctrl
Tsp-1-/- Siv
b
WT
Tsp-1-/-
Ctrl
Ctrl
Siv
Tsp-1
β-actin
c
Percent Ly6G+ cells in total lung
30
20
10
0
Ctrl
Siv
Tsp1-/-
d
CD63 MFI in Ly6G+ cells
500
400
300
200
100
0
Ctrl
Siv
Tsp1-/-

Figure 3.16

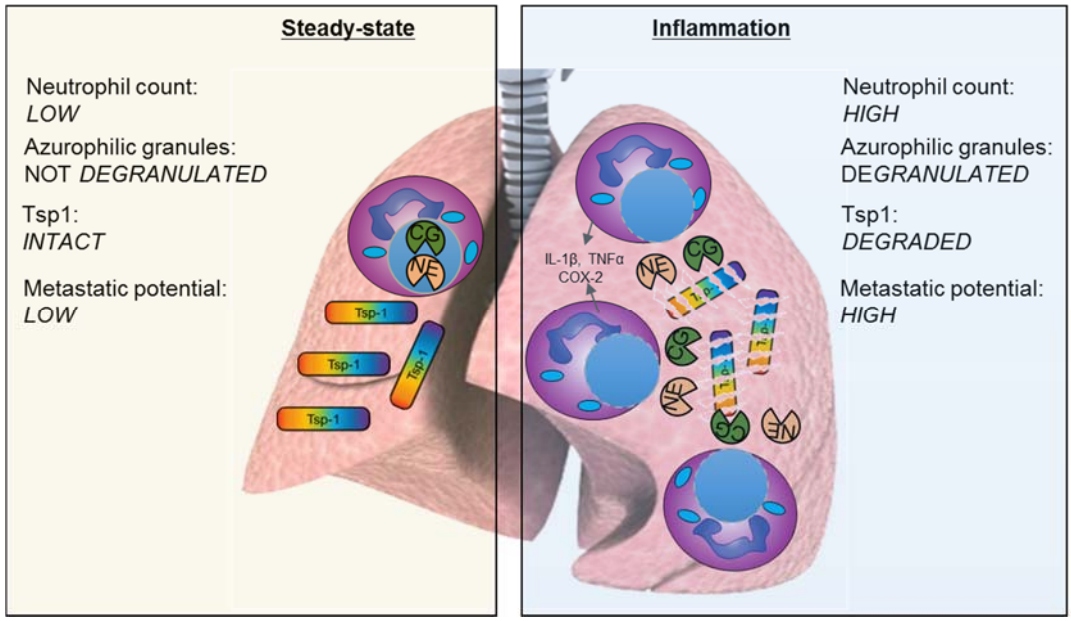

Figure 3.16. Proposed model. Under steady state, neutrophil recruitment to the lungs is minimal and Tsp-1 protein levels are maintained at a baseline necessary for lung homeostasis. Following induction of inflammation either by LPS administration or overexpression of IL-1β, myeloid cells are recruited from the bone marrow, with $Ly6G^{+}$ neutrophils being the most abundant. In the lung microenvironment, the neutrophils degranulate their azurophilic granules, releasing the serine proteases neutrophil elastase (NE) and cathepsin G (CG). NE and CG degrade the anti-tumorigenic protein Tsp-1 in the lungs, rendering the lung microenvironment more conducive to metastatic outgrowth.

Recent work has shown that LPS-induced acute lung inflammation enhances breast cancer metastasis to the lung, via a ubiquitin/CXCR4 mechanism (Yan et al., 2013), as well as via the upregulation of E-selectin on endothelial cells (Jiang et al., 2014). In our study, we have identified a novel mechanism governing enhanced metastasis in acutely inflamed lungs. By introducing LPS intranasally to induce a lung-restricted inflammatory response, we demonstrated that the release of serine proteases NE and CG by the recruited BM-derived $Ly6G^+$ neutrophils is necessary for metastasis enhancement. These proteases specifically target the potent anti-tumorigenic factor, Tsp-1, resulting in its degradation, thereby converting a metastasis-suppressive microenvironment to a metastasis-promoting microenvironment. In contrast to previous studies, where specific cleavage products of Tsp-1 mediate its function, such as the anti-angiogenic fragments generated by thrombin-mediated and ADAM-TS1-mediated cleavage (Lawler, 1986; Lee et al., 2006b; Taraboletti et al., 1997), our findings suggest a novel mechanism of Tsp-1 regulation in inflamed lungs by the combined proteolytic activity of NE and CG.

Furthermore, this study highlights the functional plasticity of $Ly6G^+$ neutrophils, which are both the source of Tsp-1 in the lungs as well as carriers of the proteases that degrade it. Under normal physiological conditions, these neutrophils appear to produce intact Tsp-1 to maintain an anti-metastatic microenvironment. However, under inflammatory conditions, the same neutrophils degranulate NE and CG from their azurophilic granules, degrading Tsp-1, and generating a metastasis-promoting microenvironment. Neutrophil plasticity has also been described in other studies. For example, tumor-derived TGFβ converts neutrophils from a cytotoxic into a protumorigenic “N2”

phenotype (Fridlender et al., 2009). In contrast, tumor-entrained neutrophils (TENs) are recruited to premetastatic lungs, where they function to block metastatic seeding (Granot et al., 2011). In our study, neutrophils are not reprogrammed by tumor cells, but rather respond to inflammatory stimuli, and Tsp-1 degradation is a consequence of this response, rendering the microenvironment more metastasis-conducive.

We have shown that Tsp-1 degradation is not unique to the LPS model of inflammation, as a similar inflammatory phenotype pertaining to neutrophil recruitment and degranulation, and cytokine production is recapitulated in a genetic model of lung inflammation, where IL-1β is ectopically expressed by lung epithelial cells. Notably, in this model, we also observed increased NE and CG activity and Tsp-1 degradation. These results suggest that the mechanism governing the metastasis-enhancing effect of inflammation is a more generalizable phenomenon, and is not only limited to LPS-mediated inflammation.

We demonstrated that LPS-mediated lung inflammation promoted metastasis of orthotopic primary tumors. However, to determine the molecular mechanisms by which neutrophil-mediated lung inflammation contributes to metastatic outgrowth, we resorted to an experimental metastasis model since the orthotopic primary tumors systemically generate BM-derived premetastatic niches with inflammatory characteristics in distal target organ (Hiratsuka et al., 2013). Consistent with this notion, the lungs of tumor-bearing control (- LPS) mice showed increased recruitment of BM-derived $CD45^+$ cells compared to non-tumor bearing mice (**Figure 3.3c**), suggesting that an experimental

metastasis model would allow us to study the effect of lung-specific external inflammation on the outgrowth of tumor cells, thus circumventing the confounding effects of primary tumor-generated inflammatory premetastatic niches.

We generated inflammation prior to tumor cell inoculation, hence preparing the microenvironment, or “soil,” for the arriving tumor cells, or “seed”. Using the orthotopic model of inflammation presented more challenges, since the timing of acute inflammation is critical to the metastatic outcome. We suspect that disseminating tumor cells that encounter the acutely inflamed lung microenvironment, with actively degranulating neutrophils, will be lysed, negatively impacting metastatic outcome. With that limitation in mind, it is not surprising that our early experiments with orthotopic tumor metastasis yielded highly variable results, since we cannot tightly control the timing of tumor cell dissemination from the primary site. This was the major reason for using the tail vein model to probe the mechanisms involved in inflammation-driven metastasis.

Of significant interest was the observation that metastasis was suppressed in mice that were deficient for NE and CG, or mice that were treated with the dual protease inhibitor Sivelestat. Furthermore, this metastasis-suppressive phenotype was abolished in Tsp-1$^{-/-}$ mice. As expected, Sivelestat, inhibited NE (Hagio et al., 2004, 2005); however, strikingly, we found that Sivelestat also inhibited CG, thereby exhibiting dual protease inhibitor activity. This dual activity can be explained by the observation that the chymotrypsin-like serine proteases CG and NE exhibit homology in primary amino acid sequence (37%

identical), homology in their tertiary structures, and the residues of the catalytic triad are at identical positions (His^{57}, Asp^{102} and Ser^{195}) (Averhoff et al., 2008).

Importantly, having observed a metastasis-inhibitory phenotype with Sivelestat treatment, and since it is currently in phase III clinical trials for the treatment of ALI associated with SIRS (Aikawa and Kawasaki, 2014; Aikawa et al., 2011; Iwata et al., 2010), we propose repurposing it for the treatment or prevention of metastatic progression. This will be discussed in greater detail in Chapter Four.

While we agree with the current notion that therapy should be targeted not only against tumor cells, but also against the host microenvironment, our studies suggest that targeting neutrophils may not be a viable strategy in light of their dual role as metastasis-suppressive and metastasis-promoting. Targeting neutrophils may neutralize their anti-metastatic effects derived from Tsp-1 production, which is why we believe that targeting the NE/CG- Tsp-1 axis may have clinical value in the prevention of metastasis or inhibition of its outgrowth.

3-4. MATERIALS AND METHODS

3-4.1. Mice and cell lines

All animal work was conducted in accordance with a protocol approved by the Institutional Animal Care and Use Committee. Wild type C57BL/6J, NE knockout B6.129X1-*Elane*^{tm1Sds}/J, and Tsp-1 knockout B6.129S2-*Thbs1*^{tm1Hyn}/J mice were obtained from The Jackson Laboratory (Bar Harbor, Maine). CG knockout Ctsg^{tm1Ley} mice in C57BL/6J strain were a gift from Dr. Christine

Pham, (Washington University, St. Louis, MO). NE, CG, and Tsp-1 knockout mice in the C57BL/6J background were bred and genotyped according to standard protocols. 8-week-old female mice of the above-mentioned genotypes were used for experiments.

CCSP-rtTA and tetO-IL-1β mice in the FBV/N background (gift from Dr. Jeffrey Whitsett, Cincinnati Children's Hospital Medical Center, Cincinnati, OH) were bred to yield the bitransgenic CCSP-rtTA; tetO-IL-1β mice. 8-week-old male and female bitransgenic mice were used for experiments.

Murine LLC cell stably expressing RFP and firefly luciferase, were cultured in DMEM supplemented with 10% fetal bovine serum (Catena et al., 2013; Gao et al., 2008).

Murine B16-BL6 melanoma cells (gift from Dr. Randolph Watnick at Boston's Children Hospital, MA) were cultured in DMEM supplemented with 10% fetal bovine serum (Nakamura et al., 2002).

3-4.2. Bone marrow isolation and transplantation

BM harvest and transplantation was performed using our published methods. BM transplantation was performed by injecting $1x10^7$ total BM cells via the retro-orbital sinus of lethally irradiated (900 rads) 8-week old C57BL/6 female mice. BM cells were harvested by flushing femurs and tibias of donor animals including Wild-type, Tsp-$1^{-/-}$, $NE^{-/-}$, $CG^{-/-}$, and $NE^{-/-}CG^{-/-}$ mice in 1X PBS. After 4 weeks of BM engraftment, reconstitution efficiency was monitored by PCR of genomic DNA from peripheral blood for absence of Tsp-1, NE, and CG.

3-4.3. Metastasis assay, bioluminescence imaging, and analysis

For experimental metastasis, 8-week old C57BL/6 mice were injected via tail vein with 5 x 10^5 luciferase-labelled LLC cells, or 2 x 10^5 B16-BL6 unlabeled melanoma cells in a volume of 100 µl PBS. LLC pulmonary metastases were monitored by live animal bioluminescence imaging (Xenogen) once per week. Briefly, mice were anaesthetized and injected in the retro-orbital sinus with 75 mg/kg of D-luciferin in 50 µL. For BLI plots, photon flux was calculated for each mouse by using the same circular region of interest encompassing the thorax of the mouse.

B16-BL6 pulmonary metastases were assessed by stereology following H&E staining of the lungs, 18 days after tumor cell intravenous injection.

To study metastasis from orthotopic tumors, 8-week old C57BL/6 mice were injected subcutaneously in the flank with 10^5 B16-BL6 unlabeled melanoma cells in a total volume of 50 µl PBS. After 3 weeks of primary tumor growth, LPS was administered intranasally on days 0, 3, and 7. Primary tumors were then resected on day 10, and a few lungs were harvested for analysis of neutrophil recruitment. Metastasis was allowed to progress for 3 more weeks, at which time all lungs were harvested for H&E staining and stereology.

3-4.4. LPS treatments

LPS derived from E. coli strain 0111:B4 was purchased from Sigma Chemical Co., (St. Louis, MO, USA). Mice were anaesthetized using isofluorane, and LPS was administered intranasally in a 50 µl volume at a concentration of 0.25 mg/ml, for a dose of 12.5 µg (Matute-Bello et al., 2004; Yan et al., 2013) on

days 0, 3, and 7. In the case of tumor-free experiments, lungs were collected at day 10 (3 days after the last LPS treatment) and analyzed.

In experiments assessing metastatic growth of tail vein-injected cells following LPS treatment, 5 x 10^5 LLC cells or 2 x 10^5 B16-BL6 melanoma cells were injected intravenously via the tail vein three days after the end of LPS treatment.

3-4.5. Sivelestat treatments

In vivo, 5 mg/kg Sivelestat dissolved in 1X PBS (ONO-5046, TOCRIS Bioscience, Bristol, UK) was administered daily via the intraperitoneal route in a volume of 100 µl. Sivelestat injections started 5 days after the intravenous injection of LLCs and were carried on until the termination of the experiment.

3-4.6. *In vitro* Tsp-1 proteolysis assays

Recombinant Tsp-1 (R&D systems, 200 ng) was incubated with recombinant Cathepsin G (Genway, 100 ng) or recombinant neutrophil elastase (R&D systems, 50 ng), in the presence of the neutrophil elastase inhibitor N-(Methoxysuccinyl)-Ala-Ala-Pro-Val-chloromethyl ketone (Sigma, 50 nmol), the cathepsin G inhibitor Z-Gly-Leu-Phe-CMK (MP Biomedicals, France, 50 nmol), or Sivelestat (TOCRIS, 1 µg).

NE or CG enzymes were pre-incubated with inhibitors for 15-30 min at room temperature. Then Tsp-1 was incubated with the enzymes or the enzyme-inhibitor reactions for 15 min at 37°C.

3-4.7. Neutrophil isolation, culture, and degranulation

Bone marrow cells were harvested from femurs and tibias of wild type C57/BL6 mice or $NE^{-/-}CG^{-/-}$ mice by flushing the bones with 1X PBS. Total bone marrow cells were then subjected to magnetic bead isolation using the anti-Ly6G microbead kit (MACS Miltenyi Biotec). $Ly6G^{+}$ cell population purity was then assessed by flow cytometric analysis.

Approximately 3 million cells were seeded in a total volume of 200 µl of serum-free RPMI in wells of a 48-well plate. Cells were cultured for 30 min at 37°C in DMSO vehicle (final concentration 0.01% DMSO), or 20nM TPA (12-O-tetradecanoylphorbol-13-acetate, Cell Signaling Technology, MA). Neutrophil cell conditioned medium was collected by centrifuging the cells (300xg for 10 min at room temperature). Degranulation of cells was measured by flow cytometric analysis using the marker CD63. The conditioned medium was incubated at 37°C for the indicated time points, with or without the addition of Sivelestat (final concentration of 0.05 µg/µl), followed by analysis for proteases activity and Tsp-1 protein levels.

3-4.8. NE and CG activity assays

After *in vitro* degranulation of $Ly6G^{+}$ cells, protease activity was measured in conditioned media. NE activity was measured using EnzChek Elastase assay kit (Molecular Probes, Oregon), and CG activity was measured using Sensolyte 520 Cathepsin G assay kit (AnaSpec, CA) according to the manufacturer's protocols.

For protease activity analysis from lung samples, lung protein was extracted in 1X RIPA buffer without protease inhibitors. For NE activity, analysis was

conducted with 40 µg of protein. For CG activity, analysis was conducted with 5 µg of protein.

3-4.9. Microscopy

Animals were euthanized at the end of experiments and lungs were quickly perfused by injecting 5 mL of 1X PBS through the right ventricle of the heart. One part of the lung from each animal was fixed in 3.7% formaldehyde overnight and the other part was collagenase-A treated to create a homogeneous cellular solution and analyzed by flow cytometry or snap-frozen for RNA or protein extraction.

For microscopy, following formaldehyde fixation, tissues were cryo-embedded in Tissue-Tek O.C.T. embedding compound (Electron Microscopy Sciences). Lungs were sectioned at a 7 µm thickness. Lung sections were stained with hematoxylin and eosin for morphometric determinations.

Immunohistochemistry for myeloperoxidase was performed using the Pierce myeloperoxidase polyclonal rabbit antibody solution (Thermo Scientific, IL), and the EnVision+ System HRP-labelled anti-rabbit (DAB+) (Dako).

3-4.10. Tissue sampling and Stereology

Lungs were perfused by injecting 5 mL of cold PBS through the right ventricle of the heart. Lungs were then fixed in 3.7% formaldehyde overnight, followed by 2 days in 30% sucrose at 4°C. To prevent tissue shrinkage that occurs during paraffin embedding, lungs were cryo-embedded in Tissue-Tek O.C.T. embedding compound (Electron Microscopy Sciences), snap frozen on dry ice, and stored at -80°C until further sampling.

For systematic uniform and random sampling (SURS) (Nielsen et al., 2001), the frozen lungs were sectioned along the coronal plane, with the first cut starting at a random position, and the entire lung cut into 1.0 mm-thick parallel slabs, resulting in six to seven slabs per lung. Cryostat sections from each slab were 7μm thick. Sections were stained with hematoxylin and eosin.
The stereological measurements of lung and metastasis volumes were performed using the Axiovision 4.8 software (Carl Zeiss Inc.) area measurement function and following the Cavalieri principle:

$$V = T * \Sigma \text{ Areas}$$

where T is the slab thickness, or intersectional distance (1.0 mm as indicated above), and Areas are measured from one section per slab, and added up for the entire 6-7 slabs.
Finally, data was presented as percent metastasis volume per lung volume.

3-4.11. Flow cytometry and cell sorting

To obtain single cell suspensions, lungs were minced and then digested in collagenase/DNase mix (Roche) for 30 min at 37ºC. Cells were washed, strained and resuspended in FACS staining buffer (PBS + 2mM EDTA, 1% BSA). For analysis of peripheral blood, blood was collected from the tails of mice in anti-coagulant buffer (PBS with 5 mM EDTA). Red blood cells were eliminated by incubation in RBC Lysis Buffer (5 Prime) for 10 min on ice. Cell suspensions were pre-blocked in FACS buffer plus Fc block (CD16/CD32, 1:100, BD Biosciences Pharmingen) and then incubated with the following primary antibodies: rat IgG2ακ and IgG2αβ isotype control (BD Pharmingen), Ly6G (Clone 1A8, BD Pharmingen), Ly6C (Clone HK1.4), Gr1 (Clone RB6-8C5, Biolegend), CD11b (clone M1/70, BD Pharmingen), CD45 (Clone 30-F1,

Biolegend), CD3 (Clone 17A2, Biolegend), B220 (Clone RA3-6B2, Biolegend), CD25 (Clone PC61, Biolegend), CD49b (Clone DX5, BD Pharmingen), cKit (Clone 2B8, BD Pharmingen), VEGFR1 (BD Pharmingen), CD11c (Clone N418, Biolegend), and CD63 (Clone NVG-2, Biolegend). SYTOX blue (Invitrogen) was added and incubated for 5 minutes at room temperature in each cell staining tube to facilitate the elimination of dead cells during flow cytometry.

Labelled cell populations were measured by LSRII flow cytometer coupled with FACSDiva software (BD Bioscience). Flow cytometry analysis was performed using a variety of controls including isotype antibodies, single color controls, and unstained samples for determining appropriate gates, voltages, and compensations required in multivariate flow cytometry. For sorting, targeted cell populations were gated within FACSDiva software and sorted by Aria II sorter (BD Bioscience). For sorting, SYTOX blue-negative gate was utilized to remove dead cells. $CD11b^+$ $Ly6G^+$ subset was isolated and processed for RNA isolation using PicoPure RNA isolation kit (Arcturus).

3-4.12. Quantitative RT-PCR analysis

Total RNA from flow cytometry sorted cells was extracted using the PicoPure RNA extraction kit (Arcturus) following the manufacturer´s protocol. RNA was converted to cDNA using qScript™ cDNA supermix (Quanta Biosciences). Q-PCR was performed with primers and iQTM SYBER Green master mix (Biorad, Hercule, CA). Each sample was duplicated to minimize pipetting error. A standard protocol of initial denaturing at 95°C for 10 min, 40 cycles of 95°C for 10 sec, 60°C for 30 sec, and 72°C for 30 sec, followed by final extension at 72°C for 5 min and melt curve analysis was applied on a BioRad CFX96 Real

Time System (BioRad) coupled with Bio-Rad-CFX Manager software. The relative abundance of each transcript compared with the control was calculated utilizing the delta-Ct method.

The primer sequences used for RT-PCR were:

Mus-GAPDH-for: CATGGCCTTCCGTGTTCCTA

Mus-GAPDH-rev: GCGGCACGTCAGATCCA

Mus-Tsp-1-for: CTTGAGGCAGATGAAGAAGACC

Mus-Tsp-1-rev: ACTGACACCACTTGTTGCTTCC

Mus-IL-6-for: AGACAAAGCCAGAGTCCTTCAG

Mus-IL-6-rev: TTAGGAGAGCATTGGAAATTGG

Mus-IL-1β-for: TGTGTAATGAAAGACGGCACAC

Mus-IL-1β-rev: TCAAACTCCACTTTGCTCTTGA

Mus-TNFα-for: GTCTACTGAACTTCGGGGTGAT

Mus-TNFα-rev: TTGAGAAGATGATCTGAGTGTGAG

Mus- Cox-2-for: CCATTGACCAGAGCAGAGAGAT

Mus- Cox-2-rev: CTTTCAATTCTGCAGCCATTTC

3-4.13. Western blot analysis

Cells were homogenized in lysis buffer (BioRad) containing protease inhibitors (Roche Applied Science). Samples were boiled for 5 min in 1x SDS sampling buffer plus 10% β-mercaptoethanol, and loaded onto 4-12% gradient Bis-Tris NuPAGE gels (Invitrogen). Western blotting was performed using antibodies specific for Tsp-1 (Clone Ab-11, Labvision) and β-actin (Sigma-Aldrich).

3-4.14. Statistical analysis

Results were expressed as mean ± SEM depicted by error bars, unless otherwise stated. Analyses of different treatment groups were performed using the Mann-Whitney U or Student t tests, using the GraphPad Prism statistics software. p values < 0.05 were considered significant.

CHAPTER FOUR

FUTURE DIRECTIONS AND CLINICAL IMPLICATIONS

4-1. FUTURE DIRECTIONS

In Chapter Two, we have demonstrated that metastasis-incompetent tumor cells, by virtue of secreting prosaposin, can induce the expression of Tsp-1 in myeloid cells recruited to the metastatic organ, rendering the lungs refractory to tumor outgrowth. We have further shown that the psap-derived DWLPK peptide, which retains the Tsp-1-inducing activity, can be used to suppress metastasis by upregulating Tsp-1 production in lung myeloid cells. In future studies, it would be of interest to determine the receptor responsible for relaying the psap/DWLPK signal leading to Tsp-1 induction in myeloid cells. Our preliminary investigations suggest that LRP1 is the receptor on myeloid cells involved in this signaling event. We plan to elucidate the signaling cascade downstream of LRP1 that leads to Tsp-1 expression. Biochemical and mutational analysis will allow us to determine the domains on LRP1 that are required for binding and responding to Psap or DWLPK. This will be carried out by expressing mutants of LRP1, each containing different clusters of ligand-binding repeats of the extracellular domain, in LRP1-deficient cells (293Ts) in the presence and absence of DWLPK. This approach was utilized to determine the α2-macroglobulin-binding domains of LRP1 (Mikhailenko et al., 2001). Based on the induction of Tsp-1 in response to culture with DWLPK, we will be able to deduce the LRP1 domains necessary and sufficient for relaying psap/DWLPK signals.

Furthermore, we will identify the intracellular signaling cascades that become activated downstream of DWLPK- ligated LRP1, leading to Tsp-1 expression. Two potential players that have been reported to be activated downstream of LRP1 are the RhoA and Rac1 GTPases (Mantuano et al., 2010). Hence, we will inhibit members of these pathways by using existing pharmacological inhibitors, and determine the subsequent response of the cells to DWLPK. For instance, RhoA activates the downstream effector Rho kinase (ROCK), which will allow us to use the Rho Kinase inhibitor, Y27632, to block that signaling cascade. We will also use the Rac1 inhibitor, NSC23766, to inhibit Rac1-mediated signaling. The absence of Tsp-1 induction would implicate the pathway or signaling component in the response of cells to DWLPK.

The findings from these experiments will allow us to address whether LRP1 on myeloid cells is required for the suppression of metastasis observed in response to DWLPK. Myeloid-specific LRP1 knockout mice ($LRP1^{f/f}$ LysM-$Cre^{+/+}$) will be treated with DWLPK and administered luciferase-labeled LLC cells via the tail vein. Metastasis will be compared to WT mice treated with DWLPK. If myeloid cell LRP1 is required for DWLPK-mediated metastasis suppression, then we expect $LRP1^{f/f}$ LysM-$Cre^{+/+}$ mice treated with DWLPK not to exhibit metastasis suppression, compared to WT mice. These transgenic mice will provide the most compelling assessment of the role of LRP1 specifically in myeloid cells, as these cells are the main producers of Tsp-1. This genetic approach provides superior specificity compared to the pharmacological inhibitor of LRP1, RAP, which will systemically block LRP1 function *in vivo* in all cells that express the receptor.

In Chapter Three, we uncovered a unique mechanism whereby neutrophils recruited to inflamed lungs degrade Tsp-1 through the action of their serine proteases, NE and CG. Notably, this mechanism enhanced metastatic outgrowth, as protease deficient $NE^{-/-}$ $CG^{-/-}$ mice intravenously challenged with LLC cells showed significant metastasis suppression, compared to their WT counterparts. It would be important to determine whether the proteases-mediated degradation of Tsp-1 is the only mechanism for the ensuing metastatic phenotype, as these proteases could also enhance metastasis by remodeling the ECM (Helske et al., 2006; Kafienah et al., 1998; Sköld et al., 1999; Zhu et al., 2001). To address this, we can generate $NE^{-/-}$ $CG^{-/-}$ $Tsp\text{-}1^{-/-}$ mice, challenge them with LPS, and monitor the metastatic outgrowth of LLC or B16-BL6 melanoma. If indeed Tsp-1 degradation is the major mechanism by which NE and CG enhance metastasis, then metastasis suppression observed in $NE^{-/-}$ $CG^{-/-}$ mice will be lost in $NE^{-/-}$ $CG^{-/-}$ $Tsp\text{-}1^{-/-}$ mice. On the other hand, if another NE and CG-mediated mechanism is also at play, then we would observe partial metastasis suppression in $NE^{-/-}$ $CG^{-/-}$ $Tsp\text{-}1^{-/-}$ mice, compared to WT mice, with $NE^{-/-}$ $CG^{-/-}$ mice showing the most efficient suppression.

Our Sivelestat metastasis suppression studies (**Figure 3.13, 3.14**) were conducted in the absence of LPS challenge, and need to be repeated in the presence of LPS-driven lung inflammation. However, this does not undermine the mechanistic results obtained with $NE^{-/-}$ $CG^{-/-}$ mice, where metastasis is suppressed in LPS-inflamed lungs in the absence of the two proteases.

4-2. CLINICAL IMPLICATIONS

Our findings suggest that therapeutic interventions that upregulate Tsp-1 levels or block its degradation could have an anti-metastatic potential.

4-2.1. Novel therapeutics to induce Tsp-1 in lung myeloid cells

Our finding that tumor-derived psap has a metastasis-inhibitory function, and our demonstration that DWLPK peptide suppresses metastasis *in vivo* offers the opportunity to develop the peptide into a therapeutic agent for the treatment or prevention of metastasis. As a therapeutic agent, the peptide provides certain advantages, as peptides are highly specific for their molecular targets, reducing the potential for undesirable off-target side-effects, which is a common shortcoming of non-peptide small molecule drugs (Craik et al., 2013). For that purpose, a more stable and bioavailable version of the peptide will have to be synthesized to increase the therapeutic benefit *in vivo*. The peptide we used in our experiments was chemically altered to include an N-terminal acetyl group and a C-terminal amide group, protecting it from serum and tissue proteases (McGregor, 2008). We will also test a cyclized version of the peptide, since cyclization is shown to further stabilize peptides against proteases (Werle and Bernkop-Schnürch, 2006). Another important factor consider to make DWLPK a viable therapeutic is increasing its bioavailability. Being a small peptide, DWLPK faces rapid clearance from the circulation by the kidneys. One way to improve its half-life in circulation is to attach polyethylene glycol (PEG) molecules to increase its molecular weight and retard its excretion (McGregor, 2008; Werle and Bernkop-Schnürch, 2006).

Another clinically relevant application of our findings is the potential activation of LRP1 signaling to induce Tsp-1 and suppress metastasis. We propose that, aside from DWLPK, we could develop an antibody that binds to the same region of LRP1 and hence mimics the effect of the peptide. This could be beneficial since the antibody would bind with even greater affinity to its antigen on LRP1 than the DWLPK peptide, improving the biological effect. Furthermore, antibody therapeutics are known to possess improved pharmacokinetic properties compared to small peptides, with serum half-lives on the order of days, compared to hours for peptides (Craik et al., 2013; Imai and Takaoka, 2006). This is because high molecular weight antibodies are rarely filtered by kidneys, and are rather reabsorbed or subjected to catabolism (Lobo et al., 2004). Moreover, based on the finding that IgG has a significantly longer serum half-life than other immunoglobulin isotypes due to its binding to the receptor FcRn (Fc receptor of the neonate), protecting it from catabolism in the lysosome, we can foreseeably develop an antibody carrying the Fc portion of IgG to extend its half-life (Beck et al., 2010; Lobo et al., 2004). Furthermore, generating a chimeric or humanized antibody will help reduce its immunogenicity and clearance when used in humans (Beck et al., 2010; Lobo et al., 2004).

4-2.2. Tsp-1 mimetic peptide ABT-510

A Tsp-1 mimetic peptide, ABT-510, has been developed that reproduces Tsp-1 anti-angiogenic activity. ABT-510 is a modified nonapeptide, derived from the anti-angiogenic properdin type 1 repeats of Tsp-1 (Baker et al., 2008). It competes with Tsp-1 for binding to endothelial cells and inhibits VEGF- and bFGF-stimulated endothelial cell migration (Baker et al., 2008). Moreover,

ABT-510 was found to inhibit angiogenesis *in vivo* and significantly suppress LLC tumor growth in lungs (Haviv et al., 2005). ABT-510 is currently in clinical trials for the treatment of several solid tumors. Despite its favorable toxicity profile, phase II trials for soft tissue sarcoma, metastatic melanoma, and advanced renal cell carcinoma have not yielded satisfying results for use of ABT-510 as a monotherapy (Baker et al., 2008; Ebbinghaus et al., 2007; Markovic et al., 2007). However, mouse experimental models using ABT-510 as an adjuvant chemotherapy have yielded more promising outcomes, as in the case of ovarian cancer, where ABT-510 boosts the antitumor effect of cytotoxic chemotherapy (Campbell et al., 2010; Greenaway et al., 2009).

Based on our results with DWLPK suppressing metastasis, we believe that DWLPK will be a more successful anti-metastatic therapeutic agent than ABT-510 because it induces the endogenous expression of full-length Tsp-1 by myeloid cells.

4-2.3. Inhibiting NE and CG proteases using Sivelestat

The metastasis-suppressive phenotype observed with Sivelestat suggests that it could be used as a therapeutic to block metastatic progression, even in the absence of external inflammation. This is based on our preliminary data showing that inflammation derived from a primary tumor exhibits a similar phenotype of Tsp-1 degradation as LPS-driven inflammation. Moreover, since Tsp-1-deficient mice didn't benefit from the effect of Sivelestat on metastases, it logically follows that Sivelestat mediates metastasis suppression via a mechanism that requires Tsp-1. Our data suggest that Sivelestat inhibits NE and CG activity, blocking Tsp-1 proteolysis, hence suppressing metastasis.

Sivelestat has been described and marketed as a specific NE inhibitor, and used for the treatment of ALI in Japan and the Republic of Korea, with phase III and a postmarketing phase IV trial finding that it enhances overall patient outcome and shows no increase in adverse events compared to placebo treatment (Aikawa and Kawasaki, 2014; Aikawa et al., 2011; Iwata et al., 2010; Zeiher et al., 2004). The pathogenesis of ALI involves lung accumulation of neutrophils, which release reactive oxygen species and several proteases, among which NE plays an important role in the etiology of ALI (Kodama et al., 2007; Zeiher et al., 2002). In that regard, Sivelestat treatment was observed to repress neutrophil recruitment and downregulate NE activity (Kawabata et al., 2000). For our purposes, having determined that Sivelestat is a dual inhibitor of NE and CG, and observing metastasis suppression in $NE^{-/-}$ $CG^{-/-}$ BMT mice, we suggest repurposing Sivelestat for the treatment or prevention of metastatic progression.

The serum half-life and bioavailability of Sivelestat are major limiting factors to its activity *in vivo*. For this reason, in the human trials for the treatment of ALI, Sivelestat is continuously administered intravenously at a rate of 0.2 mg/kg/hour for a maximum of 14 days (Aikawa and Kawasaki, 2014; Aikawa et al., 2011; Miyoshi et al., 2013). This justifies using osmotic pumps in our mouse experiments to determine more accurately the effect of Sivelestat on inflammation-enhanced metastasis. In our studies, a short serum half-life could be a hindrance to targeting protease activity and suppressing metastasis, especially in the context of inflammation, where neutrophils are constantly being recruited and releasing active proteases. Hence, by administering Sivelestat via osmotic pumps, we could determine if a

continuous low dose of Sivelestat could more steadily block protease activity and prove to be a more efficient way of suppressing metastasis. In a model of ALI in mice exposed to aerosolized LPS, intravenous infusion of Sivelestat showed reversal of the ALI phenotype, inhibiting NE activity and suppressing the recruitment of neutrophils (Kawabata et al., 2000). Similarly, intravenous Sivelestat infusion has been used as a delivery route in a model of acute pancreatitis in rats (Cao and Liu, 2013) and LPS-driven intestinal paralysis and hypotension in hamsters (Hara et al., 2008).

Given that Sivelestat can protect Tsp-1 from cleavage by neutrophil proteases, it is plausible that Sivelestat could be blocking the progression of already existing micrometastases in the lungs, either by blocking the angiogenic switch or by suppressing tumor cell proliferation. In this respect, keeping the nodules in a micrometastatic state could make them easier to target by chemotherapy, radiotherapy, or surgical resection. Hence, Sivelestat could foreseeably be used in combination with standard of care chemotherapy, radiotherapy, or in the neoadjuvant setting before surgical resection.

REFERENCES

Adams, J.C., Bentley, A.A., Kvansakul, M., Hatherley, D., and Hohenester, E. (2008). Extracellular matrix retention of thrombospondin 1 is controlled by its conserved C-terminal region. J. Cell Sci. *121*, 784–795.

Adkison, A.M., Raptis, S.Z., Kelley, D.G., and Pham, C.T.N. (2002). Dipeptidyl peptidase I activates neutrophil-derived serine proteases and regulates the development of acute experimental arthritis. J. Clin. Invest. *109*, 363–371.

Ahn, V.E., Leyko, P., Alattia, J.-R., Chen, L., and Privé, G.G. (2006). Crystal structures of saposins A and C. Protein Sci. Publ. Protein Soc. *15*, 1849–1857.

Aikawa, N., and Kawasaki, Y. (2014). Clinical utility of the neutrophil elastase inhibitor sivelestat for the treatment of acute respiratory distress syndrome. Ther. Clin. Risk Manag. *10*, 621–629.

Aikawa, N., Ishizaka, A., Hirasawa, H., Shimazaki, S., Yamamoto, Y., Sugimoto, H., Shinozaki, M., Taenaka, N., Endo, S., Ikeda, T., et al. (2011). Reevaluation of the efficacy and safety of the neutrophil elastase inhibitor, Sivelestat, for the treatment of acute lung injury associated with systemic inflammatory response syndrome; a phase IV study. Pulm. Pharmacol. Ther. *24*, 549–554.

Akira, S., Uematsu, S., and Takeuchi, O. (2006). Pathogen Recognition and Innate Immunity. Cell *124*, 783–801.

Averhoff, P., Kolbe, M., Zychlinsky, A., and Weinrauch, Y. (2008). Single Residue Determines the Specificity of Neutrophil Elastase for Shigella Virulence Factors. J. Mol. Biol. *377*, 1053–1066.

Baker, L.H., Rowinsky, E.K., Mendelson, D., Humerickhouse, R.A., Knight, R.A., Qian, J., Carr, R.A., Gordon, G.B., and Demetri, G.D. (2008). Randomized, Phase II Study of the Thrombospondin-1-Mimetic Angiogenesis Inhibitor ABT-510 in Patients With Advanced Soft Tissue Sarcoma. J. Clin. Oncol. *26*, 5583–5588.

Barnes, H., Ackermann, E.J., and van der Geer, P. (2003). v-Src induces Shc binding to tyrosine 63 in the cytoplasmic domain of the LDL receptor-related protein 1. Oncogene *22*, 3589–3597.

Beck, A., Wurch, T., Bailly, C., and Corvaia, N. (2010). Strategies and challenges for the next generation of therapeutic antibodies. Nat. Rev. Immunol. *10*, 345–352.

Bein, K., and Simons, M. (2000). Thrombospondin type 1 repeats interact with matrix metalloproteinase 2. Regulation of metalloproteinase activity. J. Biol. Chem. *275*, 32167–32173.

Beisiegel, U., Weber, W., Ihrke, G., Herz, J., and Stanley, K.K. (1989). The LDL–receptor–related protein, LRP, is an apolipoprotein E-binding protein. Nature *341*, 162–164.

Berahovich, R.D., Miao, Z., Wang, Y., Premack, B., Howard, M.C., and Schall, T.J. (2005). Proteolytic Activation of Alternative CCR1 Ligands in Inflammation. J. Immunol. *174*, 7341–7351.

Bergers, G., Brekken, R., McMahon, G., Vu, T.H., Itoh, T., Tamaki, K., Tanzawa, K., Thorpe, P., Itohara, S., Werb, Z., et al. (2000). Matrix metalloproteinase-9 triggers the angiogenic switch during carcinogenesis. Nat. Cell Biol. *2*, 737–744.

Bonnefoy, A., and Legrand, C. (2000). Proteolysis of Subendothelial Adhesive Glycoproteins (Fibronectin, Thrombospondin, and von Willebrand Factor) by Plasmin, Leukocyte Cathepsin G, and Elastase. Thromb. Res. *98*, 323–332.

Bornstein, P. (1992). Thrombospondins: structure and regulation of expression. FASEB J. *6*, 3290–3299.

Boucher, P., Liu, P., Gotthardt, M., Hiesberger, T., Anderson, R.G.W., and Herz, J. (2002). Platelet-derived Growth Factor Mediates Tyrosine Phosphorylation of the Cytoplasmic Domain of the Low Density Lipoprotein Receptor-related Protein in Caveolae. J. Biol. Chem. *277*, 15507–15513.

Brigham, K.L., and Meyrick, B. (1986). Endotoxin and lung injury. Am. Rev. Respir. Dis. *133*, 913–927.

Bu, G., Geuze, H.J., Strous, G.J., and Schwartz, A.L. (1995). 39 kDa receptor-associated protein is an ER resident protein and molecular chaperone for LDL receptor-related protein. EMBO J. *14*, 2269–2280.

Campana, W.M., Darin, S.J., and O'Brien, J.S. (1999). Phosphatidylinositol 3-kinase and Akt protein kinase mediate IGF-I- and prosaptide-induced survival in schwann cells. J. Neurosci. Res. *57*, 332–341.

Campbell, N.E., Greenaway, J., Henkin, J., Moorehead, R.A., and Petrik, J. (2010). The Thrombospondin-1 Mimetic ABT-510 Increases the Uptake and Effectiveness of Cisplatin and Paclitaxel in a Mouse Model of Epithelial Ovarian Cancer. Neoplasia N. Y. N *12*, 275–283.

Cao, J., and Liu, Q. (2013). Protective effects of sivelestat in a caerulein-induced rat acute pancreatitis model. Inflammation *36*, 1348–1356.

Catena, R., Bhattacharya, N., Rayes, T.E., Wang, S., Choi, H., Gao, D., Ryu, S., Joshi, N., Bielenberg, D., Lee, S.B., et al. (2013). Bone Marrow–Derived Gr1+ Cells Can Generate a Metastasis-Resistant Microenvironment Via Induced Secretion of Thrombospondin-1. Cancer Discov. *3*, 578–589.

Chazaud, B., Ricoux, R., Christov, C., Plonquet, A., Gherardi, R.K., and Barlovatz-Meimon, G. (2002). Promigratory effect of plasminogen activator inhibitor-1 on invasive breast cancer cell populations. Am. J. Pathol. *160*, 237–246.

Christner, P., Fein, A., Goldberg, S., Lippmann, M., Abrams, W., and Weinbaum, G. (1985). Collagenase in the lower respiratory tract of patients with adult respiratory distress syndrome. Am. Rev. Respir. Dis. *131*, 690–695.

Chung, K.F. (2001). Cytokines in chronic obstructive pulmonary disease. Eur. Respir. J. *18*, 50s – 59s.

Clausen, B.E., Burkhardt, C., Reith, W., Renkawitz, R., and Förster, I. (1999). Conditional gene targeting in macrophages and granulocytes using LysMcre mice. Transgenic Res. *8*, 265–277.

Cook, L.M., Hurst, D.R., and Welch, D.R. (2011). Metastasis suppressors and the tumor microenvironment. Semin. Cancer Biol. *21*, 113–122.

Craig, A., Mai, J., Cai, S., and Jeyaseelan, S. (2009). Neutrophil Recruitment to the Lungs during Bacterial Pneumonia. Infect. Immun. *77*, 568–575.

Craik, D.J., Fairlie, D.P., Liras, S., and Price, D. (2013). The Future of Peptide-based Drugs. Chem. Biol. Drug Des. *81*, 136–147.

Daley, J.M., Thomay, A.A., Connolly, M.D., Reichner, J.S., and Albina, J.E. (2008). Use of Ly6G-specific monoclonal antibody to deplete neutrophils in mice. J. Leukoc. Biol. *83*, 64–70.

Dameron, K.M., Volpert, O.V., Tainsky, M.A., and Bouck, N. (1994). Control of angiogenesis in fibroblasts by p53 regulation of thrombospondin-1. Science *265*, 1582–1584.

Delclaux, C., d' Ortho, M.P., Delacourt, C., Lebargy, F., Brun-Buisson, C., Brochard, L., Lemaire, F., Lafuma, C., and Harf, A. (1997). Gelatinases in epithelial lining fluid of patients with adult respiratory distress syndrome. Am. J. Physiol. *272*, L442–L451.

Descamps, O., Bilheimer, D., and Herz, J. (1993). Insulin stimulates receptor-mediated uptake of apoE-enriched lipoproteins and activated alpha 2-macroglobulin in adipocytes. J. Biol. Chem. *268*, 974–981.

Devaney, J.M., Greene, C.M., Taggart, C.C., Carroll, T.P., O'Neill, S.J., and McElvaney, N.G. (2003). Neutrophil elastase up-regulates interleukin-8 via toll-like receptor 4. FEBS Lett. *544*, 129–132.

Dick, E.P., Prince, L.R., Prestwich, E.C., Renshaw, S.A., Whyte, M.K.B., and Sabroe, I. (2009). Pathways regulating lipopolysaccharide-induced neutrophil survival revealed by lentiviral transduction of primary human neutrophils. Immunology *127*, 249–255.

Dinarello, C.A. (1996). Biologic basis for interleukin-1 in disease. Blood *87*, 2095–2147.

Doerschuk, C.M. (2001). Mechanisms of leukocyte sequestration in inflamed lungs. Microcirc. N. Y. N 1994 *8*, 71–88.

Ebbinghaus, S., Hussain, M., Tannir, N., Gordon, M., Desai, A.A., Knight, R.A., Humerickhouse, R.A., Qian, J., Gordon, G.B., and Figlin, R. (2007). Phase 2 Study of ABT-510 in Patients with Previously Untreated Advanced Renal Cell Carcinoma. Clin. Cancer Res. *13*, 6689–6695.

Erler, J.T., Bennewith, K.L., Cox, T.R., Lang, G., Bird, D., Koong, A., Le, Q.-T., and Giaccia, A.J. (2009). Hypoxia-induced lysyl oxidase is a critical mediator of bone marrow cell recruitment to form the premetastatic niche. Cancer Cell *15*, 35–44.

Ezzie, M.E., Piper, M.G., Montague, C., Newland, C.A., Opalek, J.M., Baran, C., Ali, N., Brigstock, D., Lawler, J., and Marsh, C.B. (2011). Thrombospondin-1-deficient mice are not protected from bleomycin-induced pulmonary fibrosis. Am. J. Respir. Cell Mol. Biol. *44*, 556–561.

Fahy, J.V. (2009). Eosinophilic and Neutrophilic Inflammation in Asthma. Proc. Am. Thorac. Soc. *6*, 256–259.

Faurschou, M., and Borregaard, N. (2003). Neutrophil granules and secretory vesicles in inflammation. Microbes Infect. Inst. Pasteur *5*, 1317–1327.

Fidler, I.J. (2003). The pathogenesis of cancer metastasis: the "seed and soil" hypothesis revisited. Nat. Rev. Cancer *3*, 453–458.

Fridlender, Z.G., Sun, J., Kim, S., Kapoor, V., Cheng, G., Ling, L., Worthen, G.S., and Albelda, S.M. (2009). Polarization of tumor-associated neutrophil phenotype by TGF-beta: "N1" versus "N2" TAN. Cancer Cell *16*, 183–194.

Gao, D., Nolan, D.J., Mellick, A.S., Bambino, K., McDonnell, K., and Mittal, V. (2008). Endothelial progenitor cells control the angiogenic switch in mouse lung metastasis. Science *319*, 195–198.

Gao, D., Joshi, N., Choi, H., Ryu, S., Hahn, M., Catena, R., Sadik, H., Argani, P., Wagner, P., Vahdat, L.T., et al. (2012). Myeloid Progenitor Cells in the Premetastatic Lung Promote Metastases by Inducing Mesenchymal to Epithelial Transition. Cancer Res. *72*, 1384–1394.

Garwicz, D., Lennartsson, A., Jacobsen, S.E., Gullberg, U., and Lindmark, A. (2005). Biosynthetic profiles of neutrophil serine proteases in a human bone marrow-derived cellular myeloid differentiation model. Haematologica *90*, 38–44.

Good, D.J., Polverini, P.J., Rastinejad, F., Le Beau, M.M., Lemons, R.S., Frazier, W.A., and Bouck, N.P. (1990). A tumor suppressor-dependent inhibitor of angiogenesis is immunologically and functionally indistinguishable from a fragment of thrombospondin. Proc. Natl. Acad. Sci. U. S. A. *87*, 6624–6628.

Goodman, R.B., Strieter, R.M., Martin, D.P., Steinberg, K.P., Milberg, J.A., Maunder, R.J., Kunkel, S.L., Walz, A., Hudson, L.D., and Martin, T.R. (1996). Inflammatory cytokines in patients with persistence of the acute respiratory distress syndrome. Am. J. Respir. Crit. Care Med. *154*, 602–611.

Gotthardt, M., Trommsdorff, M., Nevitt, M.F., Shelton, J., Richardson, J.A., Stockinger, W., Nimpf, J., and Herz, J. (2000). Interactions of the Low Density Lipoprotein Receptor Gene Family with Cytosolic Adaptor and Scaffold Proteins Suggest Diverse Biological Functions in Cellular Communication and Signal Transduction. J. Biol. Chem. *275*, 25616–25624.

Gout, S., Tremblay, P.-L., and Huot, J. (2008). Selectins and selectin ligands in extravasation of cancer cells and organ selectivity of metastasis. Clin. Exp. Metastasis *25*, 335–344.

Granot, Z., Henke, E., Comen, E.A., King, T.A., Norton, L., and Benezra, R. (2011). Tumor Entrained Neutrophils Inhibit Seeding in the Premetastatic Lung. Cancer Cell *20*, 300–314.

Greenaway, J., Henkin, J., Lawler, J., Moorehead, R., and Petrik, J. (2009). ABT-510 induces tumor cell apoptosis and inhibits ovarian tumor growth in an orthotopic, syngeneic model of epithelial ovarian cancer. Mol. Cancer Ther. *8*, 64–74.

Gullberg, U., Andersson, E., Garwicz, D., Lindmark, A., and Olsson, I. (1997). Biosynthesis, processing and sorting of neutrophil proteins: insight into neutrophil granule development. Eur. J. Haematol. *58*, 137–153.

Güngör, N., Pennings, J.L., Knaapen, A.M., Chiu, R.K., Peluso, M., Godschalk, R.W., and Schooten, F.J.V. (2010a). Transcriptional profiling of the

acute pulmonary inflammatory response induced by LPS: role of neutrophils. Respir. Res. *11*, 24.

Güngör, N., Knaapen, A.M., Munnia, A., Peluso, M., Haenen, G.R., Chiu, R.K., Godschalk, R.W.L., and Schooten, F.J. van (2010b). Genotoxic effects of neutrophils and hypochlorous acid. Mutagenesis *25*, 149–154.

Guo, N., Zabrenetzky, V.S., Chandrasekaran, L., Sipes, J.M., Lawler, J., Krutzsch, H.C., and Roberts, D.D. (1998). Differential Roles of Protein Kinase C and Pertussis Toxin-sensitive G-binding Proteins in Modulation of Melanoma Cell Proliferation and Motility by Thrombospondin 1. Cancer Res. *58*, 3154–3162.

Gupta, K., Gupta, P., Wild, R., Ramakrishnan, S., and Hebbel, R.P. (1999). Binding and displacement of vascular endothelial growth factor (VEGF) by thrombospondin: effect on human microvascular endothelial cell proliferation and angiogenesis. Angiogenesis *3*, 147–158.

Hachiya, O., Takeda, Y., Miyata, H., Watanabe, H., Yamashita, T., and Sendo, F. (1995). Inhibition by bacterial lipopolysaccharide of spontaneous and TNF-alpha-induced human neutrophil apoptosis in vitro. Microbiol. Immunol. *39*, 715–723.

Haegens, A., Heeringa, P., Suylen, R.J. van, Steele, C., Aratani, Y., O'Donoghue, R.J.J., Mutsaers, S.E., Mossman, B.T., Wouters, E.F.M., and Vernooy, J.H.J. (2009). Myeloperoxidase Deficiency Attenuates Lipopolysaccharide-Induced Acute Lung Inflammation and Subsequent Cytokine and Chemokine Production. J. Immunol. *182*, 7990–7996.

Hagio, T., Matsumoto, S., Nakao, S., Abiru, T., Ohno, H., and Kawabata, K. (2004). Elastase inhibition reduced death associated with acid aspiration-induced lung injury in hamsters. Eur. J. Pharmacol. *488*, 173–180.

Hagio, T., Matsumoto, S., Nakao, S., Matsuoka, S., and Kawabata, K. (2005). Sivelestat, a specific neutrophil elastase inhibitor, prevented phorbol myristate acetate-induced acute lung injury in conscious rabbits. Pulm. Pharmacol. Ther. *18*, 285–290.

Hammerstedt, R.H., Cramer, P.G., Barbato, G.F., Amann, R.P., O'Brien, J.S., and Griswold, M.D. (2001). A fragment of prosaposin (SGP-1) from rooster sperm promotes sperm-egg binding and improves fertility in chickens. J. Androl. *22*, 361–375.

Hara, S., Nemoto, K., Ninomiya, N., Kubota, M., Kuno, M., and Yamamoto, Y. (2008). Continuous infusion of sivelestat sodium hydrate prevents lipopolysaccharide-induced intestinal paralysis and hypotension in conscious guinea-pigs. Clin. Exp. Pharmacol. Physiol. *35*, 841–845.

Harmey, J.H., Bucana, C.D., Lu, W., Byrne, A.M., McDonnell, S., Lynch, C., Bouchier-Hayes, D., and Dong, Z. (2002). Lipopolysaccharide-induced metastatic growth is associated with increased angiogenesis, vascular permeability and tumor cell invasion. Int. J. Cancer *101*, 415–422.

Haviv, F., Bradley, M.F., Kalvin, D.M., Schneider, A.J., Davidson, D.J., Majest, S.M., McKay, L.M., Haskell, C.J., Bell, R.L., Nguyen, B., et al. (2005). Thrombospondin-1 Mimetic Peptide Inhibitors of Angiogenesis and Tumor Growth: Design, Synthesis, and Optimization of Pharmacokinetics and Biological Activities†. J. Med. Chem. *48*, 2838–2846.

Heissig, B., Hattori, K., Dias, S., Friedrich, M., Ferris, B., Hackett, N.R., Crystal, R.G., Besmer, P., Lyden, D., Moore, M.A.S., et al. (2002). Recruitment of Stem and Progenitor Cells from the Bone Marrow Niche Requires MMP-9 Mediated Release of Kit-Ligand. Cell *109*, 625–637.

Helske, S., Syväranta, S., Kupari, M., Lappalainen, J., Laine, M., Lommi, J., Turto, H., Mäyränpää, M., Werkkala, K., Kovanen, P.T., et al. (2006). Possible role for mast cell-derived cathepsin G in the adverse remodelling of stenotic aortic valves. Eur. Heart J. *27*, 1495–1504.

Herz, J., Goldstein, J.L., Strickland, D.K., Ho, Y.K., and Brown, M.S. (1991). 39-kDa protein modulates binding of ligands to low density lipoprotein receptor-related protein/alpha 2-macroglobulin receptor. J. Biol. Chem. *266*, 21232–21238.

Herz, J., Clouthier, D.E., and Hammer, R.E. (1992). LDL receptor-related protein internalizes and degrades uPA-PAI-1 complexes and is essential for embryo implantation. Cell *71*, 411–421.

Hiesberger, T., Hüttler, S., Rohlmann, A., Schneider, W., Sandhoff, K., and Herz, J. (1998). Cellular uptake of saposin (SAP) precursor and lysosomal delivery by the low density lipoprotein receptor-related protein (LRP). EMBO J. *17*, 4617–4625.

Hiraiwa, M., O'Brien, J.S., Kishimoto, Y., Galdzicka, M., Fluharty, A.L., Ginns, E.I., and Martin, B.M. (1993). Isolation, characterization, and proteolysis of human prosaposin, the precursor of saposins (sphingolipid activator proteins). Arch. Biochem. Biophys. *304*, 110–116.

Hiraiwa, M., Martin, B.M., Kishimoto, Y., Conner, G.E., Tsuji, S., and O'Brien, J.S. (1997). Lysosomal proteolysis of prosaposin, the precursor of saposins (sphingolipid activator proteins): its mechanism and inhibition by ganglioside. Arch. Biochem. Biophys. *341*, 17–24.

Hiratsuka, S., Nakamura, K., Iwai, S., Murakami, M., Itoh, T., Kijima, H., Shipley, J.M., Senior, R.M., and Shibuya, M. (2002). MMP9 induction by

vascular endothelial growth factor receptor-1 is involved in lung-specific metastasis. Cancer Cell *2*, 289–300.

Hiratsuka, S., Watanabe, A., Aburatani, H., and Maru, Y. (2006). Tumour-mediated upregulation of chemoattractants and recruitment of myeloid cells predetermines lung metastasis. Nat. Cell Biol. *8*, 1369–1375.

Hiratsuka, S., Watanabe, A., Sakurai, Y., Akashi-Takamura, S., Ishibashi, S., Miyake, K., Shibuya, M., Akira, S., Aburatani, H., and Maru, Y. (2008). The S100A8–serum amyloid A3–TLR4 paracrine cascade establishes a pre-metastatic phase. Nat. Cell Biol. *10*, 1349–1355.

Hiratsuka, S., Duda, D.G., Huang, Y., Goel, S., Sugiyama, T., Nagasawa, T., Fukumura, D., and Jain, R.K. (2011). C-X-C receptor type 4 promotes metastasis by activating p38 mitogen-activated protein kinase in myeloid differentiation antigen (Gr-1)-positive cells. Proc. Natl. Acad. Sci. *108*, 302–307.

Hiratsuka, S., Ishibashi, S., Tomita, T., Watanabe, A., Akashi-Takamura, S., Murakami, M., Kijima, H., Miyake, K., Aburatani, H., and Maru, Y. (2013). Primary tumours modulate innate immune signalling to create pre-metastatic vascular hyperpermeability foci. Nat. Commun. *4*, 1853.

Hogg, P.J., Jiménez, B.M., and Chesterman, C.N. (1994). Identification of possible inhibitory reactive centers in thrombospondin 1 that may bind cathepsin G and neutrophil elastase. Biochemistry (Mosc.) *33*, 6531–6537.

Horwitz, M., Benson, K.F., Duan, Z., Li, F.-Q., and Person, R.E. (2004). Hereditary neutropenia: dogs explain human neutrophil elastase mutations. Trends Mol. Med. *10*, 163–170.

Hussaini, I.M., Srikumar, K., Quesenberry, P.J., and Gonias, S.L. (1990). Colony-stimulating factor-1 modulates alpha 2-macroglobulin receptor expression in murine bone marrow macrophages. J. Biol. Chem. *265*, 19441–19446.

Imai, K., and Takaoka, A. (2006). Comparing antibody and small-molecule therapies for cancer. Nat. Rev. Cancer *6*, 714–727.

Iruela-Arispe, M.L., Liska, D.J., Sage, E.H., and Bornstein, P. (1993). Differential expression of thrombospondin 1, 2, and 3 during murine development. Dev. Dyn. Off. Publ. Am. Assoc. Anat. *197*, 40–56.

Isenberg, J.S., Jia, Y., Fukuyama, J., Switzer, C.H., Wink, D.A., and Roberts, D.D. (2007). Thrombospondin-1 Inhibits Nitric Oxide Signaling via CD36 by Inhibiting Myristic Acid Uptake. J. Biol. Chem. *282*, 15404–15415.

Iwata, K., Doi, A., Ohji, G., Oka, H., Oba, Y., Takimoto, K., Igarashi, W., Gremillion, D.H., and Shimada, T. (2010). Effect of neutrophil elastase inhibitor (sivelestat sodium) in the treatment of acute lung injury (ALI) and acute respiratory distress syndrome (ARDS): a systematic review and meta-analysis. Intern. Med. Tokyo Jpn. *49*, 2423–2432.

Jaffe, E.A., Ruggiero, J.T., and Falcone, D.J. (1985). Monocytes and macrophages synthesize and secrete thrombospondin. Blood *65*, 79–84.

Jeffery, P.K. (1998). Structural and inflammatory changes in COPD: a comparison with asthma. Thorax *53*, 129–136.

Jeyaseelan, S., Chu, H.W., Young, S.K., and Worthen, G.S. (2004). Transcriptional Profiling of Lipopolysaccharide-Induced Acute Lung Injury. Infect. Immun. *72*, 7247–7256.

Jiang, M., Xu, X., Bi, Y., Xu, J., Qin, C., and Han, M. (2014). Systemic inflammation promotes lung metastasis via E-selectin upregulation in mouse breast cancer model. Cancer Biol. Ther. *15*.

Jiménez, B., Volpert, O.V., Crawford, S.E., Febbraio, M., Silverstein, R.L., and Bouck, N. (2000). Signals leading to apoptosis-dependent inhibition of neovascularization by thrombospondin-1. Nat. Med. *6*, 41–48.

Jones, H.A., Cadwallader, K.A., White, J.F., Uddin, M., Peters, A.M., and Chilvers, E.R. (2002). Dissociation between respiratory burst activity and deoxyglucose uptake in human neutrophil granulocytes: implications for interpretation of (18)F-FDG PET images. J. Nucl. Med. Off. Publ. Soc. Nucl. Med. *43*, 652–657.

Joyce, J.A., and Pollard, J.W. (2009). Microenvironmental regulation of metastasis. Nat. Rev. Cancer *9*, 239–252.

Kafienah, W., Buttle, D.J., Burnett, D., and Hollander, A.P. (1998). Cleavage of native type I collagen by human neutrophil elastase. Biochem. J. *330*, 897–902.

Kancha, R.K., Stearns, M.E., and Hussain, M.M. (1994). Decreased expression of the low density lipoprotein receptor-related protein/alpha 2-macroglobulin receptor in invasive cell clones derived from human prostate and breast tumor cells. Oncol. Res. *6*, 365–372.

Kang, S.-Y., Halvorsen, O.J., Gravdal, K., Bhattacharya, N., Lee, J.M., Liu, N.W., Johnston, B.T., Johnston, A.B., Haukaas, S.A., Aamodt, K., et al. (2009). Prosaposin inhibits tumor metastasis via paracrine and endocrine stimulation of stromal p53 and Tsp-1. Proc. Natl. Acad. Sci. U. S. A. *106*, 12115–12120.

Kao, S.-J., Su, C.-F., Liu, D.D., and Chen, H.I. (2007). Endotoxin-induced acute lung injury and organ dysfunction are attenuated by pentobarbital anaesthesia. Clin. Exp. Pharmacol. Physiol. *34*, 480–487.

Kaplan, R.N., Riba, R.D., Zacharoulis, S., Bramley, A.H., Vincent, L., Costa, C., MacDonald, D.D., Jin, D.K., Shido, K., Kerns, S.A., et al. (2005). VEGFR1-positive haematopoietic bone marrow progenitors initiate the pre-metastatic niche. Nature *438*, 820–827.

Kawabata, K., Hagio, T., Matsumoto, S., Nakao, S., Orita, S., Aze, Y., and Ohno, H. (2000). Delayed Neutrophil Elastase Inhibition Prevents Subsequent Progression of Acute Lung Injury Induced by Endotoxin Inhalation in Hamsters. Am. J. Respir. Crit. Care Med. *161*, 2013–2018.

Kim, S., Takahashi, H., Lin, W.-W., Descargues, P., Grivennikov, S., Kim, Y., Luo, J.-L., and Karin, M. (2009). Carcinoma-produced factors activate myeloid cells through TLR2 to stimulate metastasis. Nature *457*, 102–106.

Kinoshita, A., Shah, T., Tangredi, M.M., Strickland, D.K., and Hyman, B.T. (2003). The Intracellular Domain of the Low Density Lipoprotein Receptor-related Protein Modulates Transactivation Mediated by Amyloid Precursor Protein and Fe65. J. Biol. Chem. *278*, 41182–41188.

Kodama, T., Yukioka, H., Kato, T., Kato, N., Hato, F., and Kitagawa, S. (2007). Neutrophil elastase as a predicting factor for development of acute lung injury. Intern. Med. Tokyo Jpn. *46*, 699–704.

Koochekpour, S., Zhuang, Y.-J., Beroukhim, R., Hsieh, C.-L., Hofer, M.D., Zhau, H.E., Hiraiwa, M., Pattan, D.Y., Ware, J.L., Luftig, R.B., et al. (2005). Amplification and overexpression of prosaposin in prostate cancer. Genes. Chromosomes Cancer *44*, 351–364.

Koochekpour, S., Lee, T.-J., Wang, R., Culig, Z., Delorme, N., Caffey, S., Marrero, L., and Aguirre, J. (2007a). Prosaposin upregulates AR and PSA expression and activity in prostate cancer cells (LNCaP). The Prostate *67*, 178–189.

Koochekpour, S., Lee, T.-J., Wang, R., Sun, Y., Delorme, N., Hiraiwa, M., Grabowski, G.A., Culig, Z., and Minokadeh, A. (2007b). Prosaposin is a novel androgen-regulated gene in prostate cancer cell line LNCaP. J. Cell. Biochem. *101*, 631–641.

Koochekpour, S., Lee, T.-J., Sun, Y., Hu, S., Grabowski, G.A., Liu, Z., and Garay, J. (2008). Prosaposin is an AR-target gene and its neurotrophic domain upregulates AR expression and activity in prostate stromal cells. J. Cell. Biochem. *104*, 2272–2285.

Koochekpour, S., Hu, S., Vellasco-Gonzalez, C., Bernardo, R., Azabdaftari, G., Dalin, G., Zhau, H.E., Chung, L.W., and Vessella, R.L. (2012). Serum Prosaposin Levels Are Increased in Patients with Advanced Prostate Cancer. The Prostate *72*, 253–269.

Korkmaz, B., Moreau, T., and Gauthier, F. (2008). Neutrophil elastase, proteinase 3 and cathepsin G: physicochemical properties, activity and physiopathological functions. Biochimie *90*, 227–242.

Korkmaz, B., Horwitz, M.S., Jenne, D.E., and Gauthier, F. (2010). Neutrophil Elastase, Proteinase 3, and Cathepsin G as Therapeutic Targets in Human Diseases. Pharmacol. Rev. *62*, 726–759.

Krieger, M., and Herz, J. (1994). Structures and functions of multiligand lipoprotein receptors: macrophage scavenger receptors and LDL receptor-related protein (LRP). Annu. Rev. Biochem. *63*, 601–637.

Kristensen, T., Moestrup, S.K., Gliemann, J., Bendtsen, L., Sand, O., and Sottrup-Jensen, L. (1990). Evidence that the newly cloned low-density-lipoprotein receptor related protein (LRP) is the alpha 2-macroglobulin receptor. FEBS Lett. *276*, 151–155.

Kuijpers, T.W., Tool, A.T., Schoot, C. van der, Ginsel, L.A., Onderwater, J.J., Roos, D., and Verhoeven, A.J. (1991). Membrane surface antigen expression on neutrophils: a reappraisal of the use of surface markers for neutrophil activation. Blood *78*, 1105–1111.

LaMarre, J., Wolf, B.B., Kittler, E.L., Quesenberry, P.J., and Gonias, S.L. (1993). Regulation of macrophage alpha 2-macroglobulin receptor/low density lipoprotein receptor-related protein by lipopolysaccharide and interferon-gamma. J. Clin. Invest. *91*, 1219–1224.

Lamy, L., Foussat, A., Brown, E.J., Bornstein, P., Ticchioni, M., and Bernard, A. (2007). Interactions between CD47 and thrombospondin reduce inflammation. J. Immunol. Baltim. Md 1950 *178*, 5930–5939.

Lappalainen, U., Whitsett, J.A., Wert, S.E., Tichelaar, J.W., and Bry, K. (2005). Interleukin-1β Causes Pulmonary Inflammation, Emphysema, and Airway Remodeling in the Adult Murine Lung. Am. J. Respir. Cell Mol. Biol. *32*, 311–318.

Lawler, J. (1986). The structural and functional properties of thrombospondin. Blood *67*, 1197–1209.

Lawler, J. (2002). Thrombospondin-1 as an endogenous inhibitor of angiogenesis and tumor growth. J. Cell. Mol. Med. *6*, 1–12.

Lawler, P.R., and Lawler, J. (2012). Molecular Basis for the Regulation of Angiogenesis by Thrombospondin-1 and -2. Cold Spring Harb. Perspect. Med. *2*, a006627.

Lawler, J., Sunday, M., Thibert, V., Duquette, M., George, E.L., Rayburn, H., and Hynes, R.O. (1998). Thrombospondin-1 is required for normal murine pulmonary homeostasis and its absence causes pneumonia. J. Clin. Invest. *101*, 982–992.

Lee, D., Walsh, J.D., Mikhailenko, I., Yu, P., Migliorini, M., Wu, Y., Krueger, S., Curtis, J.E., Harris, B., Lockett, S., et al. (2006a). RAP Uses a Histidine Switch to Regulate Its Interaction with LRP in the ER and Golgi. Mol. Cell *22*, 423–430.

Lee, N.V., Sato, M., Annis, D.S., Loo, J.A., Wu, L., Mosher, D.F., and Iruela-Arispe, M.L. (2006b). ADAMTS1 mediates the release of antiangiogenic polypeptides from TSP1 and 2. EMBO J. *25*, 5270–5283.

Li, Y., Wood, N., Parsons, P.G., Yellowlees, D., and Donnelly, P.K. (1997). Expression of alpha2-macroglobulin receptor/low density lipoprotein receptor-related protein on surfaces of tumour cells: a study using flow cytometry. Cancer Lett. *111*, 199–205.

Li, Y., Wood, N., Grimsley, P., Yellowlees, D., and Donnelly, P.K. (1998). In vitro invasiveness of human breast cancer cells is promoted by low density lipoprotein receptor-related protein. Invasion Metastasis *18*, 240–251.

Lillis, A.P., Duyn, L.B.V., Murphy-Ullrich, J.E., and Strickland, D.K. (2008). LDL Receptor-Related Protein 1: Unique Tissue-Specific Functions Revealed by Selective Gene Knockout Studies. Physiol. Rev. *88*, 887–918.

Lobo, E.D., Hansen, R.J., and Balthasar, J.P. (2004). Antibody pharmacokinetics and pharmacodynamics. J. Pharm. Sci. *93*, 2645–2668.

Lopez-Dee, Z., Pidcock, K., and Gutierrez, L.S. (2011). Thrombospondin-1: Multiple Paths to Inflammation. Mediators Inflamm. *2011*, e296069.

Loukinova, E., Ranganathan, S., Kuznetsov, S., Gorlatova, N., Migliorini, M.M., Loukinov, D., Ulery, P.G., Mikhailenko, I., Lawrence, D.A., and Strickland, D.K. (2002). Platelet-derived Growth Factor (PDGF)-induced Tyrosine Phosphorylation of the Low Density Lipoprotein Receptor-related Protein (LRP) EVIDENCE FOR INTEGRATED CO-RECEPTOR FUNCTION BETWEEN LRP AND THE PDGF. J. Biol. Chem. *277*, 15499–15506.

Luo, J.-L., Maeda, S., Hsu, L.-C., Yagita, H., and Karin, M. (2004). Inhibition of NF-κB in cancer cells converts inflammation- induced tumor growth mediated by TNFα to TRAIL-mediated tumor regression. Cancer Cell *6*, 297–305.

Manara, F.S., Chin, J., and Schneider, D.L. (1991). Role of degranulation in activation of the respiratory burst in human neutrophils. J. Leukoc. Biol. *49*, 489–498.

Mantuano, E., Jo, M., Gonias, S.L., and Campana, W.M. (2010). Low Density Lipoprotein Receptor-related Protein (LRP1) Regulates Rac1 and RhoA Reciprocally to Control Schwann Cell Adhesion and Migration. J. Biol. Chem. *285*, 14259–14266.

Markovic, S.N., Suman, V.J., Rao, R.A., Ingle, J.N., Kaur, J.S., Erickson, L.A., Pitot, H.C., Croghan, G.A., McWilliams, R.R., Merchan, J., et al. (2007). A phase II study of ABT-510 (thrombospondin-1 analog) for the treatment of metastatic melanoma. Am. J. Clin. Oncol. *30*, 303–309.

Matute-Bello, G., Frevert, C.W., and Martin, T.R. (2008). Animal models of acute lung injury. Am. J. Physiol. - Lung Cell. Mol. Physiol. *295*, L379–L399.

May, P., Reddy, Y.K., and Herz, J. (2002). Proteolytic Processing of Low Density Lipoprotein Receptor-related Protein Mediates Regulated Release of Its Intracellular Domain. J. Biol. Chem. *277*, 18736–18743.

McGregor, D.P. (2008). Discovering and improving novel peptide therapeutics. Curr. Opin. Pharmacol. *8*, 616–619.

McKinnell, C., and Sharpe, R.M. (1997). Regulation of the secretion and synthesis of rat Sertoli cell SGP-1, SGP-2 and CP-2 by elongate spermatids. Int. J. Androl. *20*, 171–179.

Meyer, R.C., Giddens, M.M., Schaefer, S.A., and Hall, R.A. (2013). GPR37 and GPR37L1 are receptors for the neuroprotective and glioprotective factors prosaptide and prosaposin. Proc. Natl. Acad. Sci. *110*, 9529–9534.

Miao, W.-M., Seng, W.L., Duquette, M., Lawler, P., Laus, C., and Lawler, J. (2001). Thrombospondin-1 Type 1 Repeat Recombinant Proteins Inhibit Tumor Growth through Transforming Growth Factor-β-dependent and -independent Mechanisms. Cancer Res. *61*, 7830–7839.

Mikhailenko, I., Krylov, D., Argraves, K.M., Roberts, D.D., Liau, G., and Strickland, D.K. (1997). Cellular Internalization and Degradation of Thrombospondin-1 Is Mediated by the Amino-terminal Heparin Binding Domain (HBD) HIGH AFFINITY INTERACTION OF DIMERIC HBD WITH THE LOW DENSITY LIPOPROTEIN RECEPTOR-RELATED PROTEIN. J. Biol. Chem. *272*, 6784–6791.

Mikhailenko, I., Considine, W., Argraves, K.M., Loukinov, D., Hyman, B.T., and Strickland, D.K. (1999). Functional domains of the very low density lipoprotein

receptor: molecular analysis of ligand binding and acid-dependent ligand dissociation mechanisms. J. Cell Sci. *112*, 3269–3281.

Mikhailenko, I., Battey, F.D., Migliorini, M., Ruiz, J.F., Argraves, K., Moayeri, M., and Strickland, D.K. (2001). Recognition of alpha 2-macroglobulin by the low density lipoprotein receptor-related protein requires the cooperation of two ligand binding cluster regions. J. Biol. Chem. *276*, 39484–39491.

Miyoshi, S., Hamada, H., Ito, R., Katayama, H., Irifune, K., Suwaki, T., Nakanishi, N., Kanematsu, T., Dote, K., Aibiki, M., et al. (2013). Usefulness of a selective neutrophil elastase inhibitor, sivelestat, in acute lung injury patients with sepsis. Drug Des. Devel. Ther. *7*, 305–316.

Moestrup, S.K., Gliemann, J., and Pallesen, G. (1992). Distribution of the alpha 2-macroglobulin receptor/low density lipoprotein receptor-related protein in human tissues. Cell Tissue Res. *269*, 375–382.

Morales, C.R., and Badran, H. (2003). Prosaposin ablation inactivates the MAPK and Akt signaling pathways and interferes with the development of the prostate gland. Asian J. Androl. *5*, 57–63.

Murin, S., Pinkerton, K.E., Hubbard, N.E., and Erickson, K. (2004). The effect of cigarette smoke exposure on pulmonary metastatic disease in a murine model of metastatic breast cancer. Chest *125*, 1467–1471.

Nakamura, K., Yoshikawa, N., Yamaguchi, Y., Kagota, S., Shinozuka, K., and Kunitomo, M. (2002). Characterization of mouse melanoma cell lines by their mortal malignancy using an experimental metastatic model. Life Sci. *70*, 791–798.

Neels, J.G., van Den Berg, B.M., Lookene, A., Olivecrona, G., Pannekoek, H., and van Zonneveld, A.J. (1999). The second and fourth cluster of class A cysteine-rich repeats of the low density lipoprotein receptor-related protein share ligand-binding properties. J. Biol. Chem. *274*, 31305–31311.

Ben-Neriah, Y., and Karin, M. (2011). Inflammation meets cancer, with NF-κB as the matchmaker. Nat. Immunol. *12*, 715–723.

Nguyen, D.X., and Massagué, J. (2007). Genetic determinants of cancer metastasis. Nat. Rev. Genet. *8*, 341–352.

Nielsen, B.S., Lund, L.R., Christensen, I.J., Johnsen, M., Usher, P.A., Wulf-Andersen, L., Frandsen, T.L., Dan?, K., and Gundersen, H.J.G. (2001). A Precise and Efficient Stereological Method for Determining Murine Lung Metastasis Volumes. Am. J. Pathol. *158*, 1997–2003.

Nufer, O., Corbett, M., and Walz, A. (1999). Amino-terminal processing of chemokine ENA-78 regulates biological activity. Biochemistry (Mosc.) *38*, 636–642.

Nykjaer, A., Petersen, C.M., Møller, B., Jensen, P.H., Moestrup, S.K., Holtet, T.L., Etzerodt, M., Thøgersen, H.C., Munch, M., and Andreasen, P.A. (1992). Purified alpha 2-macroglobulin receptor/LDL receptor-related protein binds urokinase.plasminogen activator inhibitor type-1 complex. Evidence that the alpha 2-macroglobulin receptor mediates cellular degradation of urokinase receptor-bound complexes. J. Biol. Chem. *267*, 14543–14546.

O'Brien, J.S., Kretz, K.A., Dewji, N., Wenger, D.A., Esch, F., and Fluharty, A.L. (1988). Coding of two sphingolipid activator proteins (SAP-1 and SAP-2) by same genetic locus. Science *241*, 1098–1101.

O'Brien, J.S., Carson, G.S., Seo, H.C., Hiraiwa, M., and Kishimoto, Y. (1994). Identification of prosaposin as a neurotrophic factor. Proc. Natl. Acad. Sci. *91*, 9593–9596.

Oganesian, A., Armstrong, L.C., Migliorini, M.M., Strickland, D.K., and Bornstein, P. (2008). Thrombospondins Use the VLDL Receptor and a Nonapoptotic Pathway to Inhibit Cell Division in Microvascular Endothelial Cells. Mol. Biol. Cell *19*, 563–571.

Orr, A.W., Pallero, M.A., and Murphy-Ullrich, J.E. (2002). Thrombospondin Stimulates Focal Adhesion Disassembly through Gi- and Phosphoinositide 3-Kinase-dependent ERK Activation. J. Biol. Chem. *277*, 20453–20460.

Orr, A.W., Elzie, C.A., Kucik, D.F., and Murphy-Ullrich, J.E. (2003a). Thrombospondin signaling through the calreticulin/LDL receptor-related protein co-complex stimulates random and directed cell migration. J. Cell Sci. *116*, 2917–2927.

Orr, A.W., Pedraza, C.E., Pallero, M.A., Elzie, C.A., Goicoechea, S., Strickland, D.K., and Murphy-Ullrich, J.E. (2003b). Low density lipoprotein receptor–related protein is a calreticulin coreceptor that signals focal adhesion disassembly. J. Cell Biol. *161*, 1179–1189.

Orr, A.W., Pallero, M.A., Xiong, W.-C., and Murphy-Ullrich, J.E. (2004). Thrombospondin Induces RhoA Inactivation through FAK-dependent Signaling to Stimulate Focal Adhesion Disassembly. J. Biol. Chem. *279*, 48983–48992.

Orth, K., Madison, E.L., Gething, M.J., Sambrook, J.F., and Herz, J. (1992). Complexes of tissue-type plasminogen activator and its serpin inhibitor plasminogen-activator inhibitor type 1 are internalized by means of the low density lipoprotein receptor-related protein/alpha 2-macroglobulin receptor. Proc. Natl. Acad. Sci. U. S. A. *89*, 7422–7426.

O'Shea, K.S., and Dixit, V.M. (1988). Unique distribution of the extracellular matrix component thrombospondin in the developing mouse embryo. J. Cell Biol. *107*, 2737–2748.

Owen, C.A., and Campbell, E.J. (1999). The cell biology of leukocyte-mediated proteolysis. J. Leukoc. Biol. *65*, 137–150.

Owen, C.A., Campbell, M.A., Sannes, P.L., Boukedes, S.S., and Campbell, E.J. (1995). Cell surface-bound elastase and cathepsin G on human neutrophils: a novel, non-oxidative mechanism by which neutrophils focus and preserve catalytic activity of serine proteinases. J. Cell Biol. *131*, 775–789.

Padrines, M., Wolf, M., Walz, A., and Baggiolini, M. (1994). Interleukin-8 processing by neutrophil elastase, cathepsin G and proteinase-3. FEBS Lett. *352*, 231–235.

Panetti, T.S., Kudryk, B.J., and Mosher, D.F. (1999). Interaction of Recombinant Procollagen and Properdin Modules of Thrombospondin-1 with Heparin and Fibrinogen/Fibrin. J. Biol. Chem. *274*, 430–437.

Park, B.S., Song, D.H., Kim, H.M., Choi, B.-S., Lee, H., and Lee, J.-O. (2009). The structural basis of lipopolysaccharide recognition by the TLR4–MD-2 complex. Nature *458*, 1191–1195.

Pham, C.T.N. (2006). Neutrophil serine proteases: specific regulators of inflammation. Nat. Rev. Immunol. *6*, 541–550.

Pidgeon, G.P., Harmey, J.H., Kay, E., Costa, M.D., Redmond, H.P., and Bouchier-Hayes, D.J. (1999). The role of endotoxin/lipopolysaccharide in surgically induced tumour growth in a murine model of metastatic disease. Br. J. Cancer *81*, 1311–1317.

Pittet, J.F., Mackersie, R.C., Martin, T.R., and Matthay, M.A. (1997). Biological markers of acute lung injury: prognostic and pathogenetic significance. Am. J. Respir. Crit. Care Med. *155*, 1187–1205.

Primo, L., Ferrandi, C., Roca, C., Marchiò, S., Blasio, L. di, Alessio, M., and Bussolino, F. (2005). Identification of CD36 molecular features required for its in vitro angiostatic activity. FASEB J.

Prince, L.R., Whyte, M.K., Sabroe, I., and Parker, L.C. (2011). The role of TLRs in neutrophil activation. Curr. Opin. Pharmacol. *11*, 397–403.

Psaila, B., and Lyden, D. (2009). The Metastatic Niche: Adapting the Foreign Soil. Nat. Rev. Cancer *9*, 285–293.

Qian, B.-Z., Li, J., Zhang, H., Kitamura, T., Zhang, J., Campion, L.R., Kaiser, E.A., Snyder, L.A., and Pollard, J.W. (2011). CCL2 recruits inflammatory monocytes to facilitate breast-tumour metastasis. Nature *475*, 222–225.

Rabhi-Sabile, S., Pidard, D., Lawler, J., Renesto, P., Chignard, M., and Legrand, C. (1996). Proteolysis of thrombospondin during cathepsin-G-induced platelet aggregation: functional role of the 165-kDa carboxy-terminal fragment. FEBS Lett. *386*, 82–86.

Raetz, C.R.H., and Whitfield, C. (2002). Lipopolysaccharide Endotoxins. Annu. Rev. Biochem. *71*, 635–700.

Ren, B., Song, K., Parangi, S., Jin, T., Ye, M., Humphreys, R., Duquette, M., Zhang, X., Benhaga, N., Lawler, J., et al. (2009). A double hit to kill tumor and endothelial cells by TRAIL and antiangiogenic 3TSR. Cancer Res. *69*, 3856–3865.

Rende, M., Brizi, E., Donato, R., Provenzano, C., Bruno, R., Mizisin, A.P., Garrett, R.S., Calcutt, N.A., Campana, W.M., and O'Brien, J.S. (2001). Prosaposin is immunolocalized to muscle and prosaptides promote myoblast fusion and attenuate loss of muscle mass after nerve injury. Muscle Nerve *24*, 799–808.

Rodriguez-Manzaneque, J.C., Lane, T.F., Ortega, M.A., Hynes, R.O., Lawler, J., and Iruela-Arispe, M.L. (2001). Thrombospondin-1 suppresses spontaneous tumor growth and inhibits activation of matrix metalloproteinase-9 and mobilization of vascular endothelial growth factor. Proc. Natl. Acad. Sci. U. S. A. *98*, 12485–12490.

Rohlmann, A., Gotthardt, M., Willnow, T.E., Hammer, R.E., and Herz, J. (1996). Sustained somatic gene inactivation by viral transfer of Cre recombinase. Nat. Biotechnol. *14*, 1562–1565.

Das Roy, L., Pathangey, L.B., Tinder, T.L., Schettini, J.L., Gruber, H.E., and Mukherjee, P. (2009). Breast cancer-associated metastasis is significantly increased in a model of autoimmune arthritis. Breast Cancer Res. BCR *11*, R56.

Ryu, S., Joshi, N., McDonnell, K., Woo, J., Choi, H., Gao, D., McCombie, W.R., and Mittal, V. (2011). Discovery of novel human breast cancer microRNAs from deep sequencing data by analysis of pri-microRNA secondary structures. PloS One *6*, e16403.

Sabroe, I., Jones, E.C., Usher, L.R., Whyte, M.K.B., and Dower, S.K. (2002). Toll-Like Receptor (TLR)2 and TLR4 in Human Peripheral Blood Granulocytes: A Critical Role for Monocytes in Leukocyte Lipopolysaccharide Responses. J. Immunol. *168*, 4701–4710.

Said, N., Sanchez-Carbayo, M., Smith, S.C., and Theodorescu, D. (2012). RhoGDI2 suppresses lung metastasis in mice by reducing tumor versican expression and macrophage infiltration. J. Clin. Invest. *122*, 1503–1518.

Schönbeck, U., Mach, F., and Libby, P. (1998). Generation of Biologically Active IL-1β by Matrix Metalloproteinases: A Novel Caspase-1-Independent Pathway of IL-1β Processing. J. Immunol. *161*, 3340–3346.

Schultz-Cherry, S., Ribeiro, S., Gentry, L., and Murphy-Ullrich, J.E. (1994). Thrombospondin binds and activates the small and large forms of latent transforming growth factor-beta in a chemically defined system. J. Biol. Chem. *269*, 26775–26782.

Schultz-Cherry, S., Chen, H., Mosher, D.F., Misenheimer, T.M., Krutzsch, H.C., Roberts, D.D., and Murphy-Ullrich, J.E. (1995). Regulation of Transforming Growth Factor-β Activation by Discrete Sequences of Thrombospondin 1. J. Biol. Chem. *270*, 7304–7310.

Shevde, L.A., and Welch, D.R. (2003). Metastasis suppressor pathways--an evolving paradigm. Cancer Lett. *198*, 1–20.

Shojaei, F., Wu, X., Zhong, C., Yu, L., Liang, X.-H., Yao, J., Blanchard, D., Bais, C., Peale, F.V., van Bruggen, N., et al. (2007). Bv8 regulates myeloid-cell-dependent tumour angiogenesis. Nature *450*, 825–831.

Simard, J.-C., Girard, D., and Tessier, P.A. (2010). Induction of neutrophil degranulation by S100A9 via a MAPK-dependent mechanism. J. Leukoc. Biol. *87*, 905–914.

Sköld, C.M., Liu, X., Umino, T., Zhu, Y., Ohkuni, Y., Romberger, D.J., Spurzem, J.R., Heires, A.J., and Rennard, S.I. (1999). Human neutrophil elastase augments fibroblast-mediated contraction of released collagen gels. Am. J. Respir. Crit. Care Med. *159*, 1138–1146.

Smith, H.A., and Kang, Y. (2013). Acute infection induces a metastatic niche: a double menace for cancer patients. Clin. Cancer Res. Off. J. Am. Assoc. Cancer Res. *19*, 4547–4549.

Stannard, A.K., Khurana, R., Evans, I.M., Sofra, V., Holmes, D.I.R., and Zachary, I. (2007). Vascular Endothelial Growth Factor Synergistically Enhances Induction of E-Selectin by Tumor Necrosis Factor-α. Arterioscler. Thromb. Vasc. Biol. *27*, 494–502.

Stathopoulos, G.T., Sherrill, T.P., Han, W., Sadikot, R.T., Yull, F.E., Blackwell, T.S., and Fingleton, B. (2008). Host Nuclear Factor-κB Activation Potentiates Lung Cancer Metastasis. Mol. Cancer Res. *6*, 364–371.

Strickland, D.K., Ashcom, J.D., Williams, S., Burgess, W.H., Migliorini, M., and Argraves, W.S. (1990). Sequence identity between the alpha 2-macroglobulin receptor and low density lipoprotein receptor-related protein suggests that this molecule is a multifunctional receptor. J. Biol. Chem. *265*, 17401–17404.

Su, C.F., Yang, F.L., and Chen, H.I. (2007). Inhibition of inducible nitric oxide synthase attenuates acute endotoxin-induced lung injury in rats. Clin. Exp. Pharmacol. Physiol. *34*, 339–346.

Su, C.-F., Kao, S.J., and Chen, H.I. (2012). Acute respiratory distress syndrome and lung injury: Pathogenetic mechanism and therapeutic implication. World J. Crit. Care Med. *1*, 50–60.

Suter, P.M., Suter, S., Girardin, E., Roux-Lombard, P., Grau, G.E., and Dayer, J.-M. (1992). High Bronchoalveolar Levels of Tumor Necrosis Factor and Its Inhibitors, Interleukin-1, Interferon, and Elastase, in Patients with Adult Respiratory Distress Syndrome after Trauma, Shock, or Sepsis. Am. Rev. Respir. Dis. *145*, 1016–1022.

Takeuchi, O., and Akira, S. (2010). Pattern Recognition Receptors and Inflammation. Cell *140*, 805–820.

Taraboletti, G., Belotti, D., Borsotti, P., Vergani, V., Rusnati, M., Presta, M., and Giavazzi, R. (1997). The 140-kilodalton antiangiogenic fragment of thrombospondin-1 binds to basic fibroblast growth factor. Cell Growth Differ. *8*, 471.

Taraboletti, G., Morbidelli, L., Donnini, S., Parenti, A., Granger, H.J., Giavazzi, R., and Ziche, M. (2000). The heparin binding 25 kDa fragment of thrombospondin-1 promotes angiogenesis and modulates gelatinase and TIMP-2 production in endothelial cells. FASEB J.

Teghanemt, A., Zhang, D., Levis, E.N., Weiss, J.P., and Gioannini, T.L. (2005). Molecular Basis of Reduced Potency of Underacylated Endotoxins. J. Immunol. *175*, 4669–4676.

Tolsma, S.S., Volpert, O.V., Good, D.J., Frazier, W.A., Polverini, P.J., and Bouck, N. (1993). Peptides derived from two separate domains of the matrix protein thrombospondin-1 have anti-angiogenic activity. J. Cell Biol. *122*, 497–511.

Tsuboi, K., Hiraiwa, M., and O'Brien, J.S. (1998). Prosaposin prevents programmed cell death of rat cerebellar granule neurons in culture. Brain Res. Dev. Brain Res. *110*, 249–255.

Vestweber, D., and Blanks, J.E. (1999). Mechanisms that regulate the function of the selectins and their ligands. Physiol. Rev. *79*, 181–213.

Vielhaber, G., Hurwitz, R., and Sandhoff, K. (1996). Biosynthesis, Processing, and Targeting of Sphingolipid Activator Protein (SAP)Precursor in Cultured Human Fibroblasts MANNOSE 6-PHOSPHATE RECEPTOR-INDEPENDENT ENDOCYTOSIS OF SAP PRECURSOR. J. Biol. Chem. *271*, 32438–32446.

Vogel, T., Guo, N.H., Krutzsch, H.C., Blake, D.A., Hartman, J., Mendelovitz, S., Panet, A., and Roberts, D.D. (1993). Modulation of endothelial cell proliferation, adhesion, and motility by recombinant heparin-binding domain and synthetic peptides from the type I repeats of thrombospondin. J. Cell. Biochem. *53*, 74–84.

Wang, D., Wei, J., Hsu, K., Jau, J., Lieu, M.W., Chao, T.J., and Chen, H.I. (1999). Effects of nitric oxide synthase inhibitors on systemic hypotension, cytokines and inducible nitric oxide synthase expression and lung injury following endotoxin administration in rats. J. Biomed. Sci. *6*, 28–35.

Weiland, J.E., Davis, W.B., Holter, J.F., Mohammed, J.R., Dorinsky, P.M., and Gadek, J.E. (1986). Lung neutrophils in the adult respiratory distress syndrome. Clinical and pathophysiologic significance. Am. Rev. Respir. Dis. *133*, 218–225.

Werle, M., and Bernkop-Schnürch, A. (2006). Strategies to improve plasma half life time of peptide and protein drugs. Amino Acids *30*, 351–367.

Wight, T.N., Raugi, G.J., Mumby, S.M., and Bornstein, P. (1985). Light microscopic immunolocation of thrombospondin in human tissues. J. Histochem. Cytochem. Off. J. Histochem. Soc. *33*, 295–302.

Williams, S.E., Ashcom, J.D., Argraves, W.S., and Strickland, D.K. (1992). A novel mechanism for controlling the activity of alpha 2-macroglobulin receptor/low density lipoprotein receptor-related protein. Multiple regulatory sites for 39-kDa receptor-associated protein. J. Biol. Chem. *267*, 9035–9040.

Willnow, T.E., Moehring, J.M., Inocencio, N.M., Moehring, T.J., and Herz, J. (1996a). The low-density-lipoprotein receptor-related protein (LRP) is processed by furin in vivo and in vitro. Biochem. J. *313 (Pt 1)*, 71–76.

Willnow, T.E., Rohlmann, A., Horton, J., Otani, H., Braun, J.R., Hammer, R.E., and Herz, J. (1996b). RAP, a specialized chaperone, prevents ligand-induced ER retention and degradation of LDL receptor-related endocytic receptors. EMBO J. *15*, 2632–2639.

Xu, X., and Håkansson, L. (2002). Degranulation of Primary and Secondary Granules in Adherent Human Neutrophils. Scand. J. Immunol. *55*, 178–188.

Yamamoto, K., Ahyi, A.-N.N., Pepper-Cunningham, Z.A., Ferrari, J.D., Wilson, A.A., Jones, M.R., Quinton, L.J., and Mizgerd, J.P. (2014). Roles of Lung

Epithelium in Neutrophil Recruitment during Pneumococcal Pneumonia. Am. J. Respir. Cell Mol. Biol. *50*, 253–262.

Yamauchi, M., Imajoh-Ohmi, S., and Shibuya, M. (2007). Novel antiangiogenic pathway of thrombospondin-1 mediated by suppression of the cell cycle. Cancer Sci. *98*, 1491–1497.

Yan, L., Cai, Q., and Xu, Y. (2013). The ubiquitin-CXCR4 axis plays an important role in acute lung infection-enhanced lung tumor metastasis. Clin. Cancer Res. Off. J. Am. Assoc. Cancer Res. *19*, 4706–4716.

Yang, J., Mani, S.A., Donaher, J.L., Ramaswamy, S., Itzykson, R.A., Come, C., Savagner, P., Gitelman, I., Richardson, A., and Weinberg, R.A. (2004a). Twist, a master regulator of morphogenesis, plays an essential role in tumor metastasis. Cell *117*, 927–939.

Yang, M., Huang, H., Li, J., Li, D., and Wang, H. (2004b). Tyrosine phosphorylation of the LDL receptor-related protein (LRP) and activation of the ERK pathway are required for connective tissue growth factor to potentiate myofibroblast differentiation. FASEB J.

Yardeni, T., Eckhaus, M., Morris, H.D., Huizing, M., and Hoogstraten-Miller, S. (2011). Retro-orbital injections in mice. Lab Anim. *40*, 155–160.

Yu, B., Hailman, E., and Wright, S.D. (1997). Lipopolysaccharide binding protein and soluble CD14 catalyze exchange of phospholipids. J. Clin. Invest. *99*, 315–324.

Zeiher, B.G., Matsuoka, S., Kawabata, K., and Repine, J.E. (2002). Neutrophil elastase and acute lung injury: prospects for sivelestat and other neutrophil elastase inhibitors as therapeutics. Crit. Care Med. *30*, S281–S287.

Zeiher, B.G., Artigas, A., Vincent, J.-L., Dmitrienko, A., Jackson, K., Thompson, B.T., Bernard, G., and STRIVE Study Group (2004). Neutrophil elastase inhibition in acute lung injury: results of the STRIVE study. Crit. Care Med. *32*, 1695–1702.

Zhu, Y.K., Liu, X.D., Sköld, C.M., Umino, T., Wang, H.J., Spurzem, J.R., Kohyama, T., Ertl, R.F., and Rennard, S.I. (2001). Synergistic neutrophil elastase-cytokine interaction degrades collagen in three-dimensional culture. Am. J. Physiol. - Lung Cell. Mol. Physiol. *281*, L868–L878.